technische universität dortmund

TÜRK ALMAN ÜNİVERSİTESİ
TÜRKISCH DEUTSCHE UNIVERSITÄT

Institut für Umformtechnik und Leichtbau

FAKULTÄT MASCHINENBAU

Master of Science in Manufacturing Technology

Institut für Umformtechnik und Leichtbau

Prof. Dr.-Ing. Dr. h.c. Matthias Kleiner

Prof. Dr.-Ing. Dr.-Ing. E.h. A. Erman Tekkaya

Master Thesis

Experimental and Numerical Analysis of Deep Drawability of Aluminium Alloys AA5754-H22 and AA6061-T6

by

Onur Erbaş

Matriculation no: 162950

Supervisors:

Prof. Dr.-Ing. Dr.-Ing. E.h. A. Erman Tekkaya

Assist. Prof. Dr. Mehmet İpekoğlu

M.Sc. Hamad ul Hassan

Submitted on 22.12.2014

Acknowledgements

This Master thesis project is carried out by the collaboration between Technical University Dortmund, Turkish-German University and Mercedes-Benz Türk A.Ş., Istanbul. This thesis has been completed under guidance and constant supervision of Prof. Dr.-Ing. Dr.-Ing. E.h. A. Erman Tekkaya (Institut für Umformtechnik und Leichtbau, TU Dortmund) and Assist. Prof. Dr. Mehmet İpekoğlu (Dept. of Mechatronic Systems Engineering, Turkish-German University).

First and foremost, I would like to express my appreciation and thankfulness to my supervisor Prof. Dr.-Ing. Dr.-Ing. E.h. A. Erman Tekkaya, for motivating me all the time with innovative ideas in metal forming technology world.

I am deeply thankful Assist. Prof. Dr. Mehmet İpekoğlu for being my supervisor and providing valuable guidance and support. His continuous help and support in all stages has always made me confident.

I would like to express my gratefulness and appreciation to M.Sc. Hamad ul Hassan for his guidance, suggestions and invaluable help. Without his encouragement, this thesis would not have materialized.

I also would like to express my deep gratitude and respect to the team manager of the production planning department Onur Darcan and my colleagues Caner Sürel and Sultan Çil for their help, support and constructive criticism.

I also want to thank to the employees of the Institute of Metal Forming and Lightweight and Zwick Avrasya Ltd. for their help in performing experiments.

Finally, yet importantly, I would like to express my heartfelt thanks to my beloved parents and my sister for their help and wishes for my success. Without their support, it would have been impossible for me to finish university easily.

Abstract

In the recent years sheet metal forming technologies are challenged by the higher fuel economy and concerns about global warming in the automotive industry. Deep drawing is one of the most commonly used sheet metal forming process in automotive industry. Lighter and safer materials are used for automotive production to reduce the weight of vehicles. Aluminium alloys, due to their low density compared to steels, are an important group of materials, in particular for light weight construction of transport vehicles.

The primary purpose of this master thesis is to determine deep drawability of two different aluminium alloys. It discusses the right material to deep draw an emergency valve cup on the bus side panel. Therefore, suitable process parameters and possible cup position according to the edge of the sheet panel are chosen for required quality of the product.

In order to estimate the formability of two different aluminium alloys, they are firstly characterized with tensile and Nakajima test. Then deep drawing experiment with different process parameters is carried out to produce emergency valve cup. The experimental investigation is followed by a numerical analysis which investigates deep drawing process through simulation software.

Keywords: Deep Drawing, Deep Drawability, Thickness Distribution, Blankholder Force, Finite Element Simulation

Table of Contents

List of Figures

List of Tables

Formula Symbols and Abbreviations

Formula Symbols

Symbol	Unit	Description
F	N	Force
D	mm	Diameter
R	mm	Radius
c	mm	Clearance
t	mm	Thickness
r	-	Anisotropy coefficient
ε	-	Strain
L	mm	Length
E	GPa	Young's modulus
$R_{P0.2}$	MPa	Yield stress
R_m	MPa	Tensile strength
n	-	Strain hardening exponent
K	MPa	Strength coefficient
k_f	MPa	Flow stress
φ	-	True strain
P	Pa	Pressure
A	mm^2	Area
R	-	Average anisotropic exponent

Indices

Indice	Description
0°	Rolling direction
45°	Diagonal direction
90°	Transverse direction
l	Length direction
t	Thickness direction
w	Width direction

Abbreviations

Abbreviation	**Description**
ACEA	European Automotive Manufacturers Association
ICCT	International Council of Clean Transportation
EAA	European Aluminium Association
AA	Aluminium Association
DR	Drawing Ratio
FLD	Forming Limit Diagram
FLC	Forming Limit Curve
IADS	International Alloy Designation System
PLC	Portevin-Le Chatelier
FEM	Finite Element Method
CAD	Computer Aided Design
3D	Three-Dimensional
DOE	Design of Experiments

1 Introduction

Sheet metal forming is one of the manufacturing processes, in which plastic deformation is used to change the shape of the flat metal sheet. It is used in almost every sector of industrial production such as automotive, aircraft, home appliance and food industry.

In the recent years automotive industry became economically and socially more significant compared to the other industries. According to the European Automotive Manufacturers Association (ACEA) 63.1 million passenger cars and 31 million commercial vehicles have been produced around the world in 2012. Now 1 billion vehicles are on the road, which is expected to reach 1.7 billion by the International Council of Clean Transportation. (ICCT)

Sheet metal forming technologies are challenged by the improvements in the automotive industry in the last several decades. More successful and economical production is the unavoidable result of increasing demands of the customer, safety requirements and market competitions. On the other hand, in recent years, environmental and safety concerns leads the industry to develop innovative new materials. (Tisza, 2013) Lighter and safer materials are used for automotive production to reduce the weight of vehicles.

Aluminium alloys, due to their low density compared to steels, are an important group of materials, in particular for light weight construction of transport vehicles. The more aluminium is used in the production of a vehicle, the less is the weight of the vehicle and the less is the fuel consumption. (Kleiner et al., 2003) European Aluminium Association (EAA) evaluates that 10% of vehicle weight reduction improves 8–10% of fuel economy. With the rising demand for environment-friendly vehicles, besides steel as a structural material, aluminium alloys in automobiles are recently also widely used in car manufacturing mostly for body production. Aluminium usage in automotive industry has grown more than 50% in the final 10 years. According to EAA (2012), the average amount of aluminium used in a vehicle produced in Europe is 140 kg.

Deep drawing is one of the most commonly used processes in sheet metal forming. According to DIN8584 deep drawing is where a sheet metal blank is formed into a hollow body open on one side or a hollow body is formed into a hollow body with a smaller cross section. This production process is used for mass production and for manufacturing of small series, such as packaging, aircraft and automotive industry. It is applied in automotive industry for the manufacturing of the vehicle body parts. (Lange, 2006)

The important variables in deep drawing are the sheet metal material, ratio of blank to punch diameter, radius of die and punch corner, blankholder force, and lubrication. Blankholder is one of the most important parameters to avoid wrinkling and tearing in the deep drawn part. (Groover, 2012)

In the deep drawing process, it is important to optimize the process parameters to obtain a product with required quality. To achieve the optimization, a large number of trials can be performed with various parameters to obtain the best result. (Ramesh and Reddy, 2013) Experimental investigations should be supported with numerical analyses such as simulations, because it is not always possible to realize all experiments. Apart from that, various other configurations of the deep drawing experiments can be investigated. Numerical investigations serve the validation of the experimental investigations.

1.1 Motivation and Objective of the Thesis

The motivation behind the thesis is to choose between two different materials for deep drawing process in terms of deep drawability to produce the emergency valve cavity on bus side panel with required quality by reducing the production cost and time.

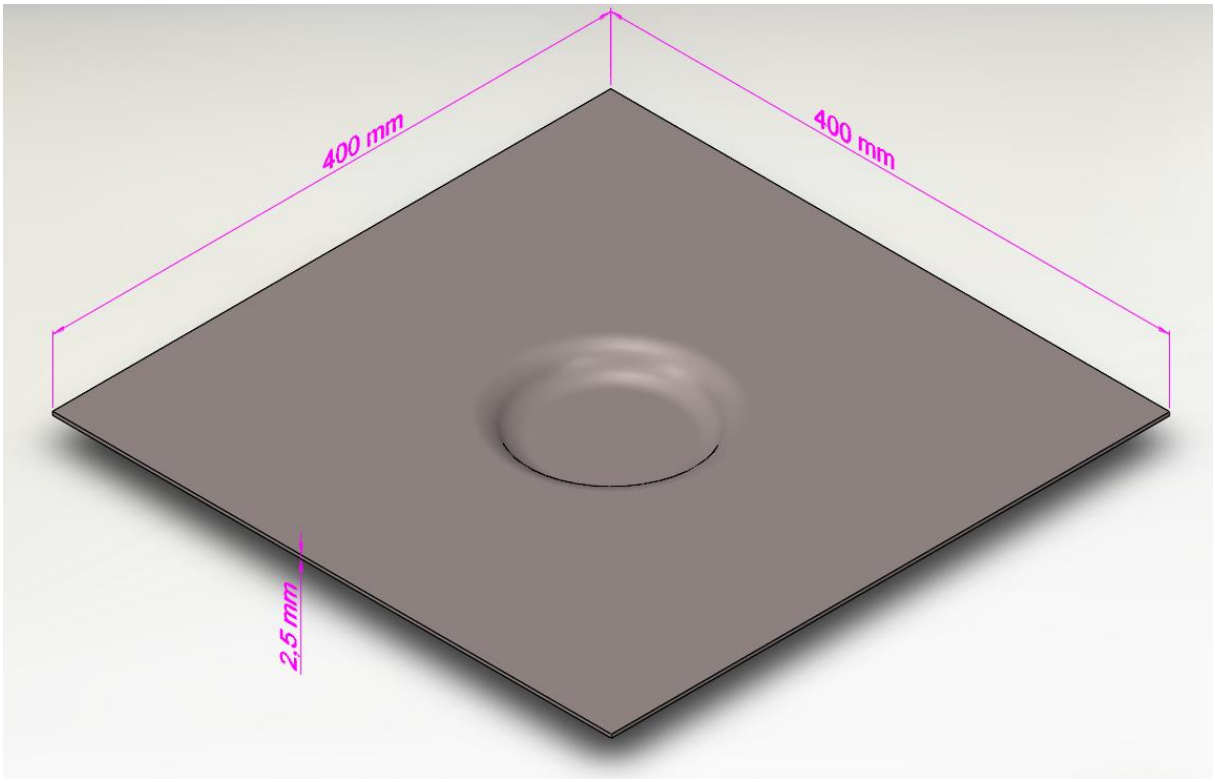

Figure 1.1: Three dimensional view of the deep drawn part

This motivation can be achieved through characterization of two different aluminium alloys AA5754-H22 and AA6061-T6, deep drawing experiment with different process parameters and its numerical analysis with a simulation software. The main objective of the thesis is to find out the best suitable material among the two options for the deep drawing, determine the required process parameters and determine a possible cavity position according to the edge of the sheet panel.

1.2 Outline of the Thesis

There are eight chapters in this thesis work. The thesis structure is organized as follows:

Chapter 1. Introduction

This chapter gives a general introduction and outline for the motivation and objective behind this thesis.

Chapter 2. State of the Art

This chapter gives an overview about the state of the art of subjects such as metal forming, deep drawing and aluminium and aluminium alloys. The metal forming processes which are bulk and sheet metal forming are briefly explained, whereas the

deep drawing is described in detail. Except the mechanics and engineering analysis of the deep drawing, detailed information about different operations and possible defects are given with the formability in deep drawing. Moreover, this chapter contains information about aluminium, aluminium alloys, AA5754-H22 and AA6061-T6 in automotive industry.

Chapter 3. Aim and Scope of the Thesis Work

This chapter describes the aim and scope of the thesis work.

Chapter 4.Experiments for Material Characterization

This chapter covers two different experiments to characterize AA5754-H22 and AA6061-T6, namely the tensile test and Nakajima test. Both tests include specimen preparation, experimental setup and results sections.

Chapter 5. Deep Drawing Experiment

This chapter includes the deep drawing experiment with different process parameters and materials to produce the desired part. It contains the experimental setup and the results of the experiments.

Chapter 6. Numerical Analysis

This chapter is devoted to the numerical analysis of the deep drawing experiments. First, it gives a short introduction about finite element analysis and the simulation software AutoForm which is used in the thesis. Next, the finite element model is described in detail and after that the results of the simulations are given. In the end of the chapter, simulation results, a comparison of the results with the results of the deep drawing experiments and further simulation investigations are discussed.

Chapter 7. Cost Analysis

This chapter contains cost analysis which explains the cost saving attained if the emergency valve cavity on bus panel is deep drawn instead of purchased.

Chapter 8. Conclusion

This chapter presents the conclusions of the thesis work and contains recommendations for further studies.

2 State of the Art

2.1 Metal Forming

Forming is defined as a group of manufacturing methods where the given shape of a workpiece is converted into another shape without altering its mass or material composition. Deformation is caused by the die which applies stresses more than the yield strength of the metal. The geometry of the die shapes the metal. Metal forming is basically divided into two main groups based on the workpiece thickness; bulk metal forming and sheet metal forming. In both processes, the surfaces of the deforming metal and the tools are in contact. In bulk forming, the input material is in billet, rod, or slab form. (Simiatin, 2005) In sheet metal forming, on the other hand, a piece of sheet metal is plastically deformed by forces, often without important changes in sheet thickness. (Lange, 2006) **Figure 2.1** illustrates how metal forming processes are classified.

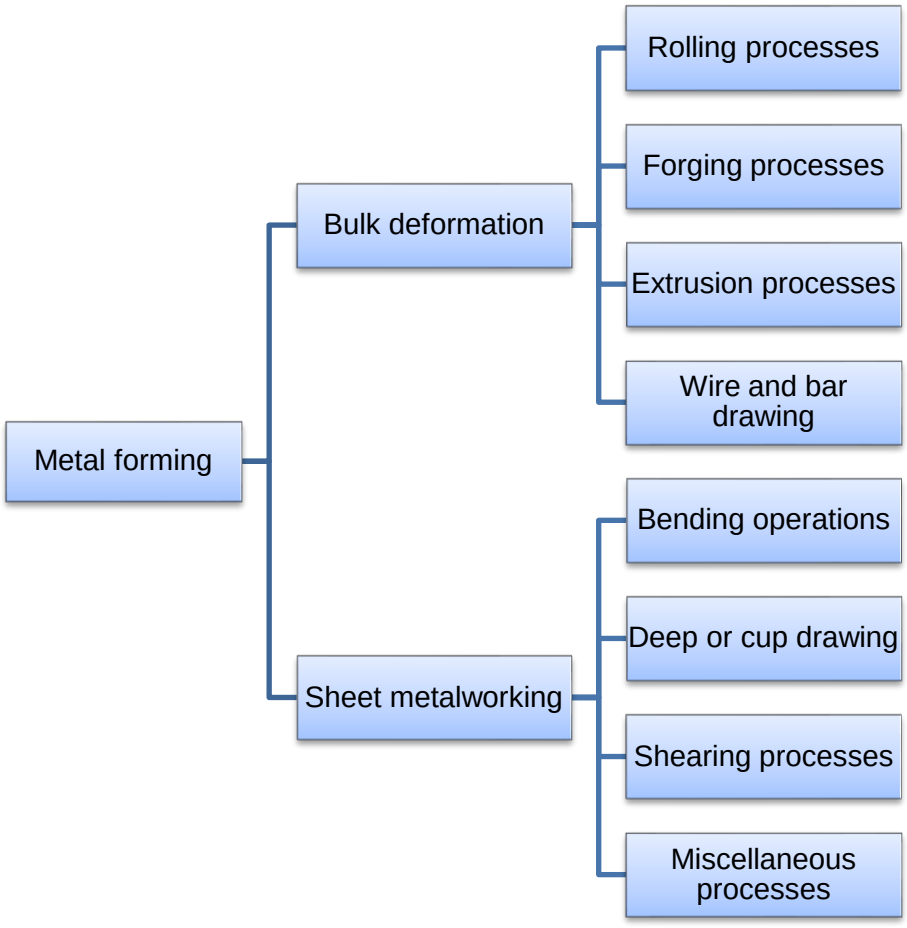

Figure 2.1: Classification of metal forming operations (Groover, 2012)

2.1.1 Bulk Metal Forming

Bulk forming is one the manufacturing processes in which plastic deformation is used to change the shape of the metal workpiece between tools or dies. Bulk forming processes involve significant amounts of plastic deformation. The cross section of workpiece changes without volume change. The surface-area-to-volume ratio is relatively small. The term bulk describes the workpiece that has this low area-to-volume ratio. Mostly, hot or warm working conditions are preferred. Basic bulk deformation processes are shown **Figure 2.2**.

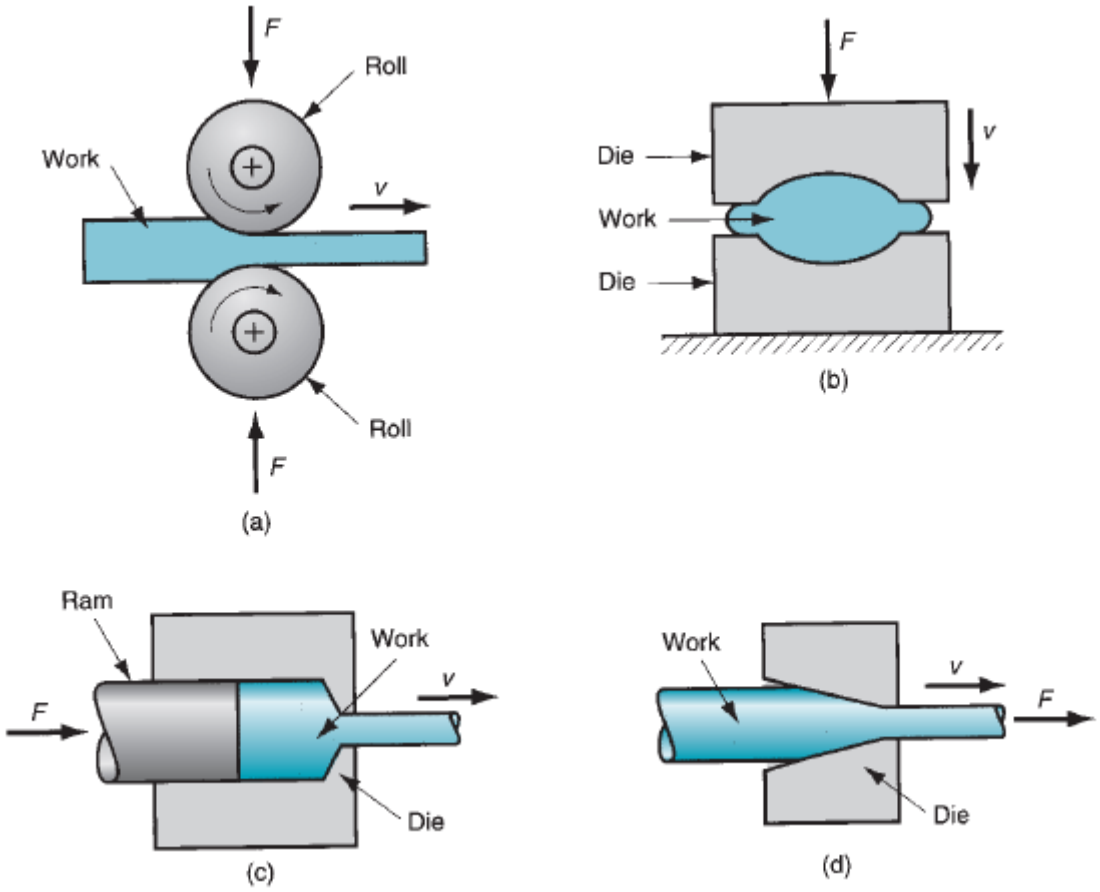

Figure 2.2: Basic bulk deformation processes: **(a)** rolling, **(b)** forging, **(c)** extrusion, and **(d)** drawing (Groover, 2012)

Rolling

In rolling, thickness of a slab or plate is reduced by two rotating cylindrical rolls. The rolls draw the workpiece into the gap and squeeze it. Most rolling processes require

high investments such rolling mills as equipment. Most of the rolling processes are hot working processes as large amount of deformation is needed. (Groover, 2012)

Forging

In forging, the workpiece is compressed between two opposing dies. The shape of the die is imparted to workpiece. It is widely used in industry to produce parts with different high strengths for automotive and other applications. Most of the operations are carried out hot or warm to reduce strength and increase ductility. (Groover, 2012)

Extrusion

In extrusion, the workpiece is forced to flow through a die opening taking its own cross section. It is a compression process which has many advantages such as shape variety, close tolerances and near or net shape forming. (Groover, 2012)

Drawing

In drawing, the diameter of a wire or bar is reduced by pulling it through a die opening. The process is similar to extrusion, the only difference is that the material is pulled through the die. Compressive stresses are important as well as tensile stresses as the metal is squeezed down while passing through the die. Drawing is called “bar drawing” when the stock materials is a large diameter bar and rod. In wire drawing small diameter stock is used. (Groover, 2012)

2.1.2 Sheet Metal Forming

Sheet metal forming deals with plastic deformation of metallic material with a high cross section to volume ratio. The workpieces used are metal sheets, strips and coils. In this process the cross section of the workpiece does not change, only the form of the workpiece changes. It is carried out with two tools called a punch and a die. Sheet metal forming has generally two types, cold forming which is carried out at room temperature and hot forming in which material is heated to higher temperatures than the recrystallization temperature of the metal that is being formed. Basic sheet deformation processes are shown **Figure 2.3**.

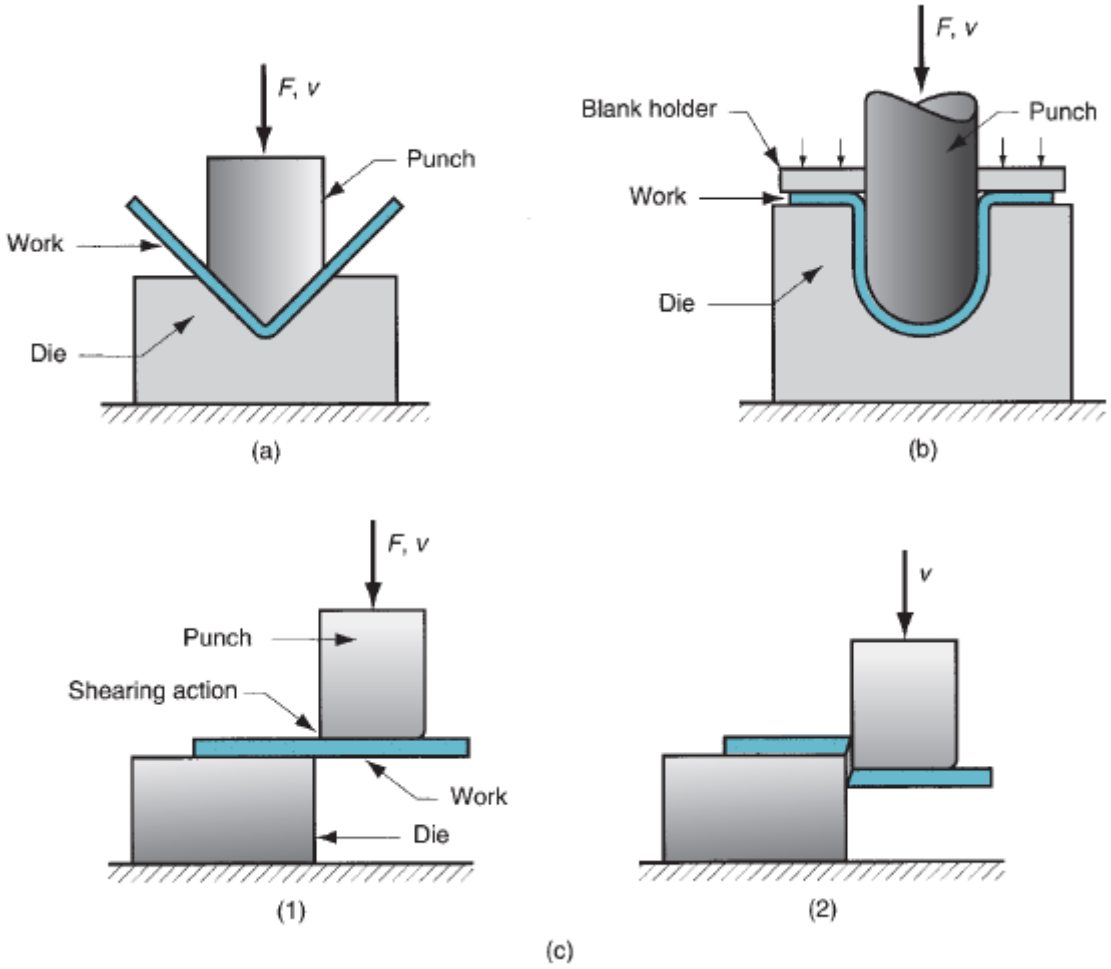

Figure 2.3: Basic sheet metal working operations: **(a)** bending, **(b)** drawing, **(c)** shearing: **(1)** as punch first contacts sheet, and **(2)** after cutting (Groover, 2012)

Bending

Bending is the straining of sheet metal around a straight axis. When it is considered that the metallic sheet has a neutral axis, the material inside is compressed while the outside material is stretched. The deformation of metal is plastic in nature thus making it permanent after the stress is removed. The change of sheet thickness in bending is negligible. V-bending and edge bending are two common methods of bending process. Sheet metal workpieces are bent to produce final desired shapes but since plastic and elastic deformation occurs during bending, springback effect occurs. When force is removed from the workpiece material due to the elasticity of the material it tends to recover its original shape. The most common problem in bending process is springback. (Groover, 2012)

Drawing

Drawing is a process used to form a sheet metal in various shapes such as cup, box, complex or hollow parts. It is carried out by pressing a sheet of metal over a die cavity with the help of a punch. The punch has the same shape but different size than die cavity. Die cavity is just sufficient to allow the sheet to be pushed by the punch into the die. The sheet metal takes the form of the die which is mostly cylindrical. (Groover, 2012)

Sheet metal cutting

Sheet metal cutting is done by either shearing or punching of the sheet metal. In shearing, the punch compresses the metal which results in plastic deformation followed by penetration of the punch and finally it ends in the fracture of the sheet metal. In blanking cutting is carried out along a closed outline in single step to separate the piece from the surrounding. The part that is cut out is the desired part in blanking and it is scrap in punching. They both have the same principles. (Groover, 2012)

2.2 Deep Drawing

Deep drawing is a manufacturing process of forming sheet metals into geometrical or irregular shapes. The sheet metal is forced by a punch to flow between surfaces of a punch and a die. (Boljanovic, 2004)

2.2.1 Mechanics of Deep Drawing

A basic drawing operation of a cup-shaped sheet metal part can be seen in **Figure 2.4**. The blank diameter is D_b is drawn into a die with a D_p punch diameter. Both punch and die have the corner radii which are respectively, R_p and R_d. There is a clearance c between the sides of the punch and die. The punch applies a downward force F which causes deformation and in the same time a downward holding force is applied to the blankholder, F_h. (Groover, 2012)

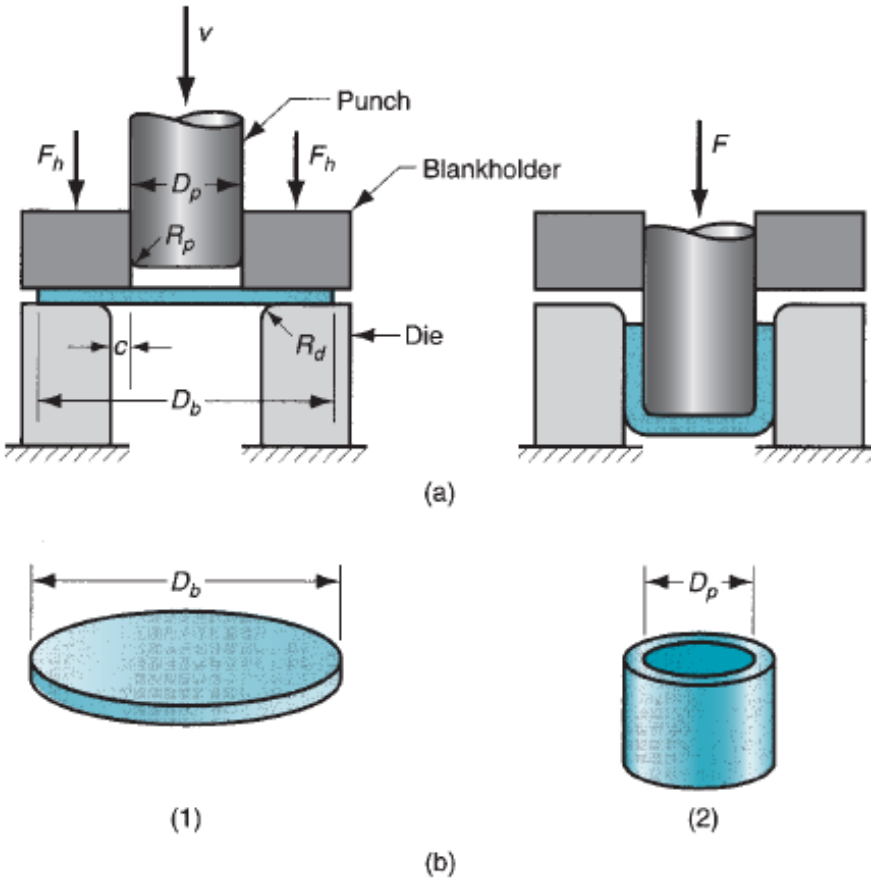

Figure 2.4: (a) Drawing of a cup-shaped part: **(1)** start of operation before punch contacts work, and **(2)** near end of stroke; and corresponding workpiece: **(1)** starting blank **(2)** drawn part (Groover, 2012)

As the punch moves downward to the final position, the workpiece is formed with the shape of the punch and die cavity. The stages of deep drawing are illustrated in **Figure 2.5**.

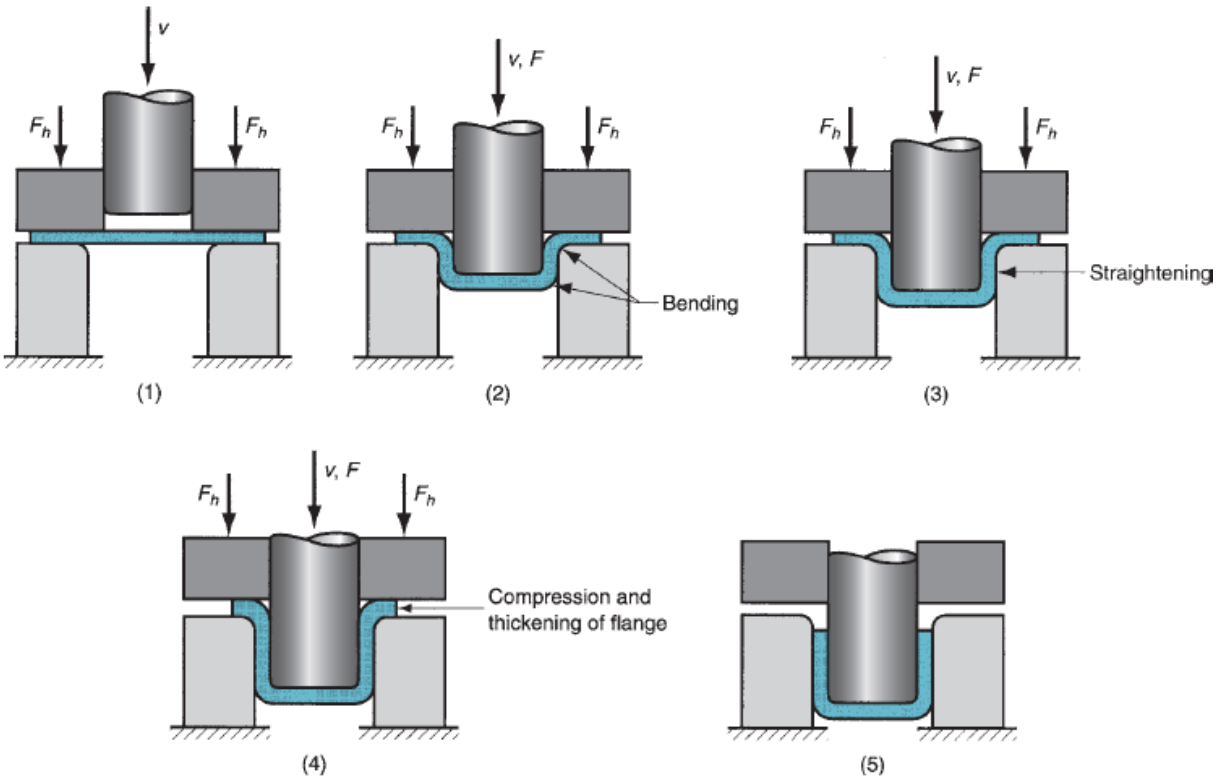

Figure 2.5: Stages in deformation of the work in deep drawing: **(1)** punch makes initial contact with work**, (2)** bending, **(3)** straightening, **(4)** friction and compression, and **(5)** final cup shape (Groover, 2012)

At step 1, the blankholder force F_h is applied and the punch begins to move towards the sheet material. In the next step, the sheet material is exposed to a bending operation. The sheet is bent over the corner of the punch and the corner of the die. In the third step, the punch keeps moving down and in the same time a straightening in the metal appears that was previously bent over the die radius. The sheet metal from the flange is drawn into the die opening to form the cylinder wall. In step 4, as the metal in the flange moves to the center, it is exposed to three different states of stress: First one is compression in the circumferential direction. Second one is the tension in the radial direction and third one is a relatively small compression in the thickness direction. Since the metal volume remains constant, and since the circumferential stress is relatively large, the sheet will be thicker as it moves in the flange area. With the downward motion of the punch, metal flow caused by drawing and compression, continues. Some thinning in the cylinder walls occurs as well. Final step shows the completed drawing process. (Groover, 2012)

2.2.2 Stress Zones of Deep Drawing

Deep drawing is defined as a tensile-compressive forming among sheet metal forming processes. During deep drawing, because of punch and blankholder force, different stress zones are formed such as force application zone at the punch region, force transmission zone and bending zone at the cup wall and forming zone at the flange. (Yalçın, 2010)

Tensile stress is produced along the surface at different points, and it has maximum value near the end of the punch. The sheet does not bend along the cup wall, and near the punch profile necking occurs. The flange is subjected to compressive hoop stress, radial tensile stress and compressive stress due to blank holder. The wall thickness decreases from top to bottom. In the **Figure 2.6** the stress distribution along the profile is shown.

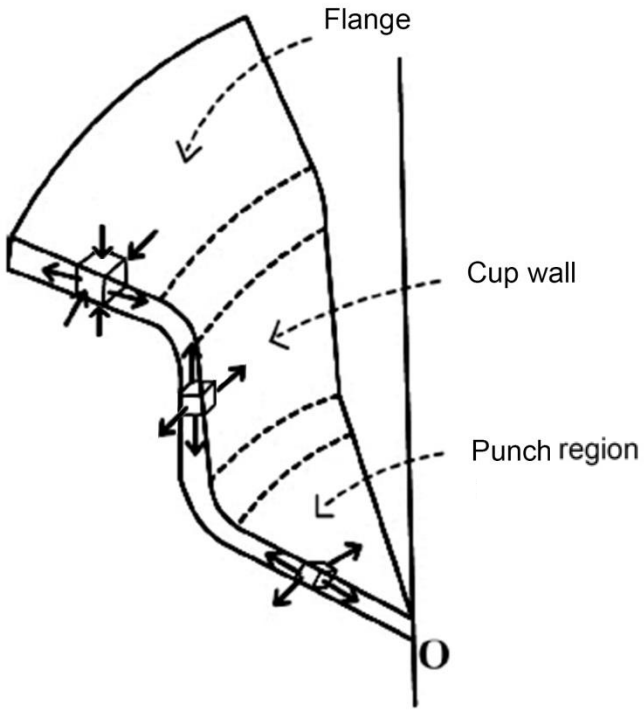

Figure 2.6: Stresses at drawn cup in deep drawing process

The flange of drawn cup is exposed to a compressive hoop stress because it is drawn towards the center and radial tensile stress. The compressive stress of the blankholder acts in the axial direction. If the compressive hoop stress is high or if the metal in the flange is not restricted, wrinkling of the metal in the flange occurs. The flange faces

compressive hoop stress and a radial tensile stress. As a result, the flange tends to swell because of the circumferential shrinking. However, because of bending under the punch and die profile, the metal undergoes thinning. The pressed metal at the center of the blank is exposed to biaxial tensile stress because of the punch. The metal in the gap between die wall and punch is subjected to longitudinal and hoop tensile stresses. (Schüler, 1998)

2.2.3 Engineering Analysis of Deep Drawing

In deep drawing there are several factors affecting the process. They are categorized into three main groups which are shown below in the **Figure 2.7**.

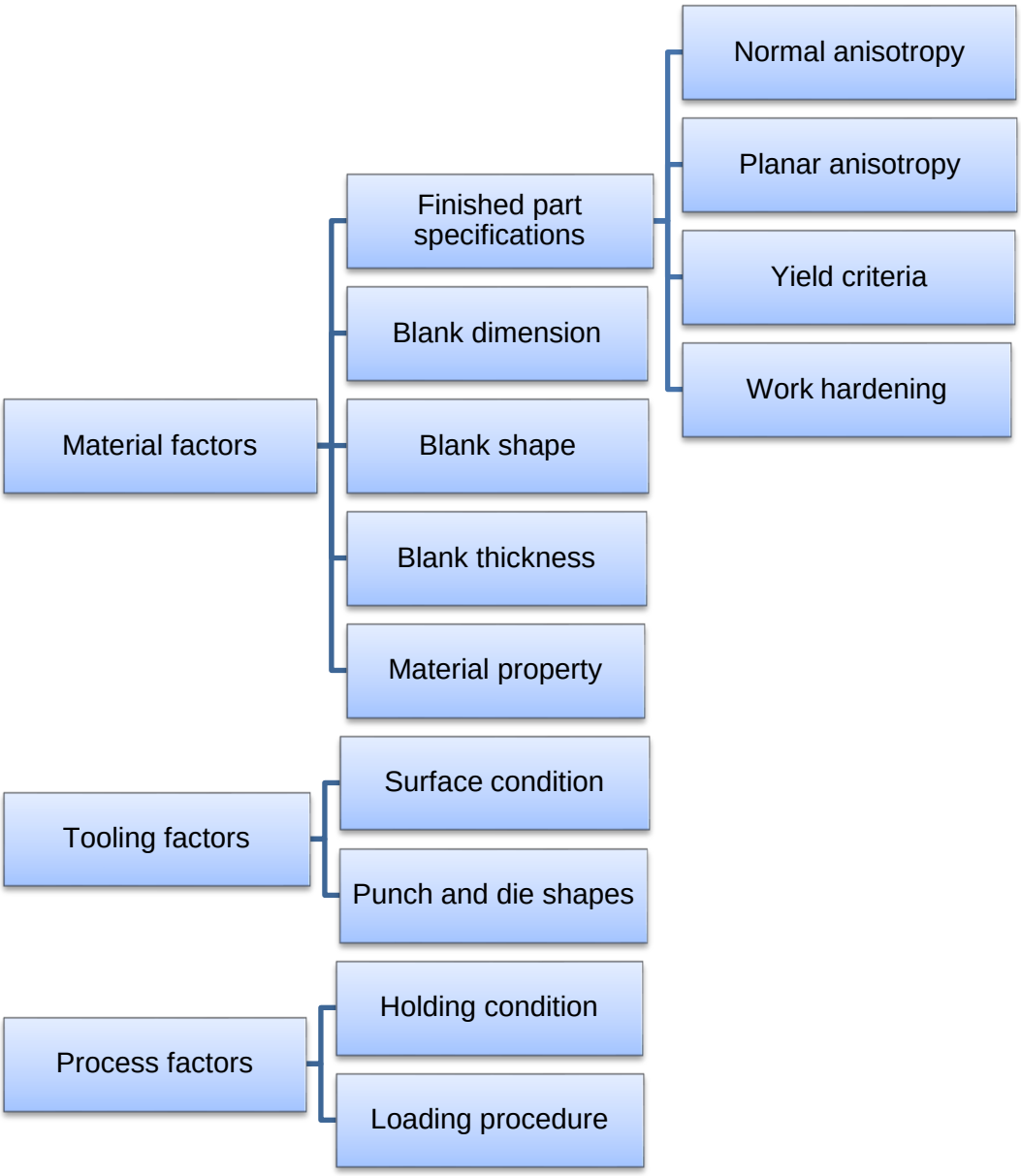

Figure 2.7: Important variables in deep drawing (Boljanovic, 2004)

The guidance to analyse deep drawing is some calculations of clearance, drawing ratio, reduction, thickness-to-diameter ratio, drawing force and holding force.

Clearance

There is a clearance *c* between the sides of the punch and die. This clearance must be about 10% greater than the sheet thickness.

$$c = 1.1\ t \quad \textbf{(2.1)}$$

Drawing ratio

Failure in deep drawn parts results from thinning of the cup wall under high tensile stresses most of the time. It should resist thinning under the stresses. Deep drawability is indicated by the drawing ratio. (Kalpakjian & Schmid, 2007)

Drawing ratio (DR) is defined as the ratio of the blank diameter D_b to the punch diameter D_p for cylindrical shape.

$$DR = \frac{D_b}{D_p} \quad \textbf{(2.2)}$$

Upper limit for drawing ratio is 2.0, although the actual limit should consider die corner radii, friction conditions, depth of drawing and characteristics of the sheet metal such as ductility.

Reduction

Reduction is related to the drawing ratio. Upper limit for reduction should be less than 0.50.

$$r = \frac{D_b - D_p}{D_b} \quad \textbf{(2.3)}$$

Thickness-to-diameter ratio

This ratio is thickness of the starting blank *t* divided by the blank diameter D_b. t/D_b is expressed as percent and it is desired to have a value higher than 1%.

Drawing force

The force needed to draw the sheet metal can be calculated by the formula given below:

$$F = \pi . D_p . t . (TS) . \left(\frac{D_b}{D_p} - 0.7\right) \quad \textbf{(2.4)}$$

F is drawing force in N; *t* is original blank thickness in mm; *TS* is tensile strength in MPa; and D_b is blank diameter in mm; and D_p is punch diameter in mm.

Holding force

The holding force in drawing operation can be calculated by the formula given below:

$$F_h = 0.015.Y.\pi.\{D_b{}^2 - (D_p + 2.2t + 2R_d)^2\} \quad \textbf{(2.5)}$$

F_h is holding force in N; Y is yield strength of the sheet metal in MPa; t is starting sheet thickness in mm and R_d is corner radius in mm. (Groover, 2012)

2.2.4 Formability in Deep Drawing

There are some tests to estimate the formability of sheet metals. The main two groups of tests are experimental and numerical analysis. For experimental analysis, mechanical tests such as tensile or Nakajima tests are carried out. (Tekkaya et al., 2000) The numerical analysis investigates the formability through simulation software.

Anisotropy

Anisotropy is a parameter to evaluate the formability of sheet materials. The reason that materials show anisotropic characteristics is crystallographic structure, which is produced by elements such as grain boundaries or phases. (Lange & Pöhlandt, 1985)

The uniaxial tensile test is executed to obtain the r value. The anisotropy coefficient, r is the ratio of width strain to thickness strain.

$$r = \frac{\varepsilon_w}{\varepsilon_t} \quad \textbf{(2.6)}$$

The anisotropy coefficient changes with longitudinal strain during the tensile test. Therefore a particular strain value e.g. in ε = 15% is can be taken in measurements.

Isotropic materials have an r value of 1. If the anisotropy coefficient is higher than 1, the material mainly flows in the width direction and possesses a high resistance to plastic flow in the direction of the sheet thickness. Otherwise, the sheet material tends to flow in the thickness direction. Most of the sheet metals show different properties with rolling (0^0), diagonal (45^0) and transverse (90^0) directions of the coil (see **Figure 2.8**).

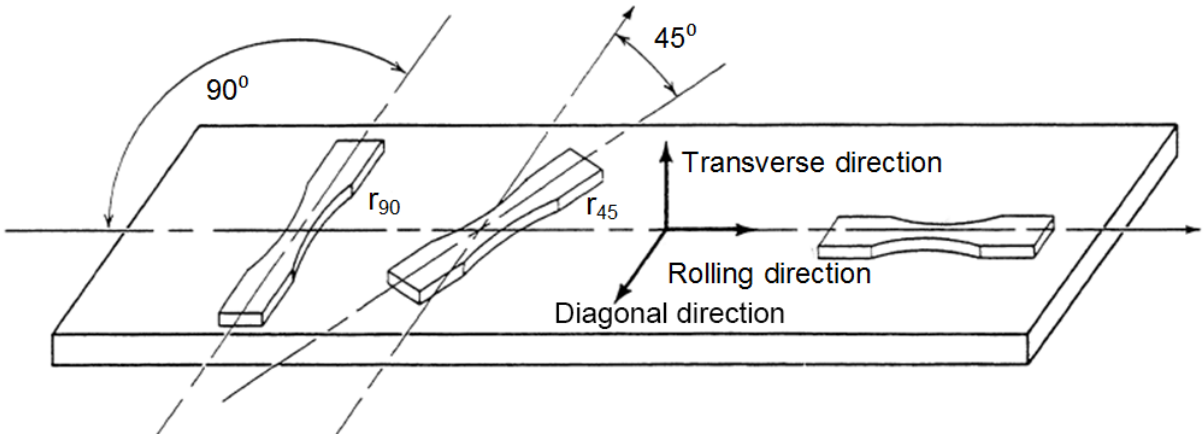

Figure 2.8: Tensile test specimen directions

The average anisotropy is calculated through the sum of the anisotropy coefficient in rolling (r_{0^0}), 2 times diagonal (r_{45^0}) and transverse (r_{90^0}) divided by 4.

$$\bar{r} = \frac{r_{0} + 2r_{45} + r_{90}}{4} \quad \textbf{(2.7)}$$

If the material has a low average anisotropy coefficient it thins more than a material with a high anisotropy coefficient. From this reason high anisotropy corresponds to good deep drawability, which means deeper drawn parts.

Another term to define the anisotropy is the planar anisotropy. The subtraction of two times r_{45^0} value from the sum of the r_{0^0} and r_{90^0} is divided by 4 indicates planar anisotropy.

$$\Delta r = \frac{r_{0} + r_{90} - 2r_{45}}{2} \quad \textbf{(2.8)}$$

The earing tendency increases as the planar anisotropy increases.

Forming Limit Diagram

The forming limit diagram (FLD) predicts the formability and the safety limit of a material in sheet metal forming processes. It includes failure limits for principal strain ratios/strain paths from equibiaxial tension/stretch forming, plane strain and uniaxial strain. It also covers the strain limit where necking begins for different principal strain ratios. The FLD can be obtained both theoretically and experimentally. Many researchers have developed different experimental methods with changing the shape and size of the specimens used in the tests such as limit dome height (LDH) test, Marciniak test or Nakajima test. The main advantage of the Nakajima test is that the

forming tool is very simple and it also allows the determination of the FLC on the whole usual domain of the strains. (Altan and Tekkaya, 2012)

Forming limit diagrams show the formability limits in the coordinate system of major (ε_1) and minor (ε_2) principal strains as shown in **Figure 2.9**. The formability limit is usually characterized by the failure (rupture) and this is called formability or fracture limit curve. (Tisza and Kovács, 2012) The forming limit diagram with these limit curves and zones is illustrated in **Figure 2.9**. Below the local necking zone, the green zone indicates the safe region of normal forming conditions in terms of major (ε_1) and minor (ε_2) principal strains. Above the FLC, the red zone shows the zone of rupture.

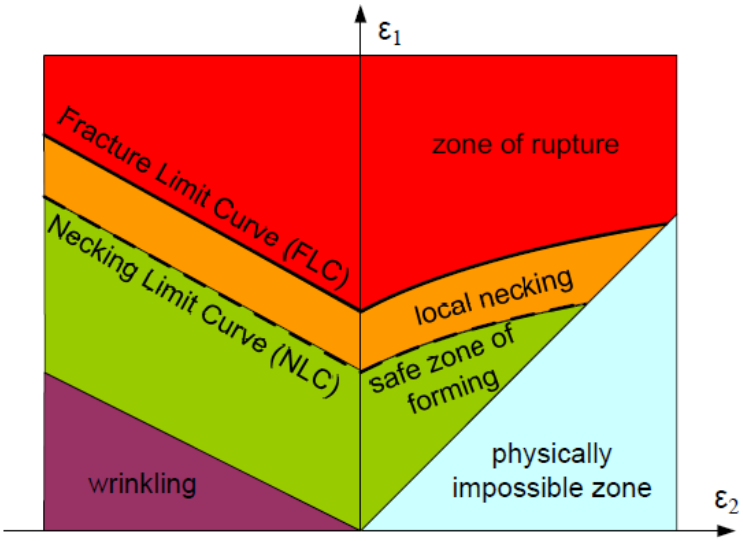

Figure 2.9: Characteristic limit curves and zones of forming limit diagram (Tisza and Kovács, 2012)

2.2.5 Deep Drawing Operations

There are other variations of basic deep drawing of a cylindrical shape which is operated by blankholder in a single step.

Redrawing

If the drawing ratio for a required shape is too high, then the drawing should be completed in more than one step. The further drawing steps are referred as redrawing. For the initial drawing step, the maximum reduction of starting blank should be 40% to 45%, for the second drawing which is the first redrawing process it should be 30% and for the further steps, the reduction should be 16%. (Groover, 2012)

Reverse Drawing

When the drawn part is placed upside down on the die to achieve a second drawing operation, it is called reversed drawing. The reverse redrawing is an easier process when compared to drawing. The reason is that the sheet metal is bent in the same direction in the outside and inside corners of the die in reverse drawing and it causes less strain hardening and drawing force. (Groover, 2012)

Ironing

The flange of the deep drawn part is compressed by squeezing of the blank perimeter which pursues a smaller circumference. Due to compression the sheet metal close to the outer edge of blank becomes thicker while moving forward. If the thickness of the stock is bigger than the drawing clearance, it will be ironed and squeezed to the clearance size. (Groover, 2012)

Various Other Drawing Operations: Shallow or tolerable depths may be used to create some specific types of parts. A part of them contains drawing, stretching or mixing of those operations. With male or female dies, parts may be embossed, which means the process of the shallow draws made on a sheet with matching male and female dies. This method is used mostly for decorative purposes. (Kalpakjian & Schmid, 2007)

At some processes the part can be drawn without a blankholder. If the thickness of the sheet metal is enough to avoid wrinkling, the deep drawing process may be applied without a blankholder. In that case, the dies should be specifically modeled. (Kalpakjian & Schmid, 2007)

Drawbead: It is often necessary to use drawbeads during deep drawing in order to control the material flow. During the process, drawbeads limit the flow of the sheet metal by bending and unbending. The beaded sheet has a higher precision and less prone to wrinkle, which reduces the amount of blackholder forces required.

2.2.6 Defects in Deep Drawing

Deep drawing operation is more complex than other sheet metal operations, which can cause some defects in the drawn parts which can be seen below in **Figure 2.10**.

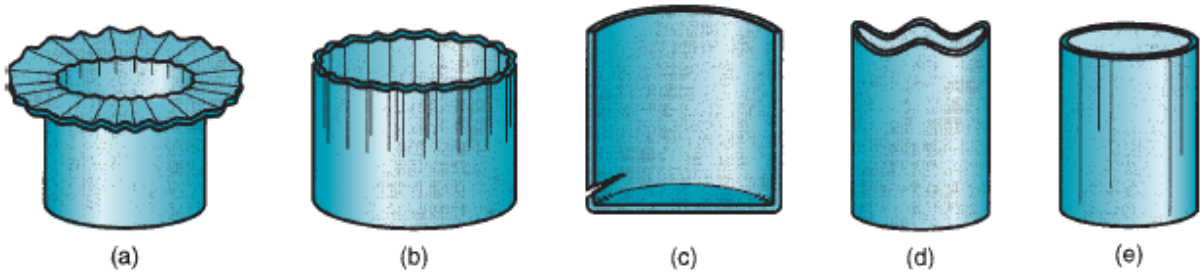

Figure 2.10: Common defects of drawn parts: **(a)** flange wrinkling, **(b)** wall wrinkling, **(c)** tearing, **(d)** earing, and **(d)** surface scratches (Groover, 2012)

Wrinkling in the flange

They are radially formed ridges in the not drawn part of the sheet metal because of the compressive stresses.

Wrinkling in the wall

When the wrinkled flange is drawn, the ridges occur in the vertical wall of the part.

Tearing

It is an open crack which is located in the vertical wall mostly close to the bottom of the drawn part. The reason for tearing is high tensile stresses which lead to thinning. Another reason can be drawing the part from a sharp die corner.

Earing

Anisotropy causes formation of irregularities such as earing, in the upper edge of drawn sheet metal. Isotropic materials do not have this defect.

Surface scratches

If the lubrication is not sufficient or the die and punch are not smooth, in surface some scratches can be observed on the surface. (Groover, 2012)

2.3 Aluminium and Aluminium Alloys

Sheet metal forming processes, especially deep drawing process is strongly dependent on the materials used. After iron, aluminium is now the second most widely used metal in the world. Aluminium and aluminium alloys have a relatively low density (2.7 g/cm^3), superior malleability, good thermal and electrical conductivity, and excellent corrosion resistance in some common environments. Because of the high ductility, most of them are easily formed. Its ductility is preserved at low temperatures as well. (Callister, 2007)

2.3.1 Comparison of Aluminium and Steel

Steel and aluminium are extensively used materials with a large range of applications. Steel is an alloy, and on the other hand aluminium is an element. However, aluminium is usually mixed with other elements and become an alloy to prevent chemical reactions. Some properties of both materials can be found in **Table 2.1.**

Table 2.1: Comparison of physical and mechanical properties of aluminium and steel

	Aluminium	**Steel**
Density	2.7 g/cm^3	7.8 g/cm^3
Young modulus	7x10^4 MPa	2.1x10^5 MPa
Poisson ratio	0.33	0.3
Melting point	660 °C	1425-1540 °C
Thermal expansion	23.1 μm/m·K	12 μm/m·K
Thermal conductivity	237 W/m·K	36.3 W/m·K

The relatively low density of aluminium is an important reason to prefer aluminium rather than steel in automotive industry. The density of steel is three times more than the density of aluminium, however to achieve the same performance a larger thickness should be used, which limits the weight reduction to half. (EAA, 2013)

The Young's modulus of aluminium is almost one third of that of steel. This causes larger springback effects and problems at the elastic recovery of aluminium sheets. Furthermore, aluminium and steel materials have different strain hardening coefficients, which means different stress–strain behavior in work hardening.

Another difference between steel and aluminium is that the normal anisotropy value of steel is larger than 1, whereas aluminium has a $\bar{r}$-value smaller than 1. This has an effect on the shape variations of steel and aluminium sheets after forming processes. Apart from that, the thickness variations of these materials for the same deep drawing operations may be different. Normal anisotropy ($\bar{r}$-value) influences the maximum drawability of the sheet, whereas planar anisotropy (Δr) leads to earing. (Öztürk et al., 2010) Sheet metals with having greater $\bar{r}$-values are more suitable for deep drawing as the thinning should be smaller and thus the formability is better. A high $\bar{r}$-value allows

deeper drawn products. In shallow parts a high value may reduce the chance of wrinkling or ripples in the part. (Marciniak et al., 2002) If the value of the planar anisotropy value is large, the orientation of the sheet with respect to the die or the part to be shaped will be important. In such cases, earing problem can occur.

Another advantage of aluminium is its high corrosion resistance. It derives from aluminium's high activity, which leads it to react simply with oxygen. When aluminium reacts with oxygen and aluminium oxygen is produced, a slab is created over the aluminium surface, which is prevented from reacting further. Opposite to the aluminium, steel shows a weaker resistance to corrosion, because its reaction with oxygen causes rust which separates from the surface and leaves it unprotected against more reactions.

Owing to different grain structures, the final surface qualities of aluminium and steel sheets are different. Especially, the formation of large grains in aluminium due to large deformations causes aesthetic problems on sheets surface.

2.3.2 Aluminium and Aluminium Alloys in Automotive Industry

The decision to choose the right material in the automotive industry is governed by several factors. The increasing need for higher fuel economy caused by concerns about global warming and energy usage has an important influence on the choice of materials. The manufacturers are trying to improve conventional engine efficiency and reduce the weight of the vehicle. European Aluminium Association (EAA) evaluates that 10% of vehicle weight reduction improves 8–10% of fuel economy. Use of lightweight materials can help reduce vehicle weight and improve fuel economy. It leads to a decreased use of steel and iron. In automotive industry, aluminium is considered better than steel because it gives a higher strength/weight ratio. Increasing use of aluminium in vehicles starting from 1990 can be seen in **Figure 2.11**.

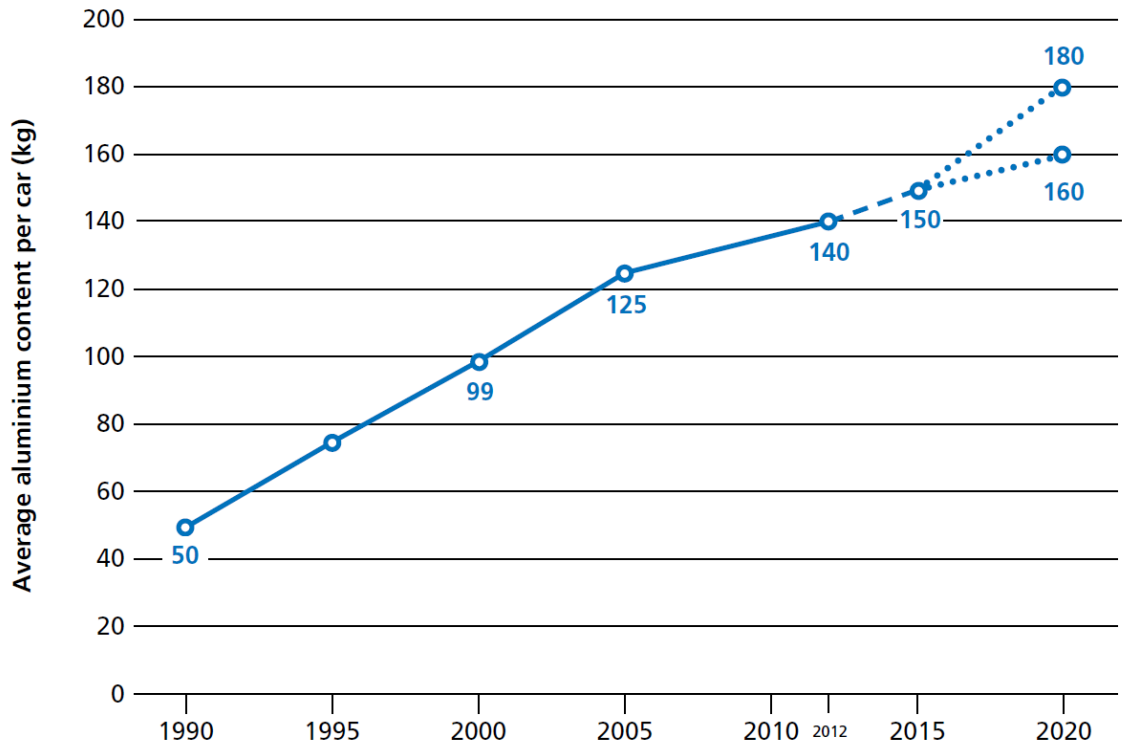

Figure 2.11: Average aluminium content per car by years (EAA)

Aluminium usage in automotive industry has grown more than 50% in the final 10 years. According to EAA a total of about 140 kg of aluminium in a vehicle in 2012 is predicted to rise to around 160-180 kg by 2020. Future use areas for aluminium applications are trunk lids, hoods and doors hanging on a steel frame.

The biggest difference between aluminium and steel is its excellent bare metal corrosion. Most of the steels are supplied zinc coated to have acceptable paint durability, which is not necessary for aluminium. Strength of aluminium as structural sheet materials may be a limiting factor in some specific areas such as impact energy absorption and good deep drawing. Wide range of aluminium materials with different surface qualities can be chosen with the help of design and process experience to satisfy customers' request. The choice of the aluminium alloys differs from region to region as well. It is shown in **Table 2.2**.

Table 2.2: Alloy choice for automotive panels: Europe vs. North America (Miller et al., 2000)

	Europe	**North America**
Alloys	6xxx-T4	5754-O
Surface texture	EDT	MF
Pre-treatment	Zr/Ti conversion	conversion
Lubrication	oil or dry-lubricant	oil

In the future it is expected that new alternative materials will gain importance. Aluminium is one of them and threats sheet steel even though it cannot be the main material of a car in the next decade. The drawback of aluminiums is the high material and manufacturing costs, recycling and regulations. (Miller et al., 2000)

2.3.3 Aluminium Alloys AA5754-H22 and AA6061-T6

The mechanical strength of aluminium can be improved by alloying, but it reduces resistance to corrosion. Main alloying elements are copper, magnesium, silicon, manganese and zinc. Aluminium alloys can be classified as cast or wrought. **Figure 2.12** describes the classification of wrought aluminium alloys according to the International Alloy Designation System (IADS). (Callister, 2007)

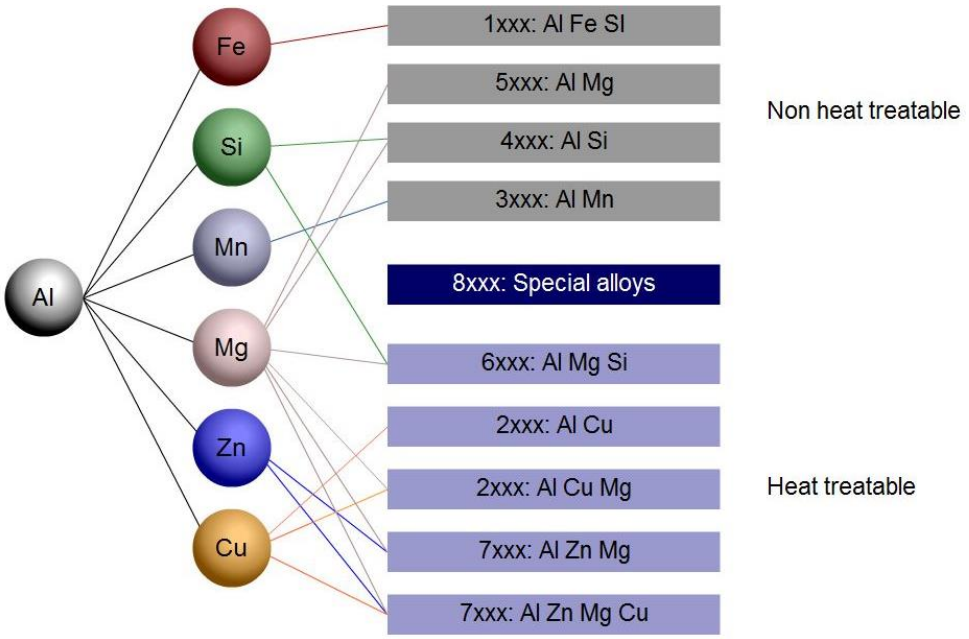

Figure 2.12: Classification of wrought aluminium alloys (Alumatter)

There are 8 types of wrought alloys. These are designated by a 4 digit number which are followed by letters. A prefix is used to show the standard AA of the Aluminium Association. The first digit indicates the series. The second digit indicates alloy modifications of an existing alloy. The third and fourth digits have different meanings, depending on the first one. For series from 2xxx to 8xxx, the two digits identify a specific alloy without physical significance. They only show to vary between various alloys. (Alumatter)

AlMg-alloys (5xxx) are recommended for high formability, adequate strength and excellent corrosion resistance. AlMgSi-alloys (6xxx) are recommended for good formability, mechanical properties after painting process and corrosion resistance, in combination with a very good surface finish. (Alumatter) In scope of the master thesis these both aluminium alloy series will be compared.

The mechanical properties of the same alloy can change depending on the thermo-mechanical processing of the alloy during or after production. There are two categories of alloys which can be seen in **Figure 2.12**: Heat treatable and non-heat treatable alloys. Heat treatable alloys can be precipitation or age hardened. They have many possibilities for tempering to achieve different mechanical properties. In heat treatable alloys, mechanical properties are achieved through hot and/or cold working mechanisms during or after production work hardening operations like strain hardening, with annealing. (Alumatter)

The type of strengthening is shown with the temper designation T or H, meaning heat treated or strain hardened, respectively. Others indicate whether the alloy is annealed (O), solution treated (W), or used as it is as-fabricated condition (F). The numbers which stand after the T or H show the amount of strain hardening, the heat treatment type, or other special aspects of the processing of the alloy. (Callister, 2007)
The metals which are used during the experiments are AA5754-H22 and AA6061-T6. Their thickness is 2.5 mm. At AA5754-H22, the temper designation H22 shows that it is work hardened by rolling then annealed to quarter hard. At 6061-T6, the temper designation T6 shows that the solution heat treated and artificially aged.

In **Table 2.3**, **2.4** and **2.5** composition and properties of both alloys used during the experiments and deep drawing are shown. (Aalco)

Table 2.3: Chemical composition of AA5754-H22 and AA6061-T6 in percentage (%) (Aalco)

AA	Mn	Fe	Mg	Si	Cu	Zn	Ti	Cr
5754-H22	0.5 max	0.4 max	2.6-3.2	0.4 max	-	-	-	-
6061-T6	0.15 max	0.7 max	0.8-1.2	0.4-0.8	0.15-0.40	0.25 max	0.15 max	0.04-0.35

Table 2.4: Physical properties of AA5754-H22 and AA6061-T6 (Aalco)

AA	Density	Melting point	Thermal expansion	Thermal conductivity	Electrical resistivity
5754-H22	2.66 g/cm³	600 °C	$24x10^{-6}$/K	147 W/m.K	$4.9x10^{-8}$ Ω.m
6061-T6	2.70 g/cm³	650 °C	$23x10^{-6}$/K	166 W/m.K	$4.0x10^{-8}$ Ω.m

Table 2.5: Mechanical properties of AA5754-H22 and AA6061-T6 (Aalco)

AA	Proof stress (MPa)	Shear strength (MPa)	Tensile strength (MPa)	Elongation (A 50 mm)
5754-H22	185-245	245-290	260	10-15%
6061-T6	270	190	310	12%

3 Aim and Scope of the Thesis Work

The company Mercedes-Benz Türk A.Ş. is currently producing coaches for distant journeys and busses for schools and municipalities in collaboration with EvoBus which belongs to Daimler AG. There are two emergency valves on the flap panels in all busses except municipality type. These valves are crucial for the vehicle as they allow people to open different type of side panels manually in an emergency case. The emergency valves are mounted into the hollow parts of flap panels. These hollow parts are produced with deep drawing process. One of them is on fuel filler flap panel which all busses have. For the time being, this hollow part is supplied by an external company and then adhered to the flap panel. After that the emergency valve is mounted to hollow part of the flap panel.

To reduce the cost of bus production, a project is started to produce these hollows by deep drawing process with the hydraulic press which is already available in Mercedes-Benz Türk A.Ş. Another major reason for trying to make an in-house production is to lower the dependence to an external supplier. If there would be a production problem in the supplier, a bottleneck can occur in Mercedes-Benz Türk A.Ş. The geometry of this hollow part is already known. For the production of this part, a die is produced by an external company. The main interest of this project is to choose the most suitable material for the production of this part and find out which process parameters lead to the deep drawing without any failure and desired quality.

An expected problem of the deep drawing of emergency valve cup is the wrinkling of the sheet metal in the edges of the flap panel preventing a straight line in the panel. Because of aesthetic concerns, emergency valve cup is located close to the edge of the flap panel. However, there is also need for space for other cables behind the cup. The position of the emergency valve cup must be optimized.

In scope of the master thesis, the materials 2.5 mm thick aluminium alloys AA5754-H22 and AA6061-T6 are examined. EvoBus and Mercedes-Benz Türk A.Ş. are already using these 2 alloys for their flap panels. Due to this reason it is suggested to investigate AA5754-H22 and AA6061-T6.

First, materials are characterized with a tensile test. The reason of not using the given values from literature is that the specifications of an aluminium alloy can vary from supplier to supplier. Even though Mercedes-Benz Türk A.Ş. purchases its aluminium alloys from the same company, the chemical composition and mechanical properties can change over time. It cannot be known how long the aluminium alloys are kept before delivery which may cause aging of aluminium. Next step is conducting Nakajima test in order to obtain formability of materials. With the help of this information deep drawing will be carried out with different blankholder forces and varying distance of the emergency valve cup to the edges of the flap panel to find the best location without any quality issues.

4 Experiments for Material Characterization

For the characterization of Aluminium Alloys 5754-H22 and 6061-T6, the tensile tests and Nakajima tests are conducted.

4.1 Tensile Test

The purpose of tensile test is to obtain data, which is used in selecting materials for engineering applications. Uniaxial tensile test is a universal test which is conducted to obtain material parameters such as ultimate strength, yield strength, % elongation, % area reduction and Young's modulus. These properties are also used to predict the material behaviour. (Davis, 2004)

4.1.1 Specimen Preparation

The tensile test specimens are prepared according to DIN ISO 6892-1 standard. This standard is for tensile testing of metallic materials in room temperature. The specimen is illustrated in **Figure 4.1**.

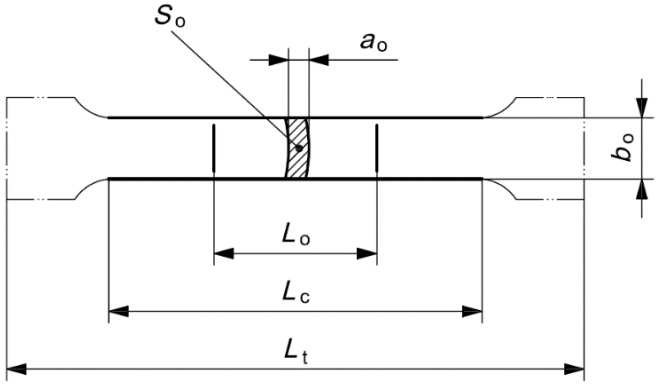

Figure 4.1: Tensile test specimen

Table 4.1: Tensile test specimen dimension

Symbol	**Explanation**	**Dimension** (mm)
a_o	original thickness of a flat test piece	2.5
b_o	original width of the parallel length of a flat test piece	20
L_c	parallel length	120
L_o	original gauge length	80
L_t	total length of test piece	280
S_o	original cross sectional area of the parallel length	-

To prepare the tensile test specimens, first the number of specimens must be determined. For the sake of accuracy, each test is repeated 5 times with each specimen set. To obverse the anisotropy of the materials 3 different types of specimens are needed, namely 0, 45 and 90 degrees according to rolling direction of sheet metal.

Tensile test specimens are prepared according to DIN ISO 6892-1 standard. The sheet metal aluminium alloys are first cut with hydraulic shearing machine Ras and then pressed in eccentric press Dirinler to the shape of a tensile test specimen. The final step of preparing specimen is to rasp the edges manually to smooth the edges and remove burrs.

5 specimens are prepared for AA6061-T6 0° as shown in **Figure 4.2**. Each specimen is labeled with material type, degree and number of specimen.

Figure 4.2: Set of tensile test specimens (AA6061-T6, 0°)

4.1.2 Experimental Setup

The tensile tests are held in the laboratory of the Zwick Avrasya Ltd. which works with the material testing department of Mercedes-Benz Türk A.Ş. The experiment is conducted according to DIN ISO 6892-1 standard, method A which donates that the speed of the cross head changes when the materials begins to yield. Zwick Roell Z250 machine is used with testXpert II 3.5 software. The tensile test setup is shown in **Figure 4.3**.

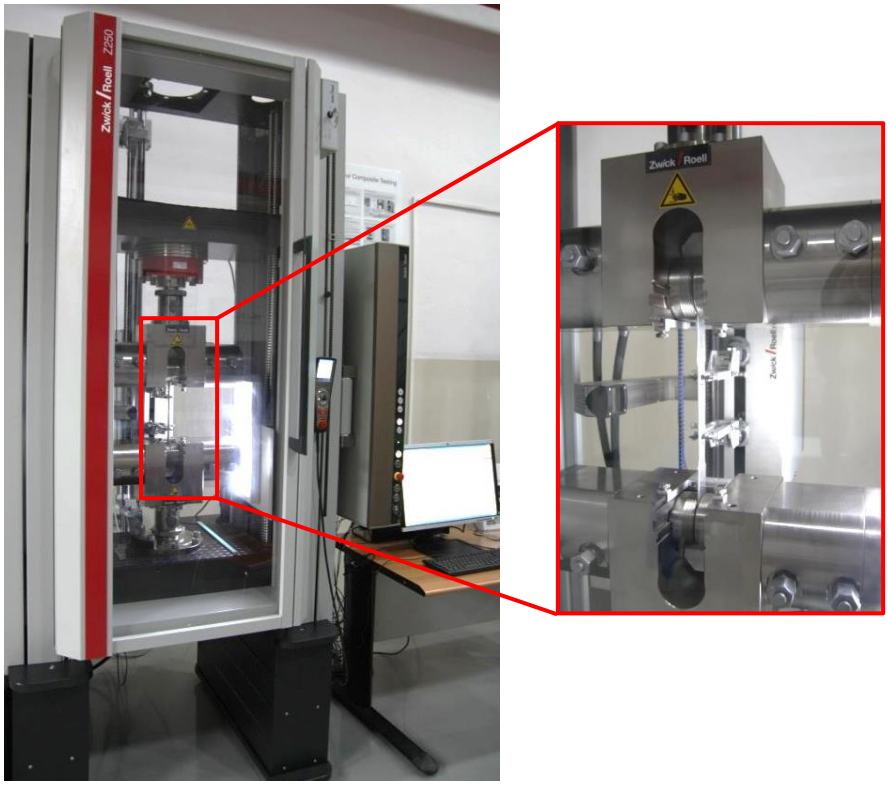

Figure 4.3: Zwick Roell Z250 tensile test machine and the specimen gripped to jaws

There are in total 30 specimens, half of them are AA5754-H22 and the other half is AA6061-T6. Each batch has 0, 45 and 90 degrees specimens. Each degree has 5 specimens so that the average can be taken to reduce the possible errors and have a more reliable result. All specimens are cleaned to remove any dust and dirt on the surface. After that the exact dimensions of the specimen is measured as length, thickness and depth.

In the beginning the machine is set to zero so that residual stresses are removed. The machine is then connected to the computer and force, change in length and width is recorded until the specimen is fractured. A fractured specimen is shown in **Figure 4.4**.

Figure 4.4: AA5754-H22 45° tensile test specimen: **a)** before the tensile test **b)** after the tensile test

4.1.3 Results

In tensile test, the force is obtained as a function of the elongation of the gauge length. There are two types of stress-strain curves: engineering and true. Both curves overlap in elastic region. In plastic region the true stress-strain curve is above of the engineering stress-strain curve. True stress-strain curve gives a more direct measure of the material's response in the plastic flow range. From this reason below, true stress-strain curve is drawn in **Figure 4.5**.

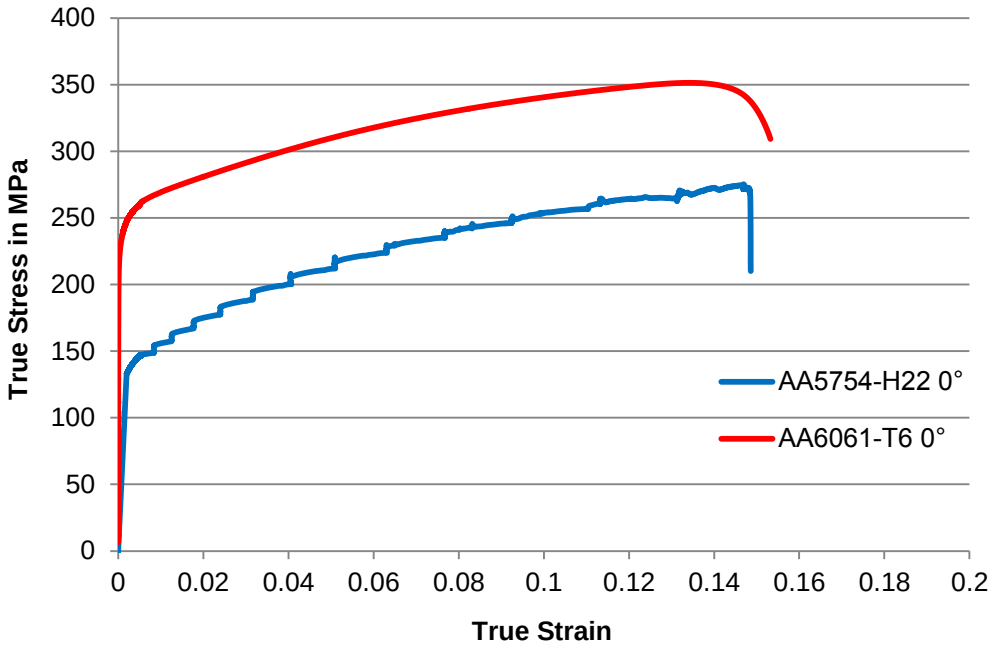

Figure 4.5: True stress-strain diagram for AA5754-H22 and AA6061-T6

The stress-strain curve of AA5754-H22 is serrated when it undergoes plastic deformation. This deformation in room temperature is discontinuous because of a phenomenon which is called as Portevin–Le Chatelier (PLC) effect. It is marked by the formation of deformation bands that not only just leave unwanted traces on the surface of the product, but also reduces the ductility of the aluminium alloy. The strength of aluminium alloys are increased their strength by alloying elements, such as magnesium, in solid solution. (Herdawandi et al., 2007)

Elastic modulus is the description of a material's tendency to be deformed elastically when a force is applied to it. On stress-strain diagram, elastic modulus can be calculated as stress divided by strain according to Hooke's law.

The values of *E*, the elastic modulus, $R_{P0.2}$, yield stress and R_m, the ultimate tensile strength are calculated directly with the testXpert II 3.5 software on computer which is installed on the Zwick tensile test machine. Yield stress is where the necking starts and the ultimate tensile strength is the maximum stress in true stress-strain curve.

Table 4.2: Elastic modulus and yield stress and ultimate tensile strength of each specimen configuration

AA	***E*** (GPa)			$\boldsymbol{R_{P0.2}}$ (MPa)			$\boldsymbol{R_m}$ (MPa)		
	0°	45°	90°	0°	45°	90°	0°	45°	90°
5754-H22	66.25	66.5	67.25	131	125.5	123.75	255.5	249	249.5
6061-T6	67.75	66.75	67.25	263.25	256.5	258.75	353	347	350.5

The anisotropy plays a very important role during forming processes. Due to anisotropy sheet shows different properties in different directions such as rolling direction, transverse and 45° of the coil. It is indicated by the r value which is the ratio of width strain to thickness strain.

For example for AA6061-T6 90 degrees, anisotropy coefficient in strain point is considered as 10%, hence;

$$\varepsilon_l = \ln\frac{l}{l_0} = \frac{88\text{ mm}}{80\text{ mm}} = 0.0953 \quad \textbf{(4.1)}$$

$$\varepsilon_w = \ln\frac{w}{w_0} = \frac{19.19\text{ mm}}{19.84\text{ mm}} = -0.0334 \quad \textbf{(4.2)}$$

To calculate the r value, volume constancy must be used.

$$\varepsilon_w + \varepsilon_t + \varepsilon_l = 0 \quad \textbf{(4.3)}$$

To find the *r* value;

$$r = \frac{\varepsilon_w}{-(\varepsilon_l + \varepsilon_w)} = 0.53 \quad \textbf{(4.4)}$$

Apart from anisotropy coefficients, the average and planar anisotropy is calculated as well, see **Table 4.3**.

Table 4.3: The *r* value, average and planar anisotropy values of each specimen configuration

AA	*r*			$\bar{r}$	Δr
	0°	45°	90°		
5754-H22	0.62	0.72	0.65	0.68	-0.09
6061-T6	0.47	0.66	0.53	0.58	-0.16

The *r* value is maximum for aluminium alloys in the direction of 45º with respect to the rolling direction. Aluminium alloys from 5 and 6 series exhibit smaller *r* values when compared to stainless steels. In such conditions, sheet metal is very prone to thinning. (Aleksandrović et al., 2009)

A high anisotropy value corresponds to good drawability. At high *r* values, the sheets exhibit significant resistance to thinning when being drawn into a part such as a cup. The difference in planar anisotropy is related to the earing tendency of the sheet metal, which increases as the planar anisotropy increases. (Öztürk et al., 2010)

The rate of work-hardening is always measured from true stress and true strain data. True stress-strain curves will fit a simple power law expression, known as the Ludwik equation:

$$\sigma = \sigma_0 + K \cdot \varepsilon^n$$

(4.5)

In the equation, σ_0 is yield stress, *n* is the strain-hardening exponent and *K* is the strength coefficient.

Table 4.4: Strain-hardening exponent and strength coefficient values of each specimen configuration

AA	*n*			*K* (MPa)		
	0°	45°	90°	0°	45°	90°
5754-H22	0.238	0.236	0.238	431.4	413.2	417
6061-T6	0.147	0.145	0.145	464.2	452.5	457.6

The strain-hardening exponent which is the slope of the flow curve in the plastic area determines how much the metal can stretch before necking. Materials with have higher

n values have better formability than those with low *n* values. Moreover, higher *n* values mean greater difference between yield and ultimate tensile strengths.

The flow curve can be determined by plotting the flow stress variation of aluminium alloy specimens with the average equivalent stress. The graph begins with the yield stress where material begins to flow. Below **Figure 4.6** and **4.7** shows the flow curves of AA5754-H22 and AA6061-T6 respectively.

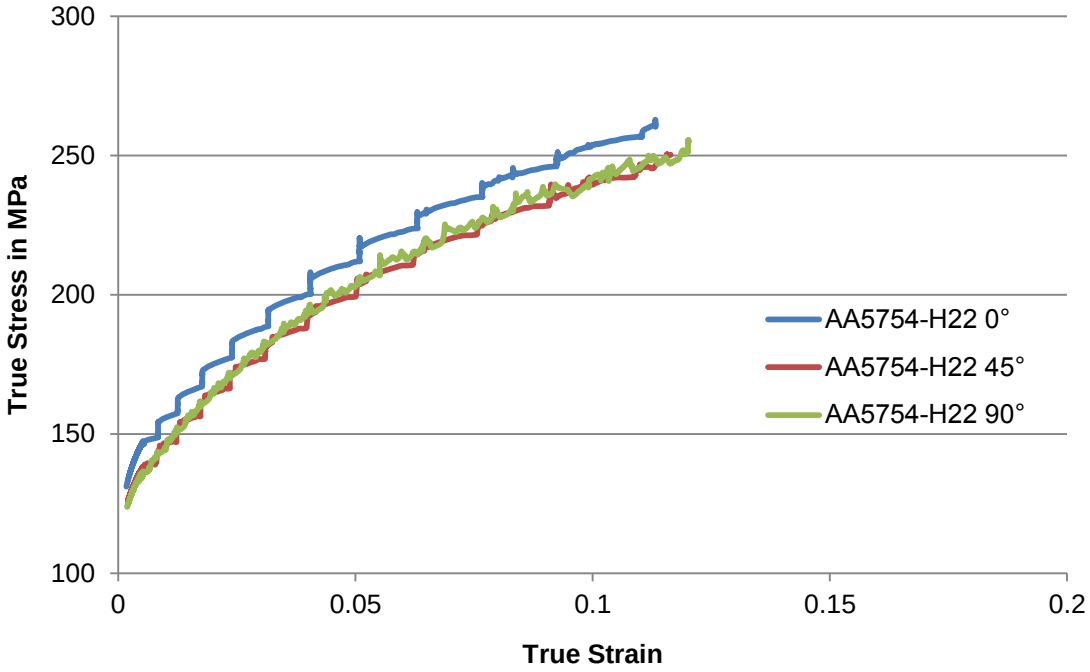

Figure 4.6: Flow curve of AA5754-H22

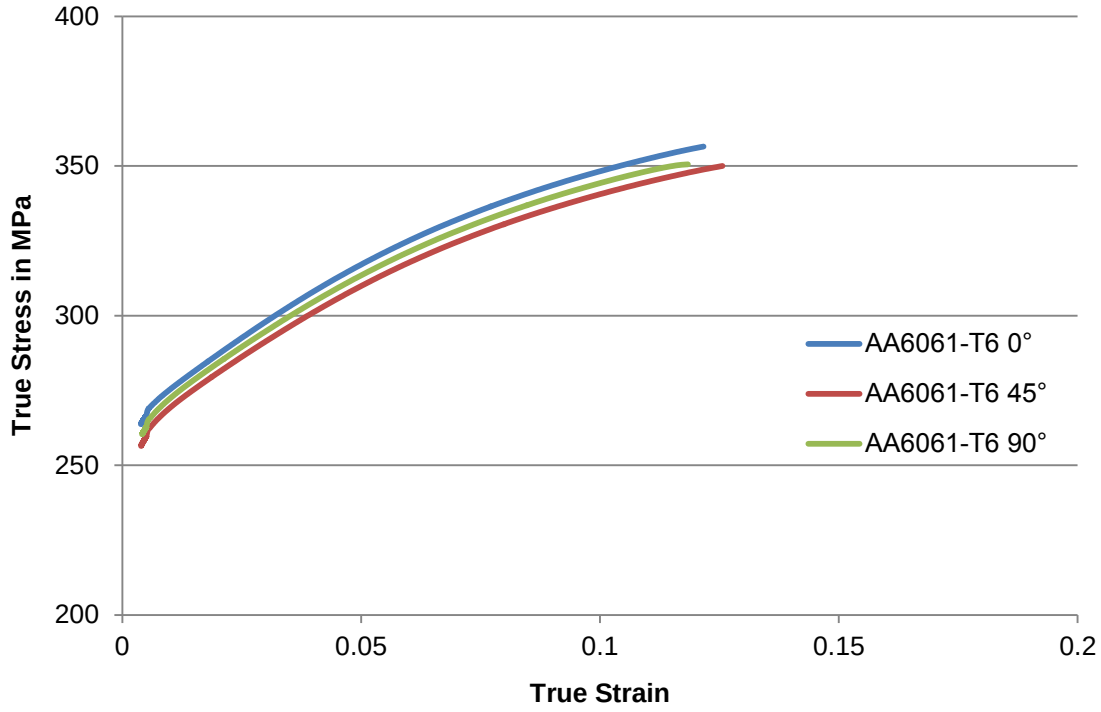

Figure 4.7: Flow curve of AA6061-T6

The values of *n*, the strain-hardening exponent and *K*, the strength coefficient are calculated directly with the testXpert II 3.5 software. Yield stress σ_0 was already calculated which shows the stress at the time at which material starts to deform plastically. Only 0 degrees of the aluminium alloys are calculated as the sheets are deep drawn in the rolling direction. The functions for aluminium alloys and their flow charts are given below. They are extrapolated according to Ludwik equation:

AA5754-H22 0 degrees, $$k_f = 131 + 431.4\,\bar{\varphi}^{0.238} \quad \textbf{(4.6)}$$

AA6061-T6 0 degrees, $$k_f = 263.25 + 464.2\,\bar{\varphi}^{0.147} \quad \textbf{(4.7)}$$

In the equation, k_f is flow stress and $\bar{\varphi}$ is equivalent strain.

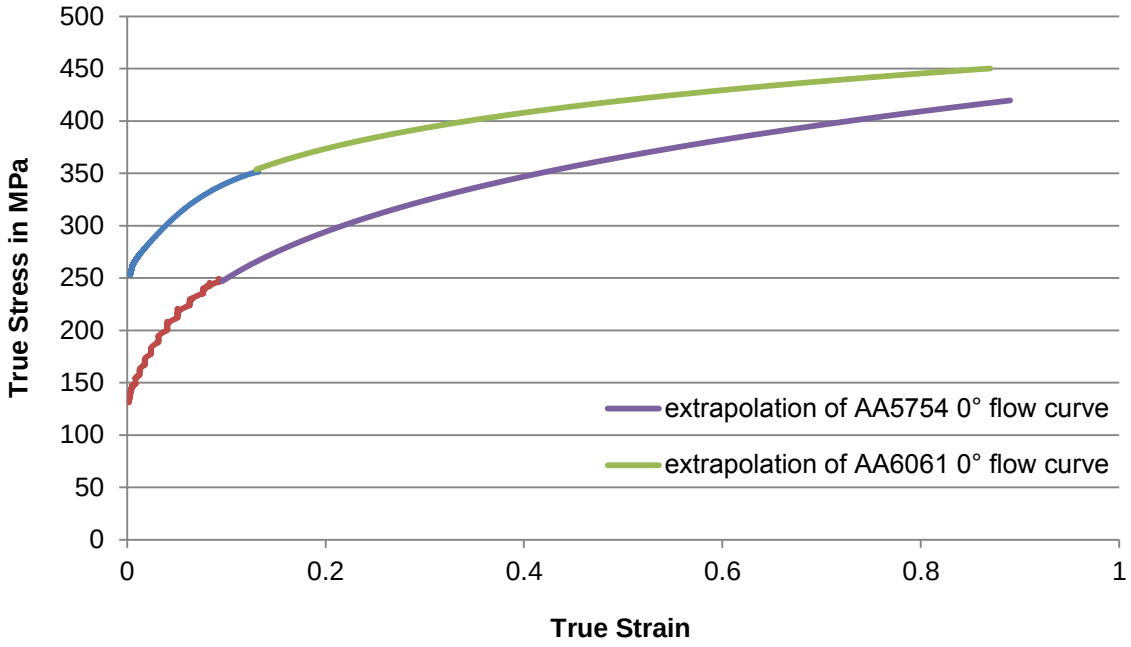

Figure 4.8: Extrapolated flow curves of AA5754-H22 and AA6061-T6

4.2 Nakajima Test

The Nakajima test is based on the principle of deforming sheet metal blanks of different geometries using a hemispherical punch until fracture occurs. The main advantage of the Nakajima test is that the forming tool is very simple and it also allows the determining of the Forming limit curve (FLC) on the cup usual domain of the strains. (Altan and Tekkaya, 2012) The FLC predicts formability and safety limit of material in sheet metal forming processes. It includes failure limits for principal strain ratios/strain paths from equibiaxial tension/stretch forming, plane strain and uniaxial strain (Girjob et al., 2010). In Nakajima test specimens with different widths are formed with a hemispherical punch and a circular female die until fracture occurs. (Nakajima et al., 1971) In this thesis Nakajima test is used to obtain FLDs for AA5754-H22 and AA6061-T6.

4.2.1 Specimen Preparation

The Nakajima test specimens are prepared according to DIN ISO 12004-2 standard. This standard is for Nakajima testing of metallic materials at room temperature. The shape and dimensions of specimen is illustrated respectively **Figure 4.9** and **Table 4.5**.

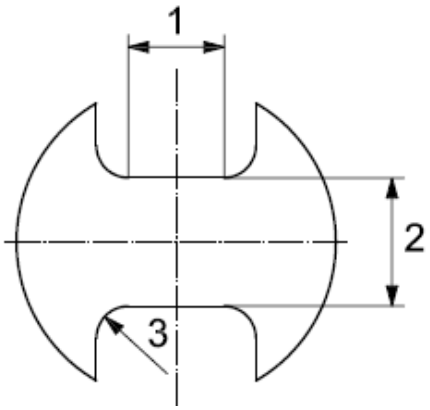

Figure 4.9: General Nakajima test specimen

Table 4.5: Nakajima test specimen dimensions

Symbol	**Explanation**	**Dimensions** (mm)
1	shaft length	60
2	remaining blank width	200, 130, 100, 70, 40, 20
3	fillet radius	25

6 various specimens are shown in the **Figure 4.10**.

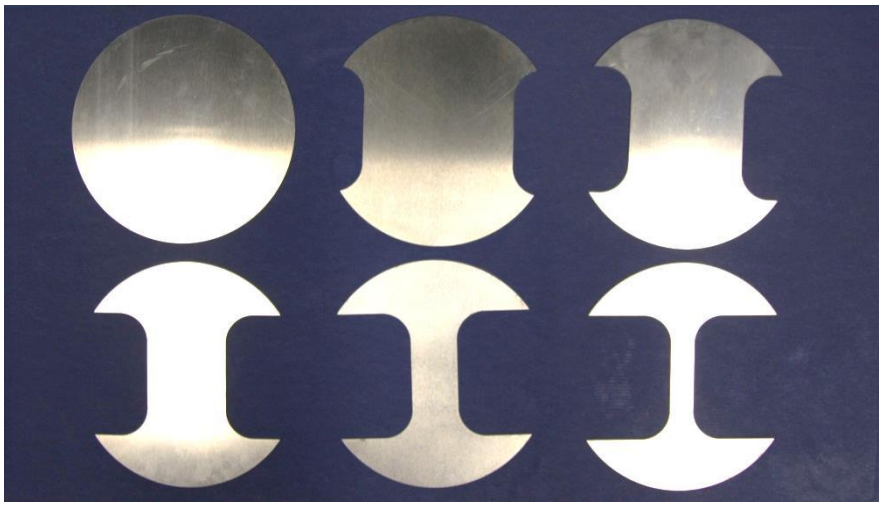

Figure 4.10: Nakajima test specimens

The drawing of specimen are generated with the Catia V5 CAD program and saved as dxf format. This file is transferred to Homag BMG 511 CNC machining center and the specimens are cut with longitudinal shaft parallel to rolling direction according to the standard for aluminium Nakajima specimens. The speed of the machine is set to low and a lubricant is also used to have a smooth cutting process.

After cutting process specimens are cleaned with ethanol to remove the oil on their surfaces. On one surface a matt white colour is sprayed and after drying, above this layer a black colour is sprayed. This generation of stochastic based white and black raster is needed for GOM Aramis software to detect and process the deformation of specimen during the experiment.

4.2.2 Experimental Setup

The Nakajima tests are carried out in the laboratory of the IUL in TU Dortmund. The experiment is conducted according to DIN ISO 12004-2 standard. Zwick Roell BUP1000 machine is used with GOM Aramis software in a computer next to the machine. The machine is shown in **Figure 4.11**. The CCD cameras of the GOM Aramis above the machine must be calibrated before the experiment begins. Calibration is important to make sharper photos of the specimen during deformation and especially just before necking. It can take upto 10 photos per second of the surface of the specimen during the experiment. Aramis software shows also major and minor strain change during the experiment which helps to draw the forming limit curve.

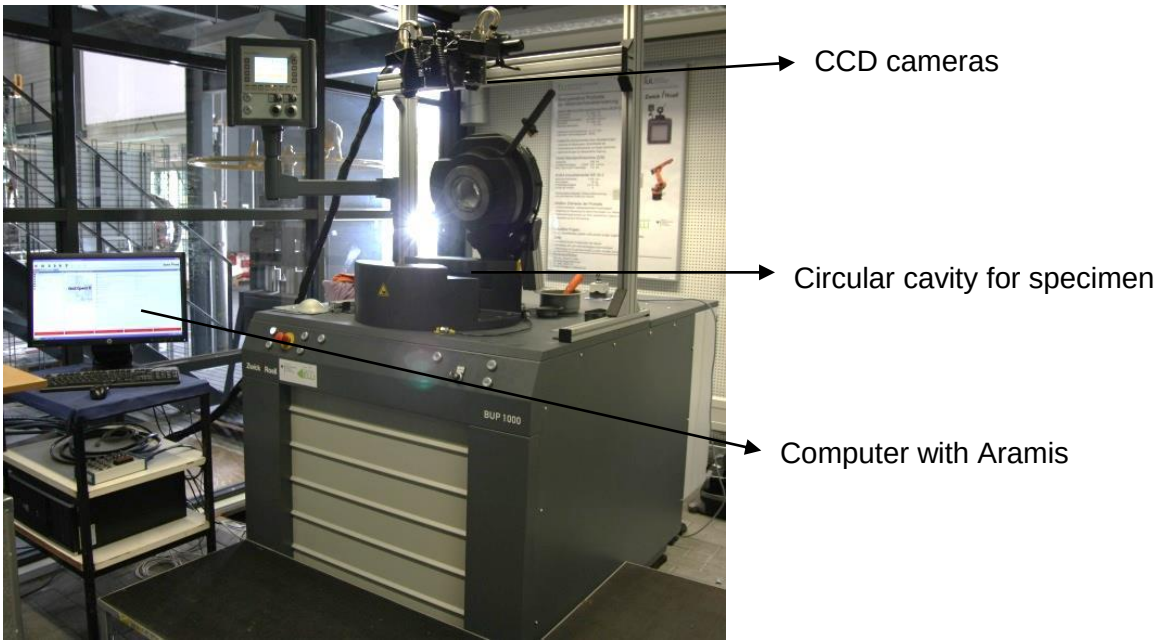

Figure 4.11: Zwick Roell BUP1000 machine

After calibration the process parameters are needed to be entered to the test machine before experiment starts. The values are chosen according to the DIN ISO 12004-2 for the Nakajima test. The tests are carried out at room temperature. The hemispherical

punch diameter of the machine is 120 mm and its speed is 1.5 mm/s. The blankholder force varies between 100-200 kN. A 1 mm thick PE foil is used as the lubrication which has creme at both sides to lower the friction. The PE foil is put above the punch and above them both, the specimen is clamped with locking beads to the testing machine. The specimen is deformed by the punch against the circular cavity until it fails. For the experiment, both machine and the Aramis software in computer are started simultaneously. The machine stops till there is a sudden drop of the force, which means a crack on the specimen surface. A specimen before and after the experiment is shown in the **Figure 4.12**. Aramis finishes recording values and taking photos as soon as the machine stops.

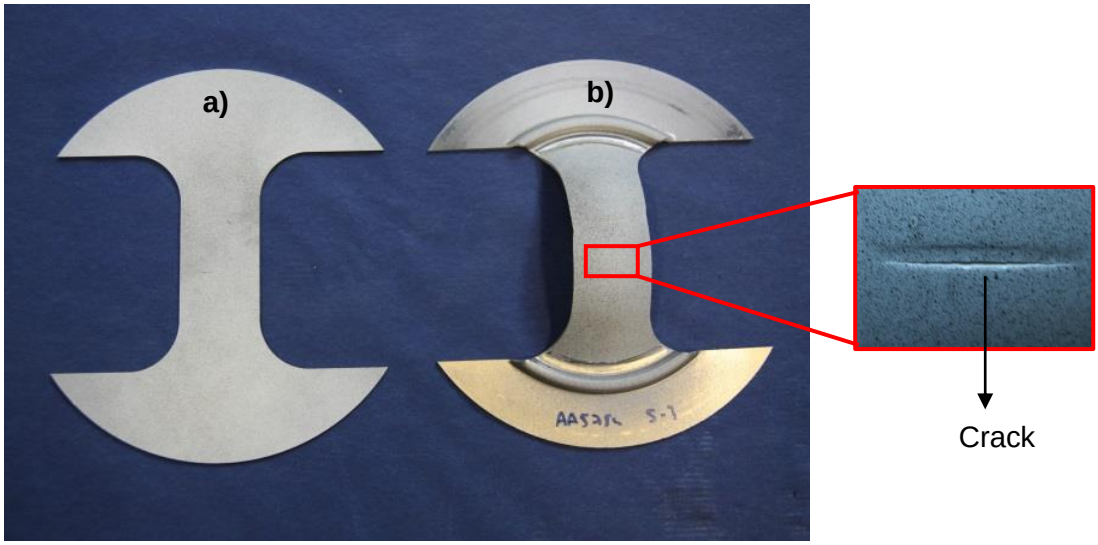

Figure 4.12: Nakajima test specimen: **a)** before the Nakajima test **b)** after the Nakajima test

There are in total 60 specimens, half of them are AA5754-H22 and the other half is AA6061-T6. Each different geometry configuration has 5 specimens in order to repeat the test. The tests are conducted until each configuration has 3 successful experimental results and after that the average is taken to reduce the possible errors and have a more reliable result. An experiment is successful where the crack occurs close to the middle of the specimen and is not apart from the middle by +/- 15mm. Some of the experiments are not successful because of the difficulties such as the punch curvature and lubrication. There is also the need for different blankholder forces for different geometries.

4.2.3 Results

The main objective of Nakajima test is to generate forming limit curves for different sheet metals. **Figure 4.13** shows the photos of the specimen before and after the fracture respectively.

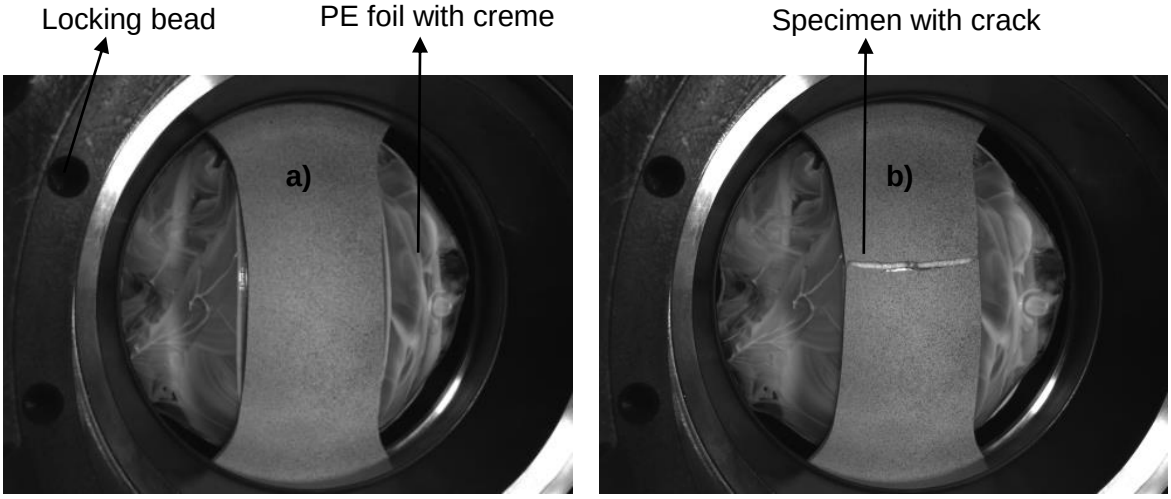

Figure 4.13: Photos of specimen which is attached to the BUP1000 machine: **a)** before the fracture **b)** after the fracture

The optical strains measurement system Aramis analyses the obtained results according to ISO 12004-2 standard. For the strains analysis, only the last stage before the fracture occurrence is chosen. Four parallel sections are selected with a distance of 2 mm between them, and as long as possible till the edge of the specimen. They all are perpendicular to the fracture. The maximum value of each line is chosen and then the average of 4 lines is taken. With this procedure the major and minor points of the forming limit curve is found out.

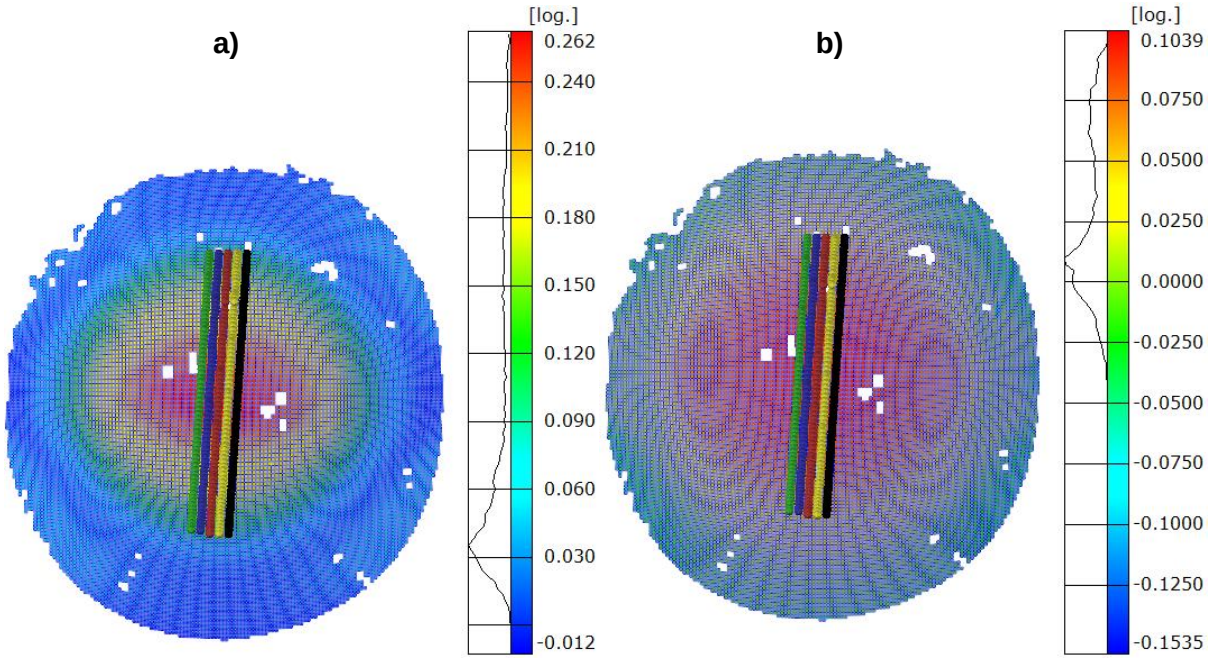

Figure 4.14: Strain distribution of AA6061-T6 before the fracture: **a)** major strain **b)** minor strain

Aramis gives the values for major and minor strains along the different sections. The position of pairs (major strain ε_1, minor strain ε_2) for each specimen geometry represents the forming limit curve which can be seen in **Figure 4.15**. A strain-length graph is drawn for different sections and a 2nd order polynomial curve is fitted for both major and minor strains. The left side of the forming limit diagram represents strain paths with strain ratios that vary from uniaxial tension (r = -0.5) to in-plane plain strain (r = 0). On the right side the strain ratios differ from in-plane plain strain to full biaxial (r = 1) stretching.

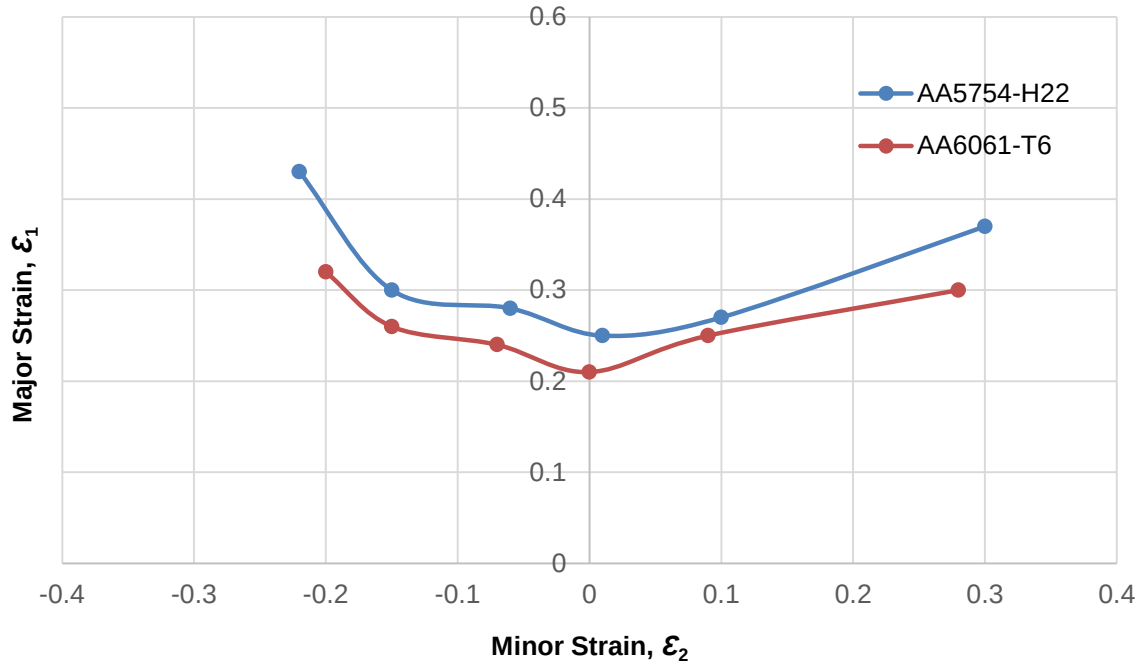

Figure 4.15: Forming limit curves of AA5754-H22 and AA6061-T6

As it can be seen from the forming limit diagram, the curve of AA5754-H22 is above the AA6061-T6 which means the formability of AA5754-H22 is higher than the AA6061-T6. The area above the curves means failure and below, it means safe to form the material. The point FLD_0 is located in the forming limit diagram where the forming limit curve crosses the ε_1-axis, and at ε_2=0. FLD_0 of AA5754-H22 and AA6061-T6 forming limit curves are 0.25 and 0.21, respectively.

5 Deep Drawing Experiment

In order to investigate the formability of both AA5754-H22 and AA6061-T6, they are drawn in the die cavity which is produced to mount the emergency valve of bus flap panel.

5.1 Experimental Setup

The deep drawing die is a square with the dimensions of 400x400 mm. Aluminium alloy sheets are cut in Ras hydraulic shearing machine with the same dimensions, so the initial blank dimension is 400x400x2.5 mm.

Before the experiment, the aluminium alloy specimens are prepared according to the experiment schedule. The number of specimens is chosen as 180, because of 60 different configurations and each of them is drawn three times. The varied process parameters are listed in the **Table 5.1** below. Other parameters such as die shoulder radius, punch nose radius and clearance are already obtained from the company and given in the **Table 5.2**.

Table 5.1: Deep drawing experiment parameters

Material	**Blankholder force** (kN)	**Distance of cup center to the edge of the die** (mm)
AA5754-H22, AA6061-T6	200, 800, 1200, 1600, 2000	80, 90, 100, 110, 120, 130

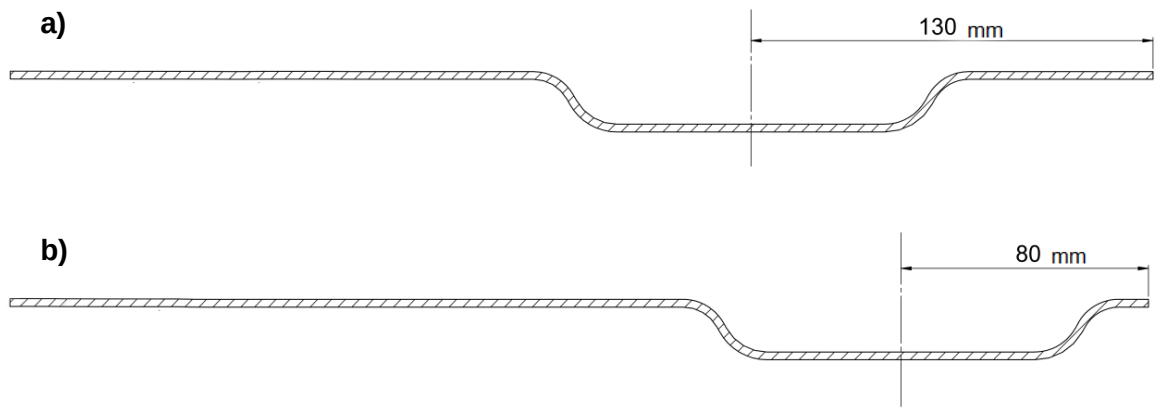

Figure 5.1: Distance of cup center to the edge of the die: **a)** 130 mm **b)** 80 mm

The aluminium alloy sheets are drawn in HSP-DM 630 double acting hydraulic press of Hidromode. The upper plate has a constant force of 2500 kN to able to observe the effect of blankholder force. The lower plate of the press has a maximum pressure of 260 bars. Therefore, different pressures are selected from 20 to 240 bars with almost equal increments. They are converted to force where the pressure values are multiplied with the lower cylinder's area.

$$F = P.A \quad \textbf{(5.1)}$$

$$F_1 = 22 \text{ bar}. 882.5 \text{ cm}^2 = 200 \text{ kN}$$

Other blankholder forces can be seen in the **Table 5.1**. The press speed is chosen as 10 mm/s. During the experiment two different aluminium alloys are drawn without lubrication. The blankholder force and the distance of cup center to the edge of the die is altered according to experimental design. The photo of the tool setup can be seen from the **Figure 5.2**.

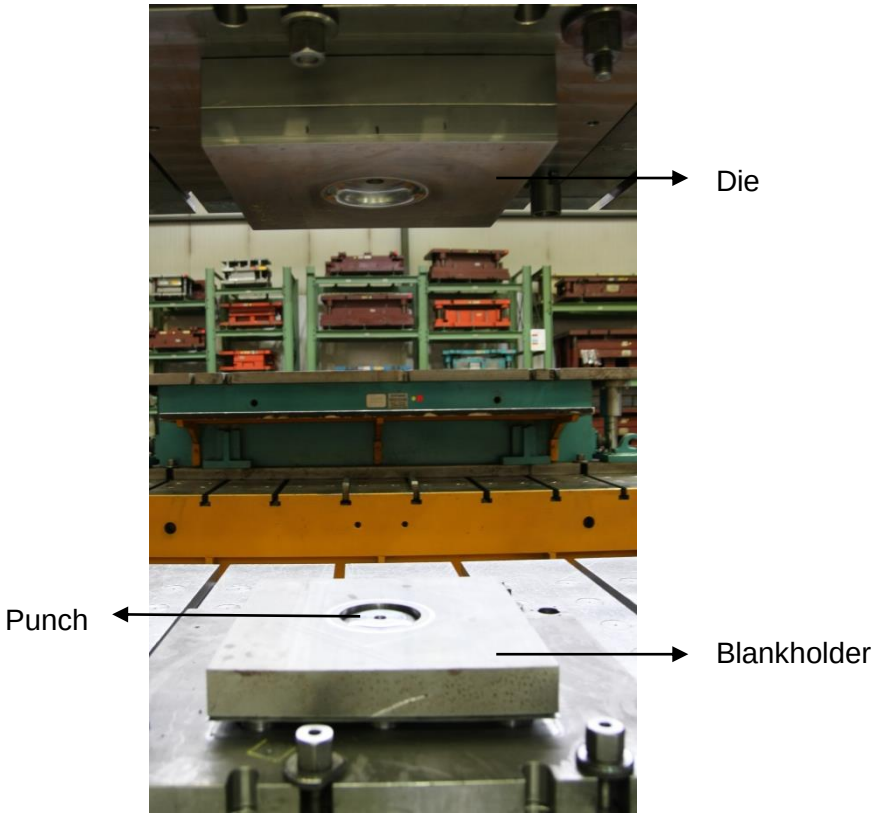

Figure 5.2: Tool setup for deep drawing

The tool setup drawing of the deep drawing experiment can be seen in **Figure 5.3** and its dimensions are given in the **Table 5.2**.

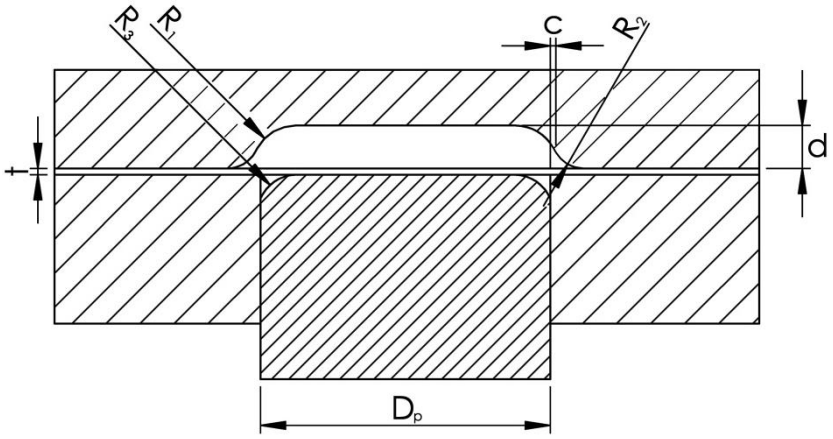

Figure 5.3: CAD drawing of deep drawing tool setup

As it can be seen from **Figure 5.2** and **5.3**, die is attached to the upper plate. The blankholder is attached to lower plate and the punch is fixed to the table of the hydraulic press. The aluminium alloy blank stands at the top of the blankholder before the experiment starts.

Table 5.2: Dimensions of deep drawing tool setup

Symbol	**Explanation**	**Dimension** (mm)
t	thickness	2.5
c	clearance	2.2
d	depth of die	17
D_p	punch diameter	115
R_1	inner radius of die	17.5
R_2	outer radius of die	12.5
R_3	outer radius of punch	15

The **Figure 5.4** shows the working principle of the double acting hydraulic press for deep drawing. First, the blank is put in the top of the blankholder and punch which is fixed to the lower plate. The punch is in the same level with the blankholder. The die is fixed to the upper plate. Secondly, after giving the necessary parameters to the hydraulic press, the die begins to move downwards till it touches the blank. The final step is moving downwards of both die and blankholder together until the necessary stroke length. The blank is filled in the die cavity and has the shape of the die.

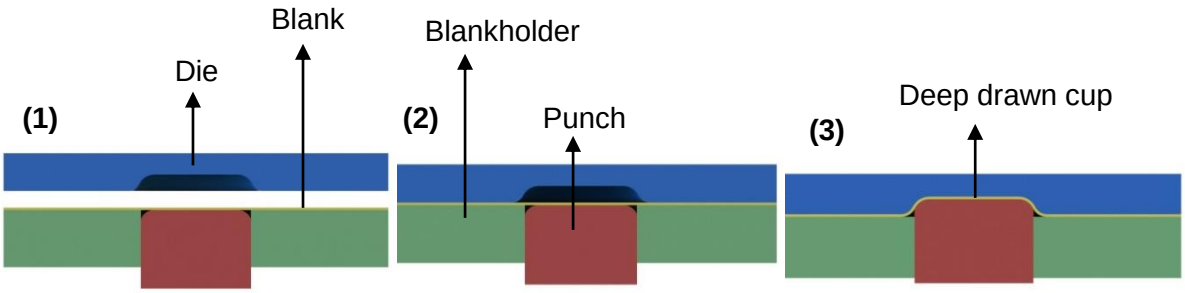

Figure 5.4: Stages of deep drawing experiment: **(1)** positioning **(2)** initial contact **(3)** deep drawing

5.2 Results

The results of the deep drawing experiment consist of two parts: first part gives the results of the thickness variation and the second part gives the straightness of the edge.

5.2.1 Thickness Distribution of the Drawn Parts

After the sheet is drawn, the unnecessary part of the product is removed to measure the thickness variation. The specimen and its cutting steps are shown respectively in **Figure 5.5** and **5.6.** First, the cup is cut into half till the end of the blank. Next, the already cut part is turned around and cut into two halves. The final step is to cut a thin layer of 20 mm thickness so that it can be observed under the microscope.

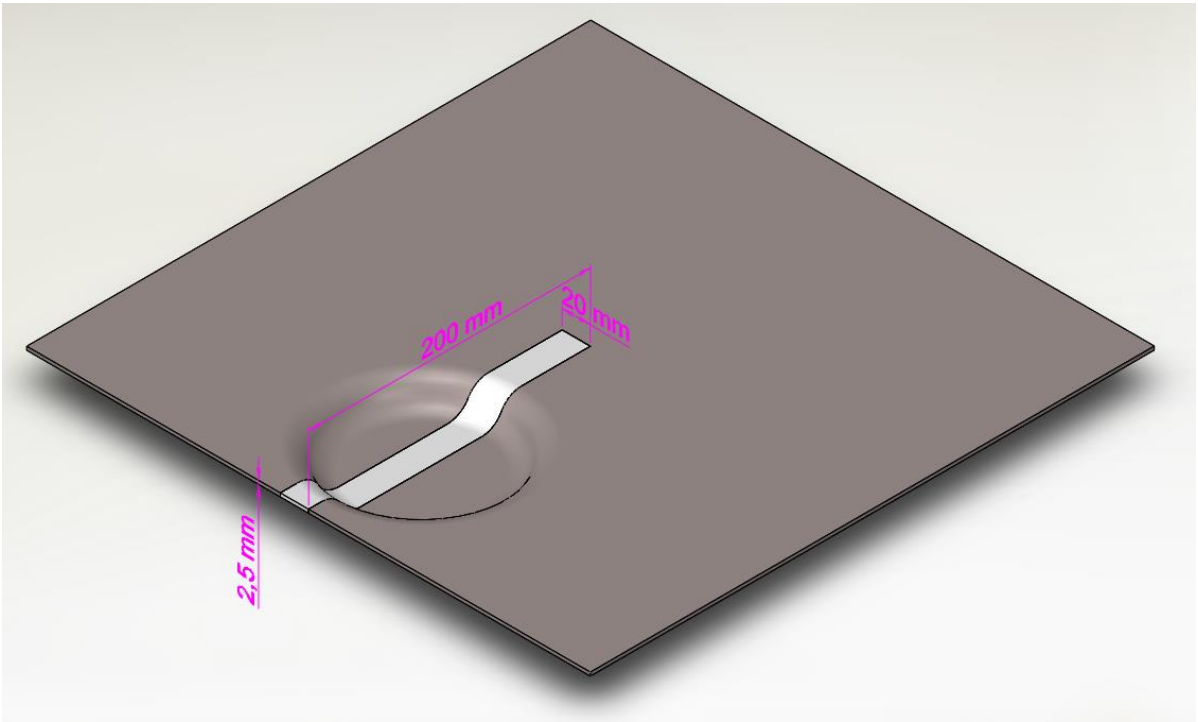

Figure 5.5: The aluminium alloy specimen for thickness measurement

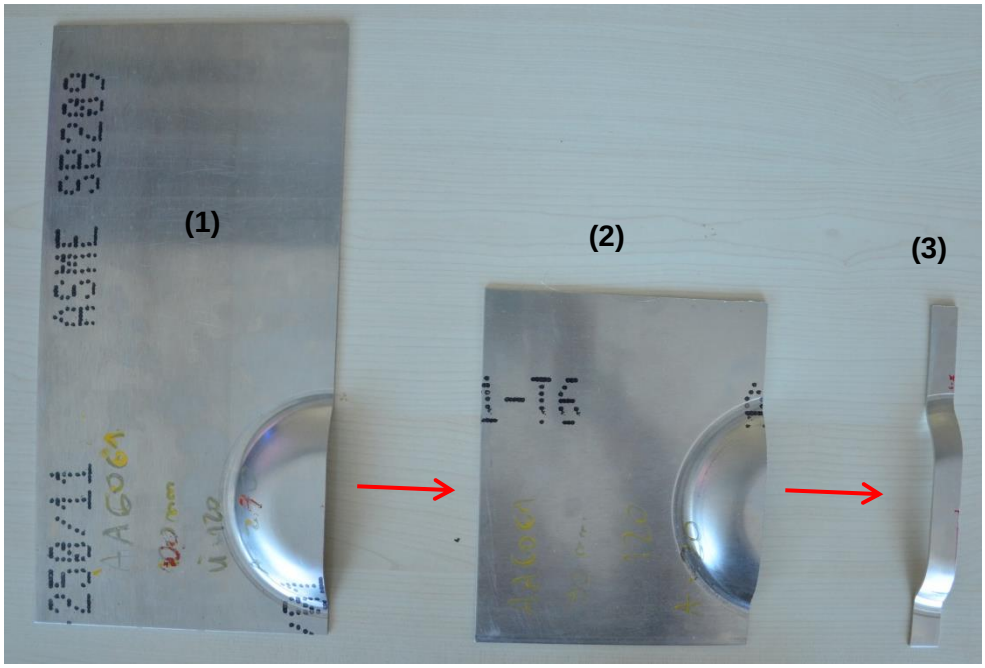

Figure 5.6: Preparation of the specimen for thickness measurement: **(1)** first cut **(2)** second cut **(3)** third cut

The thin layer of the drawn product is brought under the microscope Mitutoyo QuickScope. The part is placed so that the cross section is seen under the light of the microscope. It is observed under x50 magnification and the magnified image of the specimen is transmitted to the computer. The software of the microscope shows live image of the cross section and enables to capture an instant image.

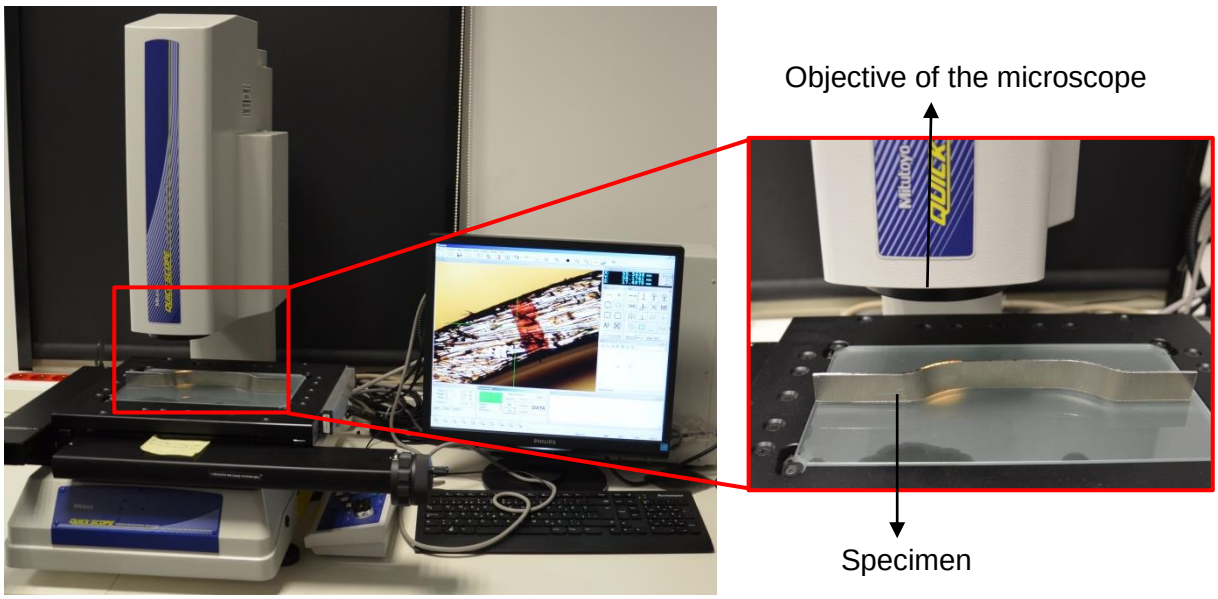

Figure 5.7: Thickness measurement setup and the specimen under microscope

After having an image of the specimen, with the help of the software, some points in the cross section (see **Figure 5.8)** are measured. Each specimen is measured three times and the average is taken for the calculations.

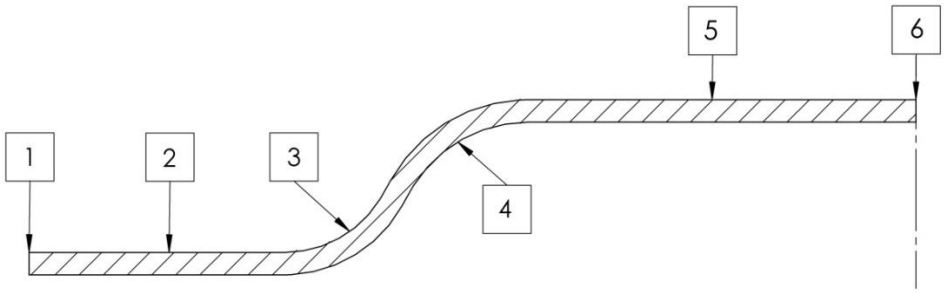

Figure 5.8: Cross section of the deep drawn part with different thickness measurement points

Point 1 shows the edge of the flange area and point 6 shows the center point of base of the cup. Point 2 and 5 are center points of the straight parts till sidewall of the cup. Point 3 is top fillet area and point 4 is bottom fillet area.

The material in the locations 5 and 6 will form the base of the cup which is in contact with the face of the punch. This material stretches and slides over the surface of the punch. The points 3 and 4 represent the cup bottom and top radius respectively, which have undergone bending around the die radius first. Next, the material is unbent and finally bent again around the punch radius in the opposite direction. The material in the locations 1 and 2 form the flange of the cup. It has undergone bending around the die radius.

Demirci et al. that for aluminium alloy AA5754-O, with increasing blankholder force the wall thickness of the drawn cup decreases during the deep drawing experiment. The authors also showed that wall thickness varies especially in the corners.

Influence of blankholder force on the thickness distribution of the drawn cup is depicted in **Figure 5.9**.

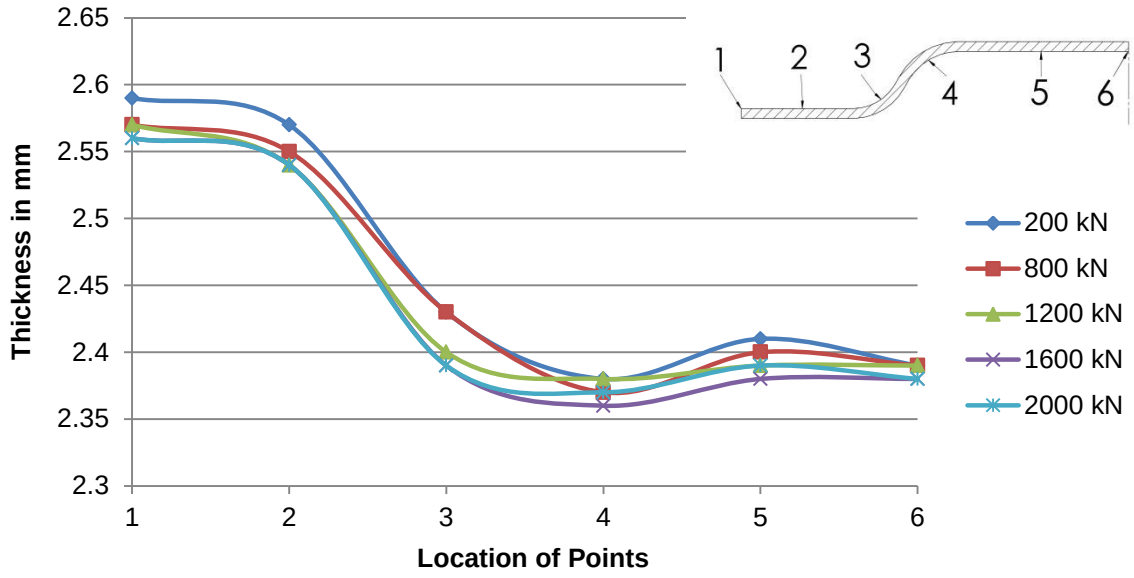

Figure 5.9: AA5754-H22 thickness distribution with different blankholder forces for 80 mm distance away from the cup center to the edge of die

As it can be seen from the graph, when the blankholder force increases, the thickness of the cup decreases. The highest thickness value of the drawn cup is observed for 200 kN blankholder force. It has maximum value of 2.59 mm at the edge of the flange. On the other hand, for 2000 kN blankholder force, the lowest thickness value is measured in the bottom fillet area is measured. It can be concluded that, blankholder force must be chosen as low as possible to avoid the excessive thinning.

Raju et al. investigated the thickness distribution of aluminium alloy AA6061 sheet from the center of the cup to the edge of the flange. According to their study, the thinnest values were observed at the punch nose radius and thickest values at edge of the flange.

The effect of distance of cup center from the edge of the die on the thickness distribution of the drawn cup is shown in **Figure 5.10**.

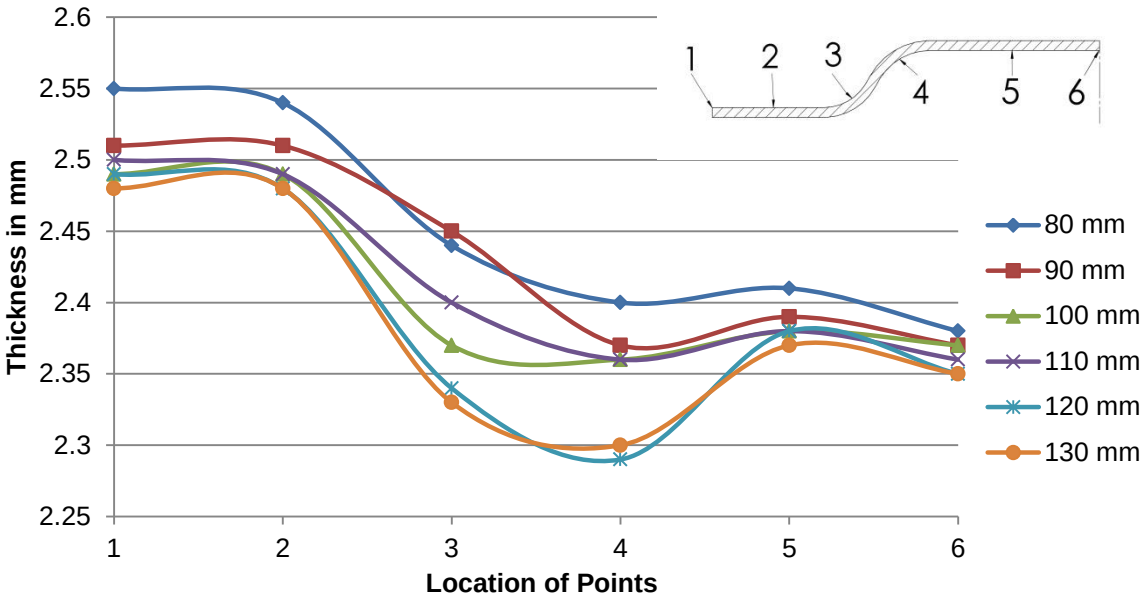

Figure 5.10: AA6061-T6 thickness distribution with different distances away from the cup center to the edge of die for 200 kN blankholder force

The highest reduction in thickness values can be observed when the cup center is 130 mm from the edge of the die. If the distance of the cup center to the edge of die becomes smaller, then the thickness reduction decreases. The thickest part of the cup is observed on the first point at the edge of the flange area. The thickness is lowest when the distance is selected to be 130 mm from edge of the die. To avoid excessive thinning, the distance away from the cup center to the edge of die must be chosen as small as possible.

Both **Figure 5.9** and **5.10** show the thickness distribution of the drawn cup in selected points over the section. Thickening occurs in the flange area and thinning occurs in the side wall and just above punch nose radius. The thickest location of the cup is observed in point 1 where the edge of the flange is and the thinnest is in point 4 where the bottom fillet area is.

The relation between two different aluminium alloys is illustrated in **Figure 5.11.** The blue tone curves show AA5754-H22 and red tone curves show AA6061-T6.

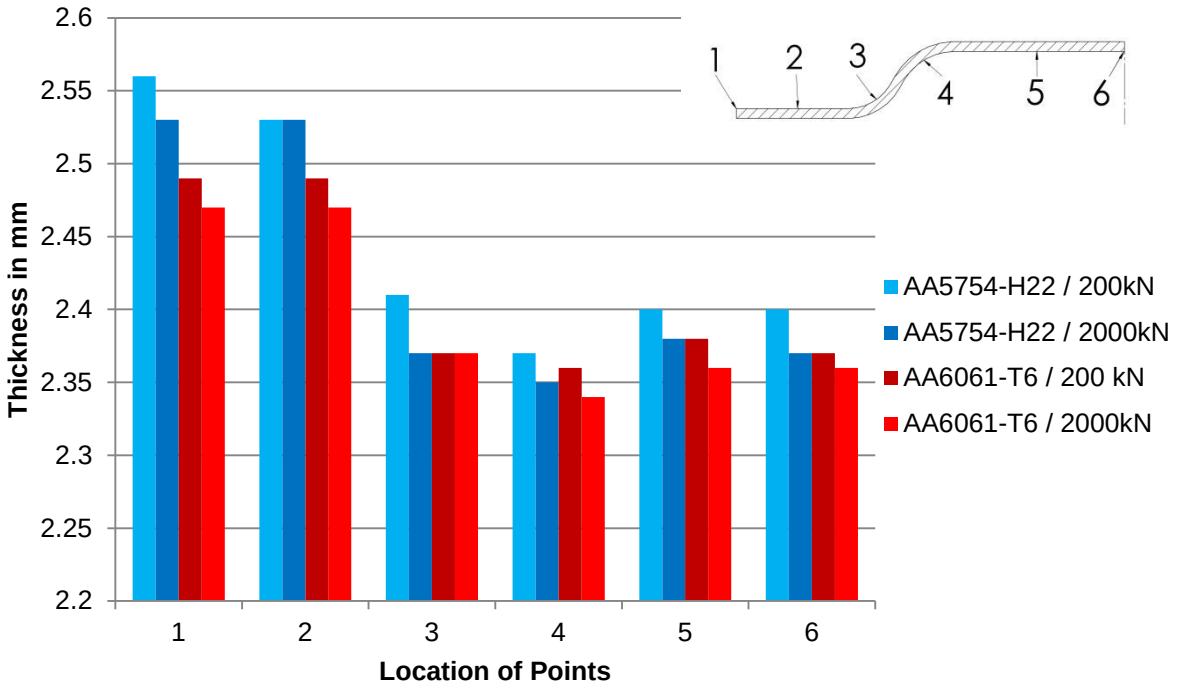

Figure 5.11: Thickness distribution of AA5754-H22 and AA6061-T6 for 200 kN and 2000kN blankholder force with 100 mm distance away from the cup center to the edge of die

In **Figure 5.11** it can be observed that AA5754-H22 has higher thickness values than AA6061-T6 which shows thatAA5754-H22 is more resistant to thinning as compared to AA6061-T6. Since AA5754-H22 has a higher average anisotropy value (0.68) than AA6061-T6 (0.58) it is more resistant to thinning. Resistance to thinning is important in deep drawing processes. If the thickness reduction of the cup is more than a critical limit, the material necks and then cracks. This excessive thinning is a failure in deep drawing and can be prevented with selection of different process parameters. When these two aluminium alloys are compared, AA5754-H22 is a more suitable choice for drawing since thinning is less than AA6061-T6 which means it has lower risk to fail.

From the previous graphs, it can be concluded that lower blankholder force and smaller distance of the cup center from the edge of die causes less thinning and will be preferred in the deep drawing process.

However, there are some deviations in the results of the thickness measurement which occurs because of some minor errors. The chosen distance of the cross section of the part can vary from experimenter to experimenter and it is an observational mistake.

Because of this reason the measurements are repeated 3 times and using the average value, the errors are tried to be minimized. After deep drawing, the product is cut and it has some burrs which prevent to measure the thickness in a correct way. From this reason the edges of the part are rasped. While removing the burrs the thickness of the part can vary which causes deviations during measurement.

5.2.2 Straightness of the Edge of the Drawn Parts

The straightness of the edge depends on how much the drawn part is close to the edge of the blank. As it can be seen from the **Figure 5.12** below, there is certain gap between the part and a straight surface when the distance of the cup center to the edge of die is 80 mm.

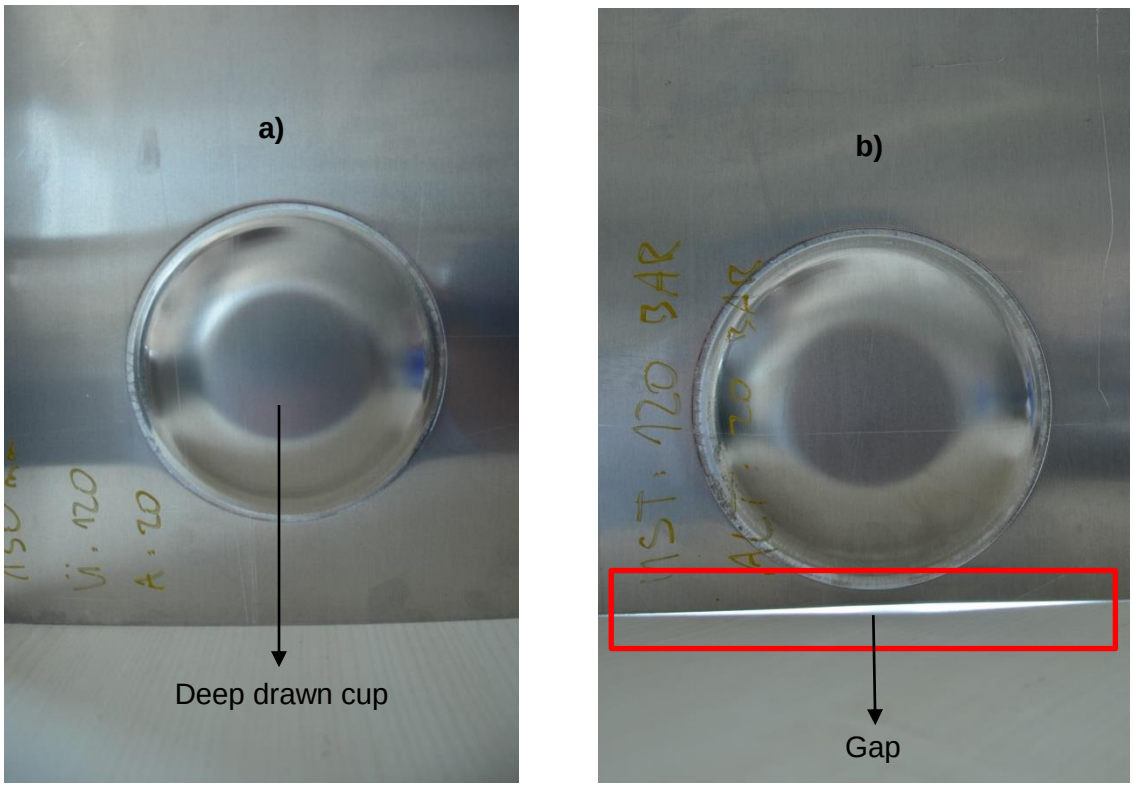

Figure 5.12: The edge of the drawn cup in flange area with different distances away from the cup center to the edge of die: **a)** 130 mm distance **b)** 80 mm distance

It shows that the part is straight when the drawn part has larger distance from the edge. For both of the aluminium alloys, with the cup at 80 mm and 90 mm distance from the edge respectively, the gap can be observed with naked eye. **Table 5.3** shows the gap distance values for different parameters.

Table 5.3: Gap distances of AA5754-H22 and AA6061-T6 for different distances of cup center to the edge of the die and different blankholder forces

Distance of cup center to the edge of the die (mm)	**Blankholder force** (kN)	**Gap distance** (mm)	
		AA5754-H22	AA6061-T6
80	200	0.45	0.4
80	2000	0.22	0.19
90	200	0.28	0.26
90	2000	0.18	0.15

The drawn AA5754-H22 cup with 80 mm distance from the edge has a gap of around 0.45 mm, whereas the one with 90 mm distance has 0.28 mm for 200 kN blankholder force. It shows that when the drawn cup moves away from the edge, the gap distance becomes smaller. The reason is that the compressive stresses are higher when the drawn cup is closer to the edge. The cup with 80 mm distance from edge has a larger thickness at the edge than the one with 90 mm distance, which causes shape distortion at the edge of the part and causes a bigger gap. When the cup distance is close to the edge, the area which the blankholder can hold becomes smaller and it causes smaller pressure even if the force is the same. This causes that the gap becomes larger as the material can flow easier.

With increasing blankholder force, the gap between the part and the straight surface decreases. The reason is that the blankholder prevents material to flow. If not, thickening of the edge occurs which causes the gap.

The gap distance values of AA5754-H22 and AA6061-T6 are close to each other, whereas AA5754-H22 has smaller gap values than other the aluminium alloy. As it can seen from the previous graphs, more thickening occurs in AA5754-H22 as compared to AA6061-T6. If the thickening becomes larger at the edge of the drawn part, then the gap between part and flat surface becomes larger. For instance, the edge thickness of the part of AA5754-H22 for 80 mm distance from the edge and 200 kN blankholder force is 2.59 mm, whereas for AA6061-T6 with the same parameters this

value is 2.55 mm showing that the thickness of the edge has an influence on the gap between edge of the drawn part and straight surface.

When the distance from the edge is 100 mm or above, no gap between the part and straight surface is observed. Both alloys can be drawn to produce emergency valve cavity in the bus panel without causing any aesthetic problems.

6 Numerical Analysis

In the previous chapter experimental procedure of the deep drawing is investigated and the results regarding the mechanical properties are evaluated. Experimental investigations should be supported with numerical analyses, because it is not always possible to realize all experiments or do complicated calculations. Numerical analysis can both support the conducted experiments and can give an idea about further experiments which eliminates the expensive and time consuming trial-and-error method. (Zein et al., 2013)

6.1 Introduction to Finite Element Analysis and AutoForm

Finite element analysis was common for research and development purposes only, however its real industrialization did not start until around 1990 (El Khaldi, 2002). By that time, with considerable efforts the finite element analysis is started be accessible to industry to use this technology in industrial problems. Before the numerical simulation methods were widespread, the process design including die design and improvement projects were extremely costly and time consuming. In the recent years, finite element method (FEM) is the most frequently used tool in analysis and simulation of sheet metal forming processes. (Firat, 2007) The reason is that the computer software used for process simulation has become more reliable and more user friendly.

FEM is a numerical method for finding approximate solutions to boundary value problems. It utilizes various methods to minimize an error function and produce a stable solution. Simulation programs allow visualization of metal forming processes, and provide information about the distribution of stresses, strain and displacements.

In experimental study, drawability of different aluminium alloys, blankholder force, distance of the cup center to the edge of die are analyzed, but finite element analysis allows to calculate thickness change, in deep drawing known as thinning and wrinkling over the deformed zone and cross section of the formed specimen. In this work, deep drawing experiment is modeled in AutoForm^{plus} R3 where the code type is

a special static implicit. (Altan and Tekkaya, 2012) Numerous simulations are run and according to the results, they are optimized.

AutoForm is a finite elements simulation program which has been developed by the Swiss software developer AutoForm Engineering GmbH. It is used for die making and mostly for sheet metal forming simulations so that reliability in planning is improved and try out time is reduced. (AutoForm, 2014) Autoform^{plus} is an integrated system with specialized functions to analyse review and optimize each step in the manufacturing process. AutoForm^{plus} R3 focuses on accurate results with short computational times. (Autoform, 2011) This forming finite element analysis software is based on an implicit solver. Implicit formulation provides higher computational speed and lower memory requirements for the simulations.

6.2 Modeling of the Deep Drawing Experiment

The CAD drawings of die, punch, blank and blankholder, which is also known as binder, are imported to the simulation. In AutoForm^{plus} R3 a new process plan is generated and the tools are imported as the .igs files. The tools which are the elements used in the simulation are shells. After choosing the tools, they are aligned according to each other and the movement. Their directions are chosen for each of them separately. It can be seen in **Figure 6.1**.

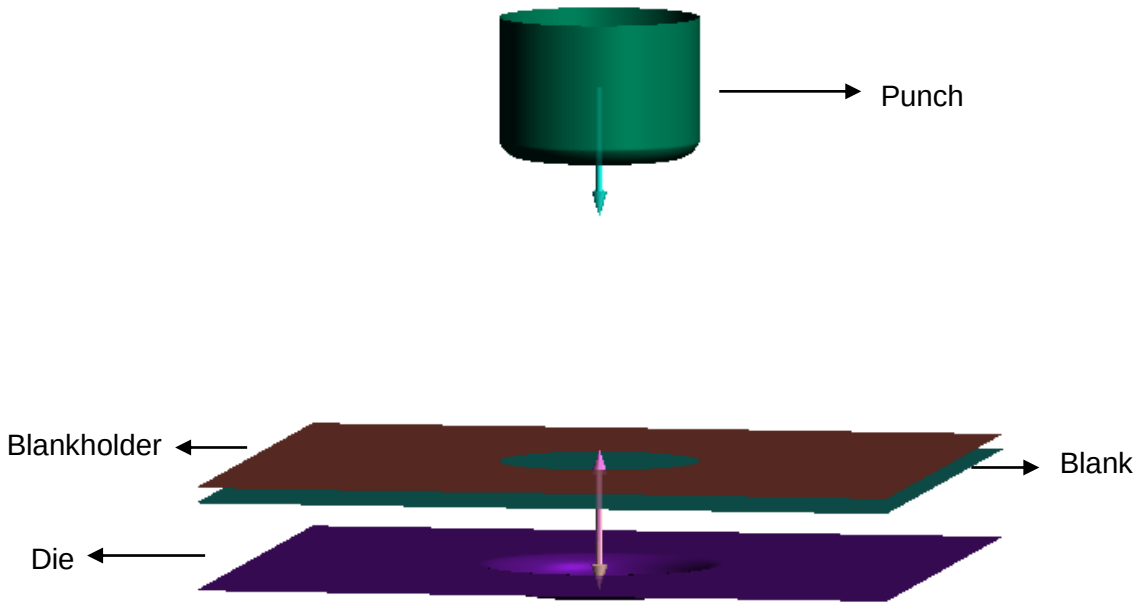

Figure 6.1: 3D finite element model of the deep drawing

There is a rigid die at the bottom. Above it, there is a blank which moves downwards when the simulation starts and stops until touches the die. Above them, there is a blankholder which is stationary. At the top, the rigid punch moves downwards with a constant speed until forms the blank through the blankholder and fills the die cavity. There is no gravity in the simulation.

The process can be summed up with three steps which can be seen in **Figure 6.2.**

1)

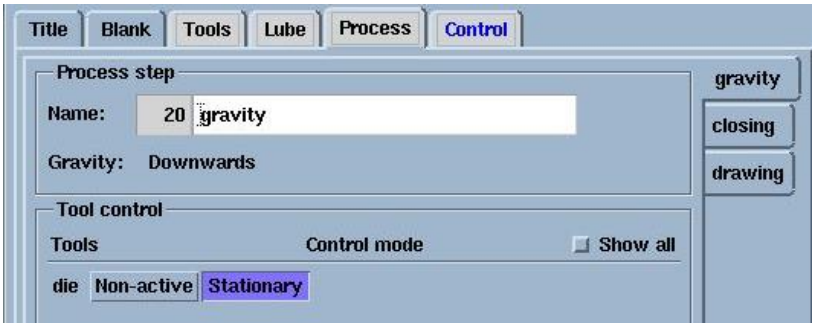

2)

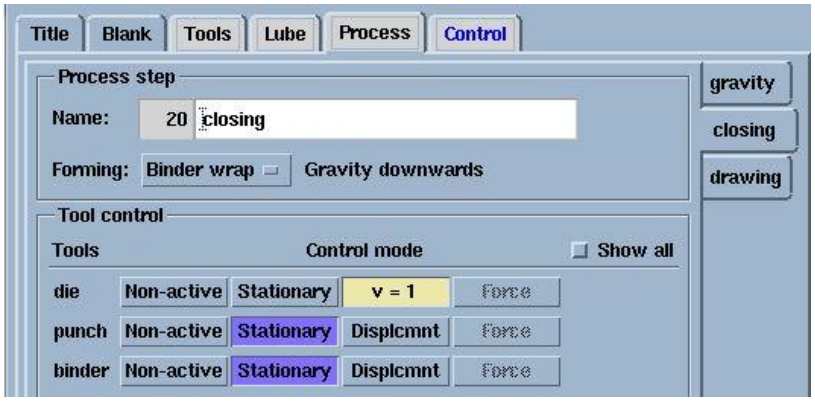

3)

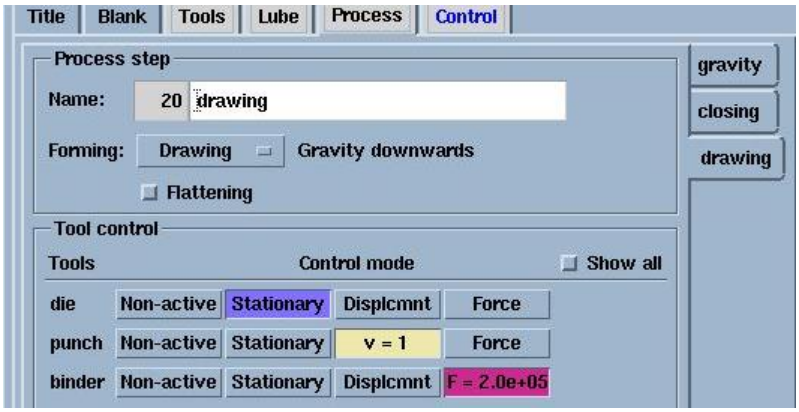

Figure 6.2: Process generator for deep drawing process in AutoForm^{plus} R3: **1)** gravity **2)** closing **3)** drawing

First one is gravity where the die is stationary. Second one is where the closing punch and binder are stationary but the die moves with a constant speed. And finally, in the

third step the drawing is carried out. In drawing, the die is stationary, punch has a displacement with a constant speed and binder is given a force value which presses the sheet against the die.

The mechanical properties of both aluminium alloys are determined experimentally with tensile test and Nakajima test. According to tensile test results, Young's modulus values for AA5754-H22 and AA6061-T6 0 degree are imported to material viewer program of AutoForm^{plus} R3 for the blank. Next, the hardening curve is selected according to Ludwik and the values of yield stress (σ_0), strain-hardening exponent (n) and the strength coefficient (K) are imported to simulation software. The reason for this is that all values in the tensile test are calculated according to Ludwik hardening law. Additionally initial flow curve values are Hill's criterion is selected as the field criteria and the anisotropy values of aluminium alloys for 0, 45 and 90 degrees are given to the AutoForm^{plus} R3. For other yielding criterions like Barlat, not only tensile tests but also bi-axial and shear tests have to be conducted. The forming limit curve which is drawn with the help of the Nakajima test is also used for both materials in the simulation. Other values such as Poisson's ratio and specific weight are taken from literature. The properties which are imported to AutoForm^{plus} R3 are shown in the screenshot with red rectangles in the **Figure 6.3**.

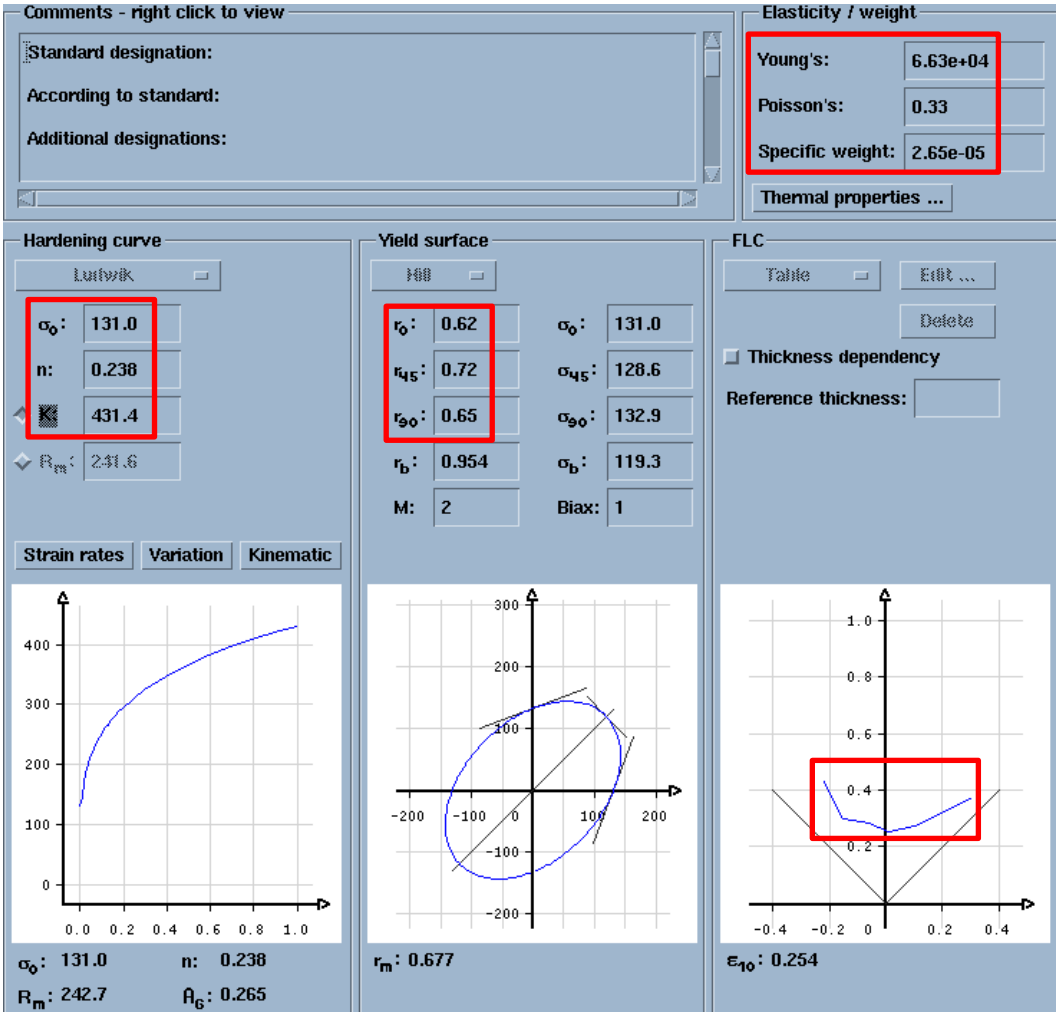

Figure 6.3: Material chart for AA6061-T6 in AutoForm^{plus} R3

FEM is an approximate numerical solution, and the accuracy of the results is dependent on the number of elements used. Element formulation is shear soft shell formulation which means elastic plastic shell. Element type is three node triangular elements.

For the comparison with deep drawing experiment, mesh is generated automatically by the AutoForm^{plus} R3. In the mesh section, the radius penetration and maximum element angle is chosen for meshing. In AutoForm^{plus} R3, element angle is given to set the accuracy of the simulation. The number of elements is determined by AutoForm^{plus} R3 where the element edge lengths do not exceed the given value. It is linked to the initial element size. The meshing and remeshing properties used in the simulation are shown below **Figure 6.4.**

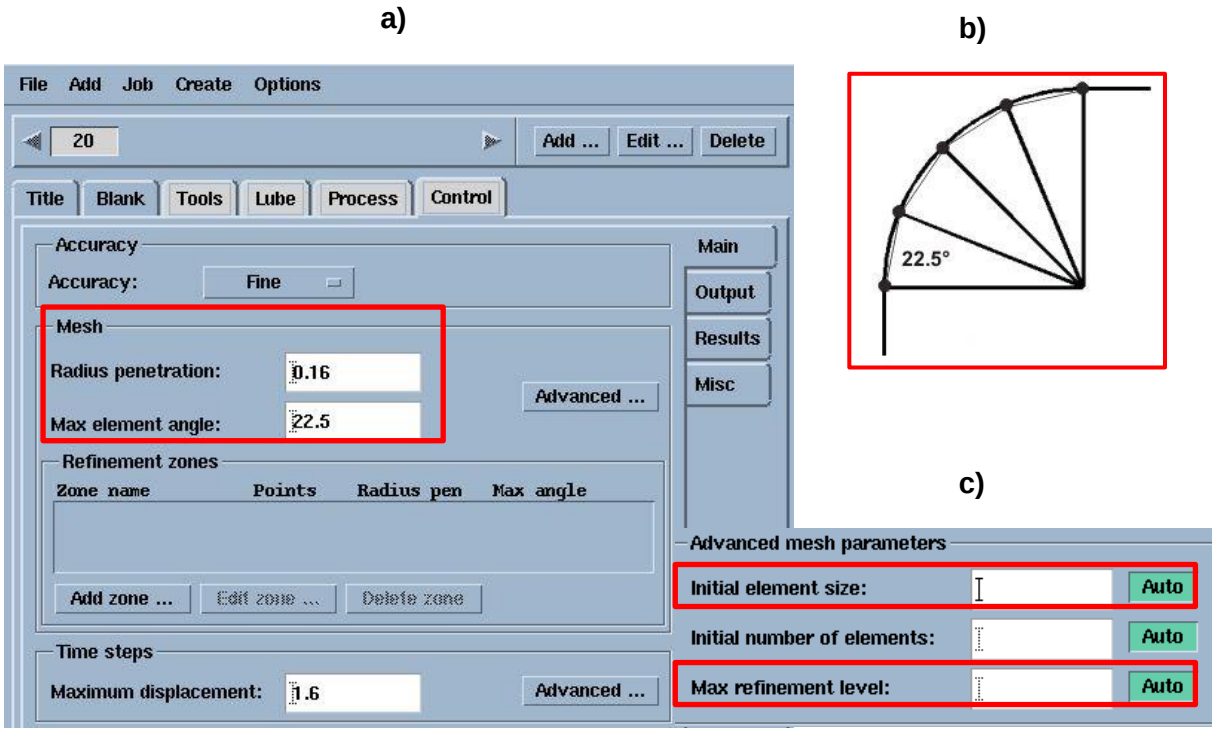

Figure 6.4: Mesh properties in AutoForm^{plus} R3: **a)** accuracy of the mesh **b)** max. element angle **c)** advanced mesh parameters

If the accuracy is chosen as fine, the radius penetration becomes automatically 0.16 mm and the max. element angle 22.5° for a radius of 90°. Radius penetration defines the acceptable penetration of the blank with the tool in the length unit used. If acceptable penetration is exceeded, the mesh is refined locally. Maximum element angle is another control parameter which defines the maximum enclosed angle between two adjacent elements. If the value for the max. element angle is exceeded, the element is refined. For remeshing the maximum refinement level is chosen automatically. In **Figure 6.5** mesh of the product can be seen before and after the deep drawing process.

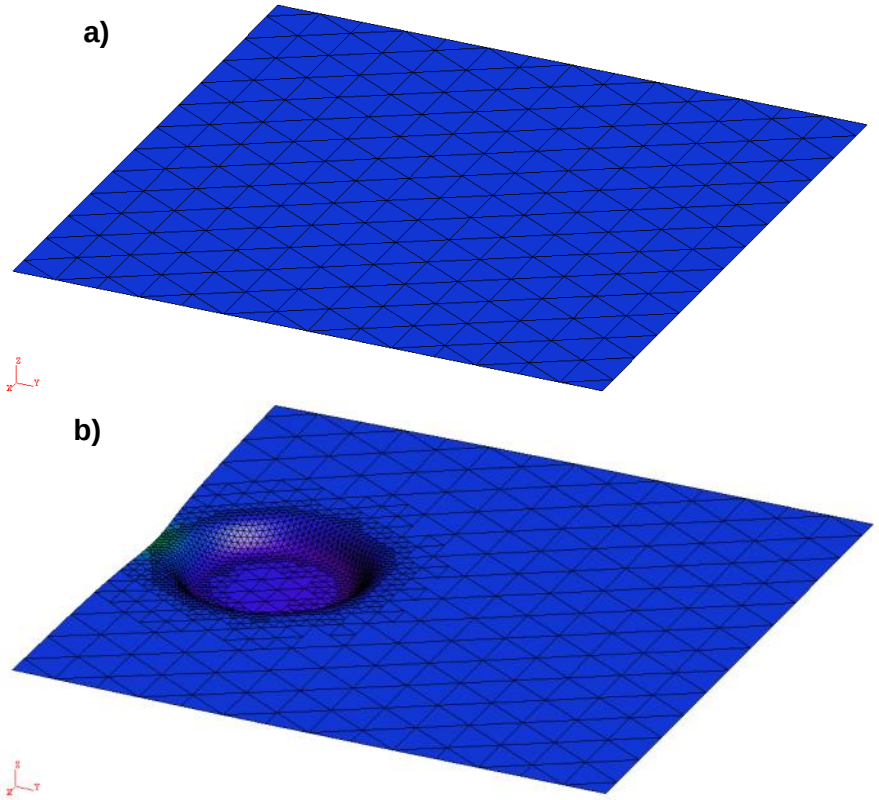

Figure 6.5: Meshing in AutoForm^{plus} R3: **a)** mesh of the sheet before deep drawing **b)** meshing of the deep drawn cup

The deep drawing experiment is conducted without any lubricant in clean and dry environment. Various frictions such as the ones between punch/blank, blankholder/blank and, die/blank affect the deep drawing process. It is not easy to predict these friction coefficients. The study of Aleksandrović et al. shows that the friction coefficient of AlMg4.5Mn changes with different process parameters from 0.4 to 0.2 during deep drawing process. Because of this reason, the friction coefficient is chosen as 0.2 and imported to AutoForm^{plus} R3.

6.3 Results

The results of the numerical analysis are divided into four parts: In the first part, the thickness distribution results of drawn part are given which have the same process parameters like deep drawing experiment. The second part includes the FLD diagrams and wrinkling criterions of both aluminium alloys. In the next part, simulation results are compared with the deep drawing experiment results for validation. In the fourth and final part, the results of the comparison of deep drawing experiment and

simulation are interpreted and further simulations are conducted with different process parameters.

6.3.1 Thickness Distribution of the Drawn Parts

In the results of the simulations, two types of aluminium alloys are compared in terms of their thickness reduction. The thickness reduction of the deep drawn part in the end of simulation is shown in **Figure 6.6** below.

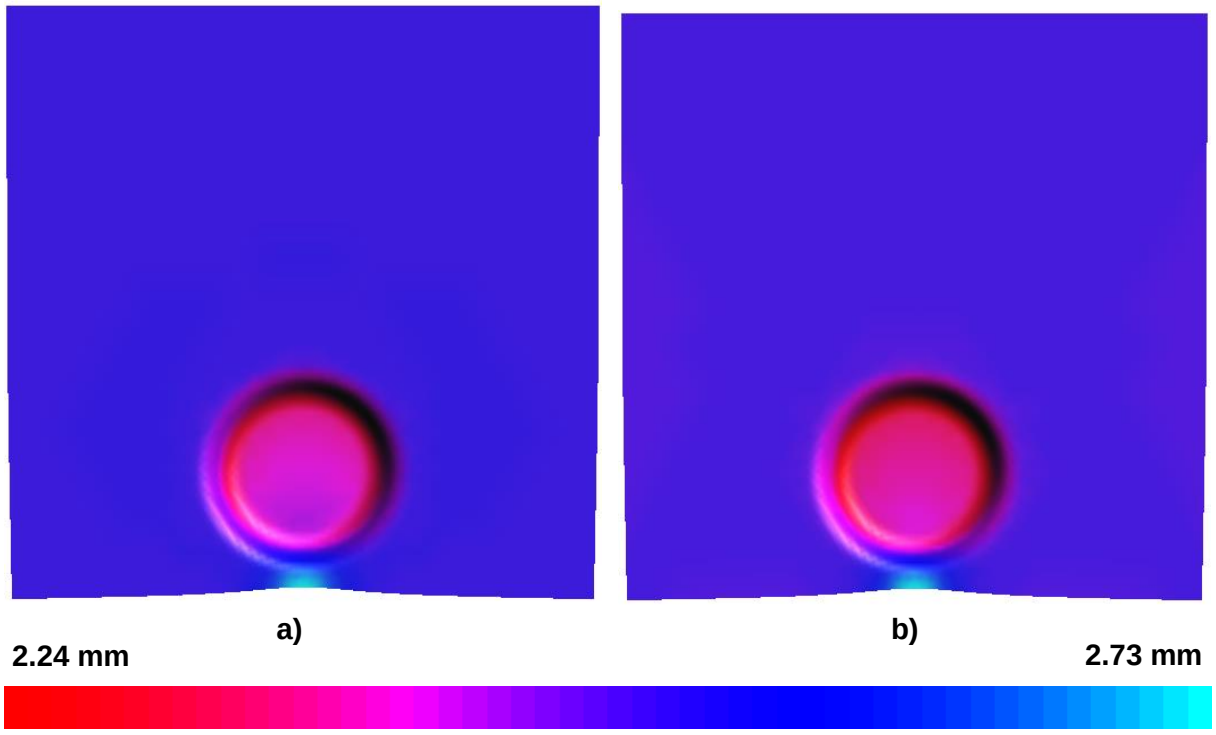

Figure 6.6: Thickness distribution of deep drawn part for 200 kN blankholder force and 80 mm distance away from the cup center to the edge of die: **a)** AA5754-H22 **b)** AA6061-T6

AA5754-H22 has its thickest value of 2.73 mm and thinnest value of 2.25 mm. AA6061-T6 has values of 2.73 mm and 2.24 mm respectively. Both AA5754-H22 and AA6061-T6 have same thickness values close to the edge of the flange are. This thickened part is shown with light blue colours. The difference in AA6061-T6 is that the bottom fillet area has lower thickness values than AA5754-H22. The red coloured areas are the weakest points of the drawn cup, which can result in splits or cracks with higher drawing ratio.

After the thickness distribution, the thinning distribution of both aluminum alloys for 2000 kN blankholder force is shown in **Figure 6.7.**

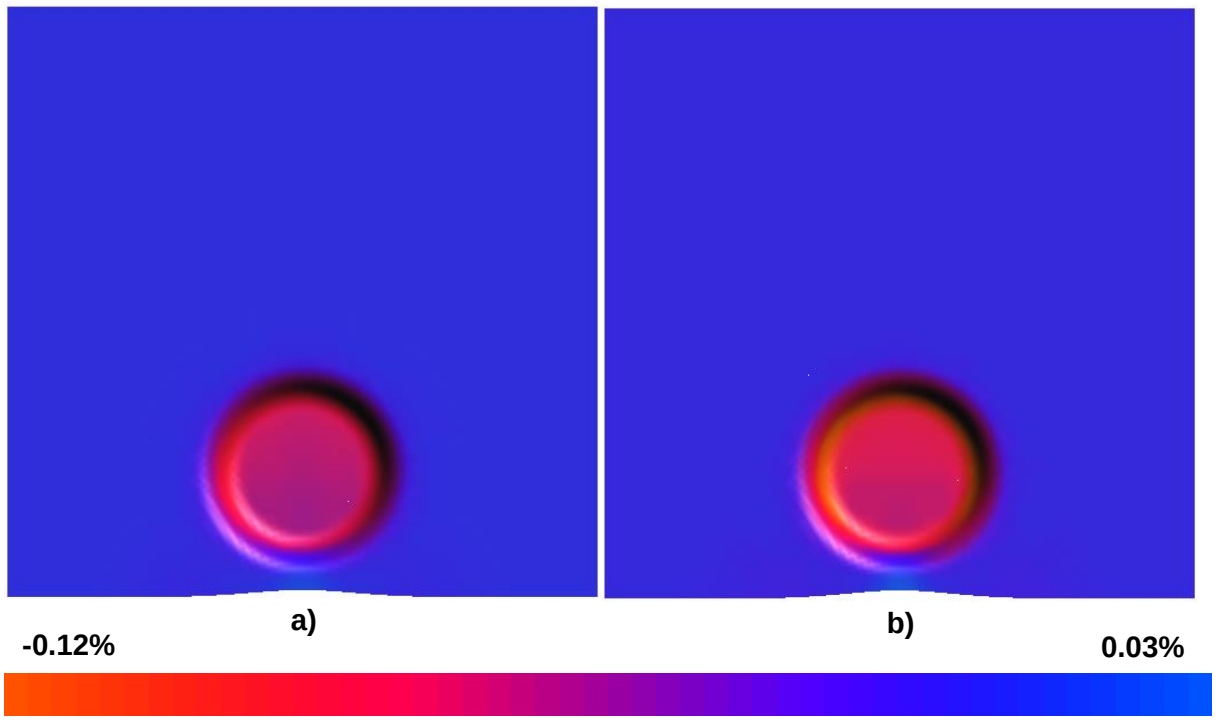

Figure 6.7: Thinning distribution of deep drawn part for 2000 kN blankholder force and 80 mm distance away from the cup center to the edge of die: **a)** AA5754-H22 **b)** AA6061-T6

The thinning values are given in percentage. As it can be seen, AA6061-T6 has lighter red tones compared to AA5754-H22, which shows higher thinning at the bottom fillet area. The lowest thickness value of AA6061-T6 is 2.21 mm, which is equal to 0.15% thinning when initial thickness is considered as 2.5 mm. The maximum thickening is observed at the edge of the drawn part and the value is around 0.03% for both aluminium alloys. The maximum thickness of AA5754-H22 is 2.57 mm, whereas it is 2.56 mm for AA6061-T6. The values are close to each other and they have the same blue colour at the edge of the part.

If **Figure 6.6** is compared with **Figure 6.7,** the effect of blankholder force can be observed. For both aluminium alloys with increasing blankholder force, the thinning becomes larger. In both of the above figures it can be observed that AA5754-H22 has higher thickness values than AA6061-T6. It shows that AA6061-T6 is more prone to thinning as compared to AA5754-H22. AA6061-T6 has lower average anisotropy

value (0.58) than AA5754-H22 (0.68) which means it is more prone to thinning. Another observation is that the edge of the blank is not straight where it is close to drawn part. A similar observation can be made also during the deep drawing experiment.

6.3.2 Forming Limit Diagram and Wrinkling Analysis of the Drawn Parts

The most important criteria to evaluate the forming processes is formability. The analysis of the deformation based on forming limit diagram helps to identify the potential failure during forming of the sheet metal. The formability regions of an FLD are shown in **Figure 6.8**.

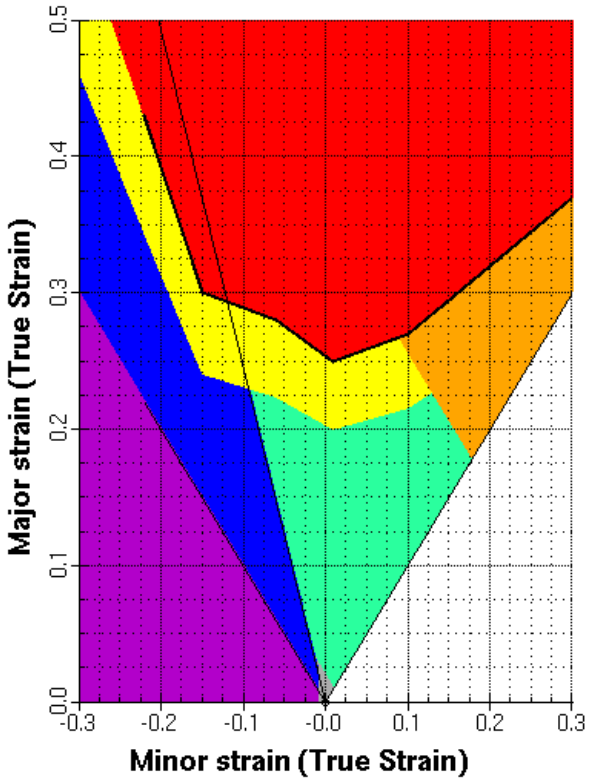

Figure 6.8: Formability regions of forming limit diagram

The formability regions are explained below:

- Splits (Red): Areas where blank has split or crack. It is above the FLC.
- Excessive Thinning (Orange): Areas where thinning of blank is higher than 30% of original sheet thickness.
- Risk of Splits (Yellow): Areas where blank may split or crack. It is between the FLC and 20% below the FLC.

- Safe (Green): Areas where blank has no wrinkles, thinning or splits.
- Insufficient Stretching (Gray): Areas where blank has not enough strain (below 2%)
- Compression (Blue): Areas where blank has compressive stresses. It causes wrinkling tendencies.
- Thickening (Purple): Areas where blank becomes thicker. It may cause wrinkles.

Forming limit diagrams for different process parameters are drawn below in **Figure 6.9, Figure 6.10 and Figure 6.11**. First figure compares FLD of both aluminium alloys with the same process parameters.

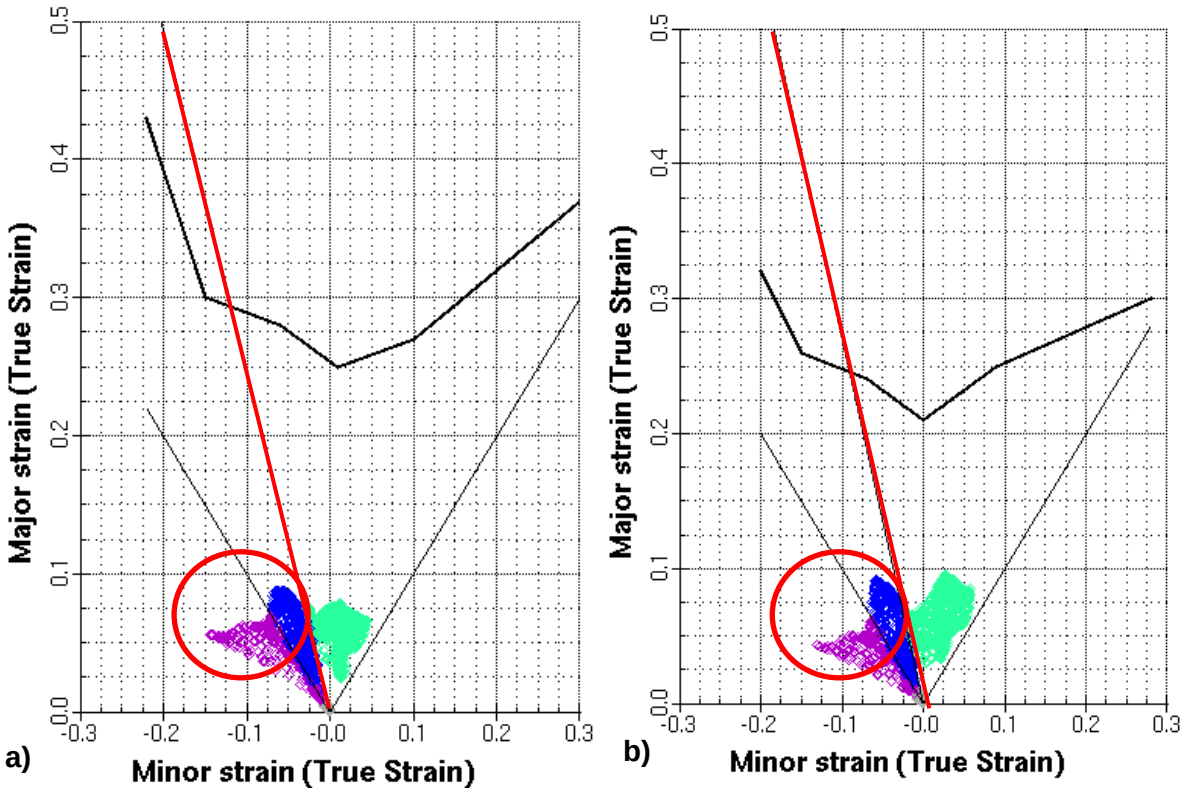

Figure 6.9: Forming limit diagrams of both aluminium alloys with 80 mm distance away from the cup center to the edge of die and 200 kN blankholder force:
a) AA5754-H22 **b)** AA6061-T6

Figure 6.9 shows the difference between aluminium alloys AA5754-H22 and AA6061-T6. With the same process parameters, their major and minor strain values are observed to be different than each other. In FLD, there are three lines in total. Two

of the lines are diagonal and the third red line is uniaxial tensile line which shows the thickening border of the drawn part. This means that the areas below this line show the inclination of wrinkling. The red circle shows these areas which are in blue and purple colours. As mentioned before, blue colour shows areas with compression stresses and purple shows thickening of the drawn part. AA6061-T6 has less purple areas than AA5754-H22, which shows it has less wrinkling than the other aluminium alloy. However, in total the difference is small as they have almost the same amount of blue areas.

The next figure compares different aluminium alloys with the same process parameters, however with a different blankholder force than the previous figure.

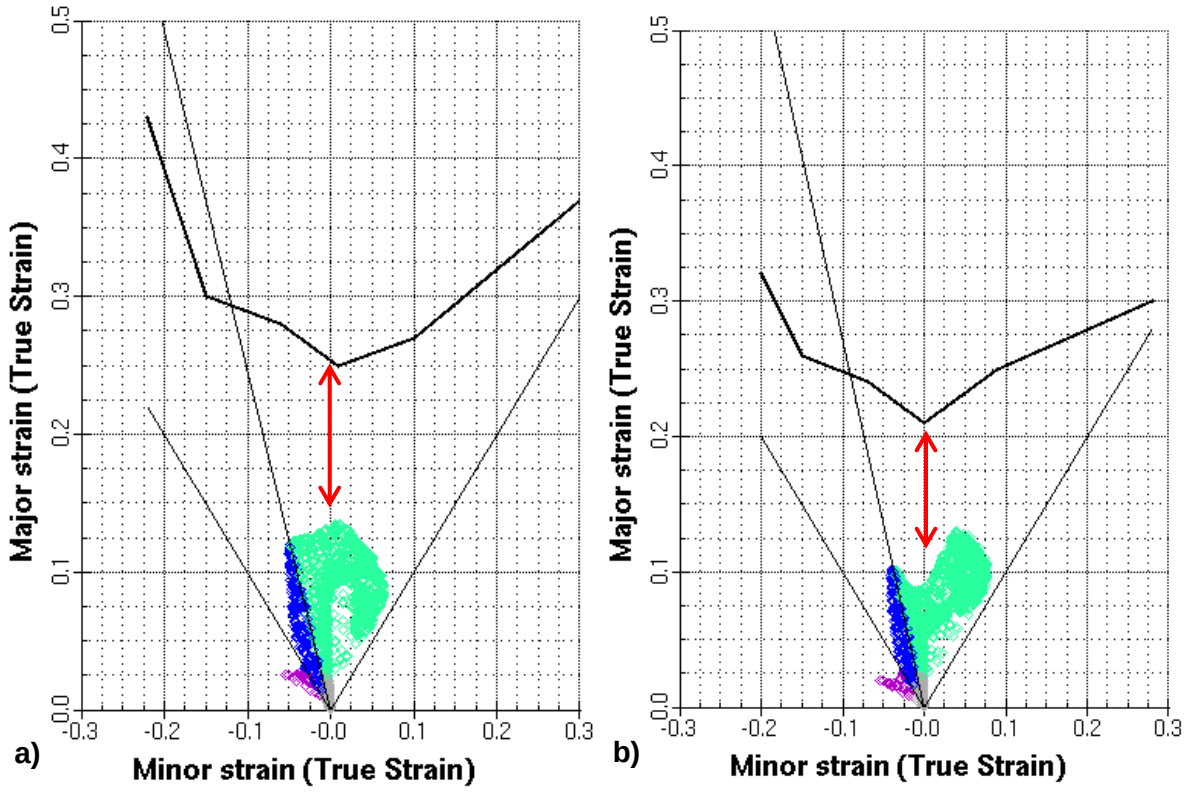

Figure 6.10: Forming limit diagrams of both aluminium alloys with 80 mm distance away from the cup center to the edge of die and 2000 kN blankholder force:
a) AA5754-H22 **b)** AA6061-T6

Figure 6.10 shows the difference between aluminium alloys AA5754-H22 and AA6061-T6. With the same process parameters, their major and minor strain values are observed to be different than each other. The red arrow shows the distance between maximum major strain and FLD_0 point. The FLD_0 point of AA5754-H22 is 0.25 which

is 0.4 higher than AA6061-T6. According to FLD, AA5754-H22 has a similar maximum strain value when compared to AA6061-T6. Therefore, the red arrow of AA5754-H22 is longer when compared to AA6061-T6. This shows that AA5754-H22 has longer distance to the bottom of the forming limit curve where the drawn part will split or crack. It means AA5754-H22 is safer to be drawn deeper parts compared to other aluminium alloy. Both of the drawn cups have undergone a safe deep drawing process which is shown with green areas. The drawing operation is shallow and there is no risk of splits or excessive thinning.

If **Figure 6.9** is compared to **Figure 6.10,** the effect of blankholder can be observed. With increasing blankholder force, the compression stress and thickening becomes smaller, whereas the sheet becomes thinner which may cause risk of splits. This means major strain values become higher and minus minor strains become smaller.

The final figure shows the effect of the distance away from the cup center to the edge of die on the forming limit diagram.

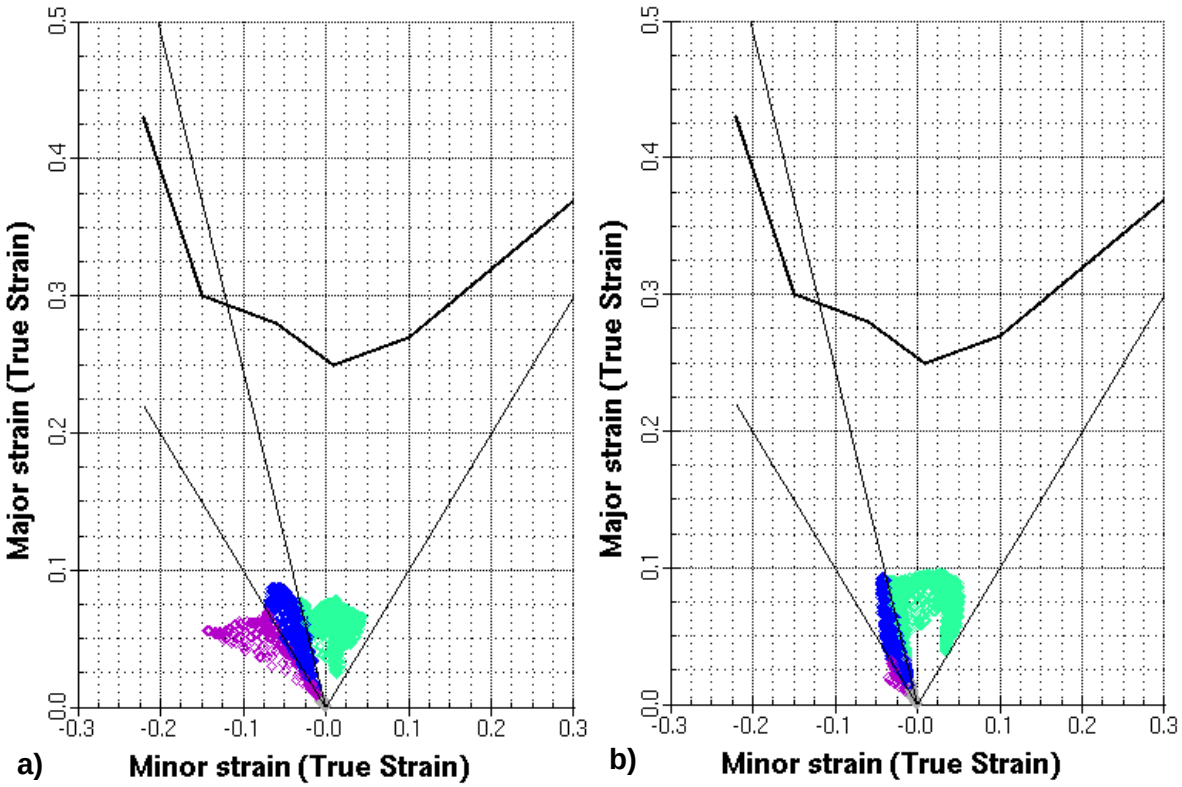

Figure 6.11: Forming limit diagrams of AA5754-H22 with 200 kN blankholder force: **a)** 80 mm distance away from the cup center to the edge of the die **b)** 130 mm distance away from the cup center to the edge of the die

Figure 6.11 shows that 80 mm distance away from the cup center to the edge of the die has significantly larger blue and purples areas than 130 mm distance. Shorter distances away from the cup center to the edge of the die cause thickening which increases the chance of wrinkling. This thickening occurs at the flange of the drawn part which causes a gap between part and straight surface. As it can be seen, the gap becomes smaller if the distance away from the cup center to the edge of die becomes larger.

Apart from FLD, in AutoForm^{plus} R3 wrinkling criterion is used to identify the areas where the material has wrinkling tendency.

The wrinkling is a failure in the sheet metal forming processes which results from the compressive stress in the direction of membrane. There are many factors which influence the wrinkling such as material, friction, tool shape and blankholder. Because of this reason, it is not easy to predict the wrinkling tendency.

The formula of wrinkling criterion which predict wrinkling is shown as follows:

$$\varepsilon_{wc} = max\left[-\left(\varepsilon_2 + \frac{R}{1+R}\varepsilon_1\right), 0\right] \quad \textbf{(6.1)}$$

In the formula, R is average anisotropic exponent and ε_1 and ε_2 are major strain and minor strain respectively. Below the **Figure 6.12** visualizes the strain value for wrinkling criterion ε_{wc} on a standard FLD.

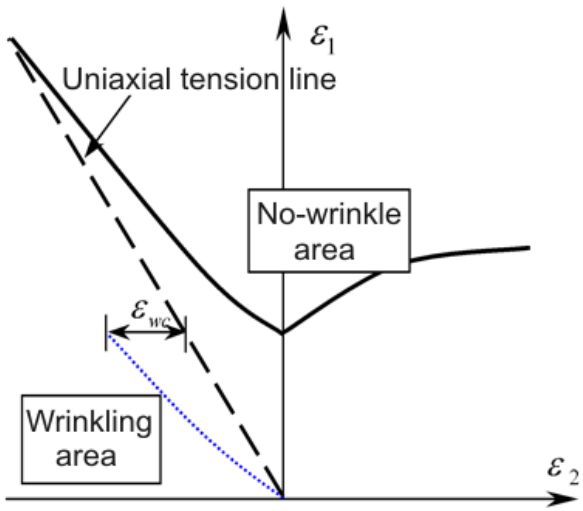

Figure 6.12: Forming limit diagram with ε_{wc}

ε_{wc} is the strain value which shows the shifted distance from the uniaxial tension line. If the distance is larger, then the deep drawn part has larger wrinkling. The wrinkling area is on the compression side of the FLD and also below the uniaxial tension line.

Table 6.1: Maximum wrinkling criterion strain values of AA5754-H22 and AA6061-T6 for different distances of cup center to the edge of the die and blankholder forces

Distance of cup center to the edge of the die (mm)	**Blankholder force** (kN)	**Max.** $\boldsymbol{\varepsilon_{wc}}$	
		AA5754-H22	AA6061-T6
80	200	0.12	0.1
80	2000	0.04	0.04
130	200	0.03	0.02
130	2000	0.001	0.001

As it can be seen from the table above, the wrinkling of both aluminium alloys are close to each other, whereas AA5754-H22 is more prone to wrinkle as the strain values are higher than AA6061-T6. As mentioned before, with the increasing blankholder force and distances of cup center to the edge of the die, the strain value becomes smaller, which means wrinkling becomes less.

If this table is compared with the **Table 6.1** in the previous chapter, it can be concluded that thickening/wrinkling is proportionally related to the gap distance between the drawn part and straight surface. The thickening causes the gap to be larger.

6.3.3 Comparison of Deep Drawing Experiment and Simulation Results

In the simulation, the same six points from the cross section of the drawn part are measured as in the experiment. AutoForm^{plus} R3 has dynamic section menu where the section can be cut according to the axis with a specific distance.

First, the thickness distribution results of two different aluminium alloys for both experiment and the simulation are illustrated in **Figure 6.13**. The red coloured curves show the results of the experiment and blue coloured curves show the results of the simulations.

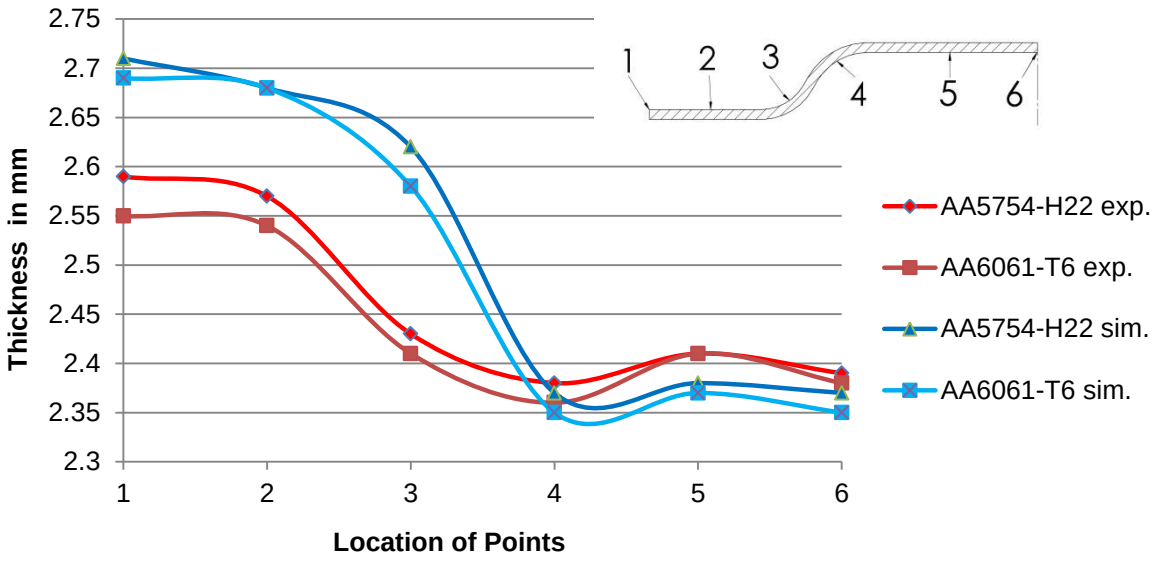

Figure 6.13: Thickness distribution of AA5754-H22 and AA6061-T6 for 200 kN blankholder force with 80 mm distance away from the cup center to the edge of die for both experiment and simulation

As it can be seen from the figure above, the maximum and minimum thickness values simulation results. The initial thickness of the part was 2.5 mm and specifically at the edge of the AA5754-H22 part, it becomes 2.71 mm in the simulation and 2.59 mm in the experiment. The difference is 0.12 mm which is around 5%. The thinnest thickness values of experiment and simulation are close to each other, where the difference is not more than 0.2 mm. The simulation graph rapidly falls beneath the experimental graph after point three although, it starts on the top at point one. This creates a greater interval in the simulation data compared to the experimental data. On the other hand, the trend of the lines is similar, which means the lowest value is observed in the fourth location, and the highest in the first location. In both graphs AA6061-T6 has lower thickness values than AA5754-H22. According to the results of the simulation the thickness difference between both aluminium alloys are smaller as compared to experiment.

Zein et al. confirm the previously stated point that the thickest location of the cup is observed in point 1 where the edge of the flange is and the thinnest is in point 4 where the bottom fillet area is.

The thickness distribution of AA5754-H22 is illustrated in **Figure 6.14** to compare the experiment and simulation results with two different blankholder forces. The red coloured curves show the results of the experiment and blue coloured curves show the results of the simulations.

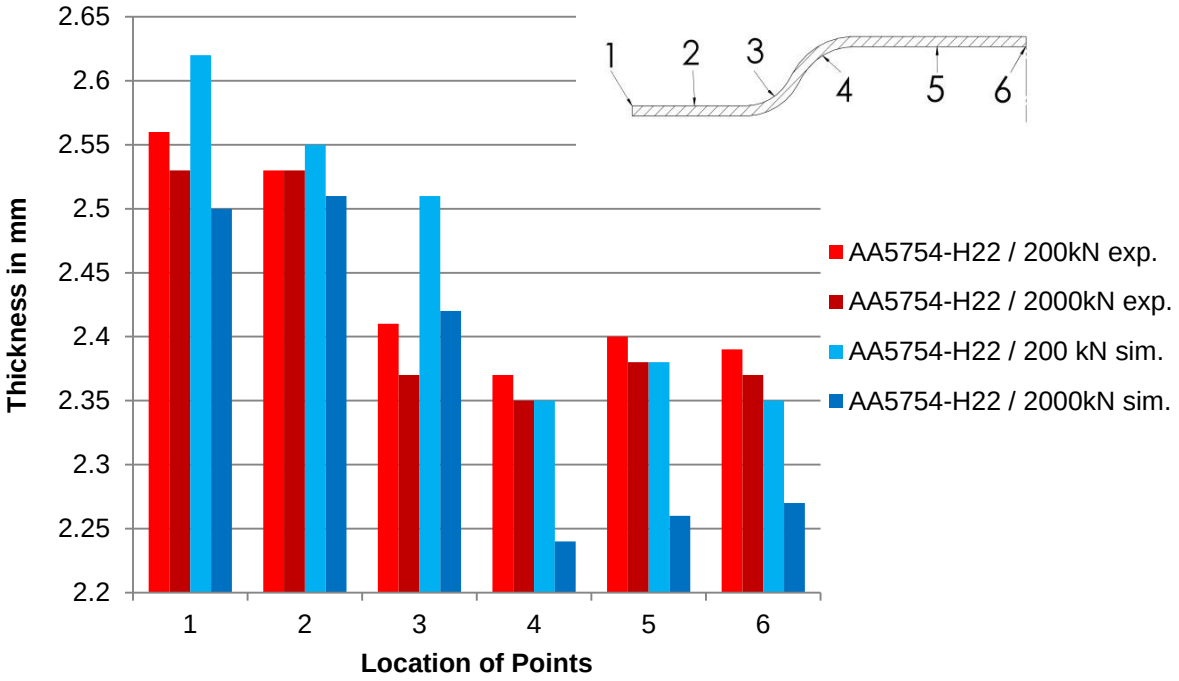

Figure 6.14: Thickness distribution of AA5754-H22 for 200 kN and 2000 kN blankholder force with 100 mm distance away from the cup center to the edge of die for both experiments and simulations

As it can be seen from the figure above, the results of the simulation is higher from first up to the third location and lower from the fourth to the sixth location compared to the experiment. The thinnest value is observed in fourth location with 2000 kN and the thickest value in first location with 200 kN blankholder forces in the simulations. It means that with increasing blankholder forces, the thickness of the drawn cup becomes less for both the experiment and the simulation. The difference between them is that the effect of blankholder force in the simulation is bigger when compared to the experiment. For example, the maximum thickness difference at the third location between 200 kN and 2000 kN in simulation is 0.11, whereas in experiment it is 0.04. This can be observed also at the other points. Furthermore, it can be seen that both results are in agreement and show the same trend in the columns.

When simulation results are compared to the experiment results, maximum errors in prediction are around 5% in the flange area and 2% in the cup bottom area. Eventough the results are generally in harmony, the difference between the results can be explained with the following reasons:

- The material chart in the simulation has different hardening curves. Ludwik is calculated with data of the uniaxial tensile test and used in the simulation. Another hardening law like Swift or Ghosh may give closer results to the experiment. Another approach may be conducting bulge test to obtain more precise *n* and *K* values.
- Another material property in the simulation is yield criteria. The paper published by Cosovici et al. investigates the major influence of the yield criterion on the quality of the numerical results obtained when simulating a deep-drawing process. R values are imported to simulation according to Hill's criterion. Model of Barlat can be utilized if required shear test is conducted.
- Various frictions are observed during the deep drawing process and many factors affect the friction coefficient. Because of this, it is not easy to predict the friction. In the simulation the friction coefficient is taken as 0.20. It can be altered and other values can be taken to conduct more simulations to see the effect on results.

In terms of deep drawability, AA5754-H22 is chosen over AA6061-T6. Both experiments and simulations show that the material is more resistant to thinning which is an important criteria for deep drawability. Thinning can lead to cracks and splits when it is excessive. Apart from that, AA5754-H22 has higher formability which can be seen from the forming limit diagram. If the depth of the cup is altered to produce deeper cup, AA5754-H22 would be a better choice. The AA6061-T6 can withstand less forming without any failure.

The reason to investigate deep drawability of different aluminium alloys is not only to optimize the process, but also to choose the more inexpensive material if possible,. The price of aluminium alloy AA5754-H22 is 1 €/kg less than the price of AA6061-T6. This economically justify the choice of AA5754-H22 over AA6061-T6.

From the results of the experiments and the simulations it can be concluded that the drawing of the cup can be achieved most efficiently and with required quality with 100 mm distance away from the cup center to the edge of the die and by using 200 kN blankholder force. The first parameter, 100 mm distance to the edge of the drawn cup, provides a straight edge of the cup. Distances higher than 100 mm can be also chosen but closest distance to edge is preferred by the company due to aesthetic concerns. The second parameter, 200 kN blankholder force, has more wrinkling compared to higher blankholder forces. However, wrinkling cannot be observed when the distance is chosen as 100 mm. Apart from that, the lowest blankholder force has the highest thickness values. Therefore, for further simulations these parameters were chosen for aluminium alloy AA5754-H22.

6.3.4 The Effect of Lubrication and Mesh Size on Simulation Results

Further simulations are run with different parameters for the blankholder and the distance to the edge of the drawn cup, chosen as 200 kN and 100 mm, respectively. Other parameters such as the mesh size and the lubrication are varied. **Table 6.2** shows the parameters of AA5754-H22 deep drawing simulation.

Table 6.2: Deep drawing simulation parameters

Material	Lubrication	Mesh size
AA5754-H22	no lubricant (0.2), normal (0.1), special lubricant (0.05)	normal (0.22/30), fine (0.16/22.5), extra fine (0.05/6)

The mesh size used throughout the simulation is fine. Two different mesh sizes are used to observe the effect of the mesh on the results. If the accuracy is chosen as normal, the radius penetration becomes automatically 0.22 mm and the max. element angle 30° for a radius of 90°. The mesh size can also be defined by the user as it is shown in the table such as extra fine. In the simulations, the friction coefficient for lubrication is chosen as 0.2. In the deep drawing experiments, no lubrication is used. It is easier to apply lubrication on simulation. According to Soliman, the friction values, between 0.05 and 0.25 are typically used in simulation programs. Therefore, two

friction values lower, which are also suggested by AutoForm^{plus} R3, were chosen to observe the effect of this parameter.

First, the effect of lubrication is investigated. For extra fine mesh, three different friction coefficients, 0.2 (no lubricant), normal (0.1) and special lubricant (0.05) are compared. **Figure 6.15** shows the thickness distribution of AA5457-H22 for different lubrication conditions.

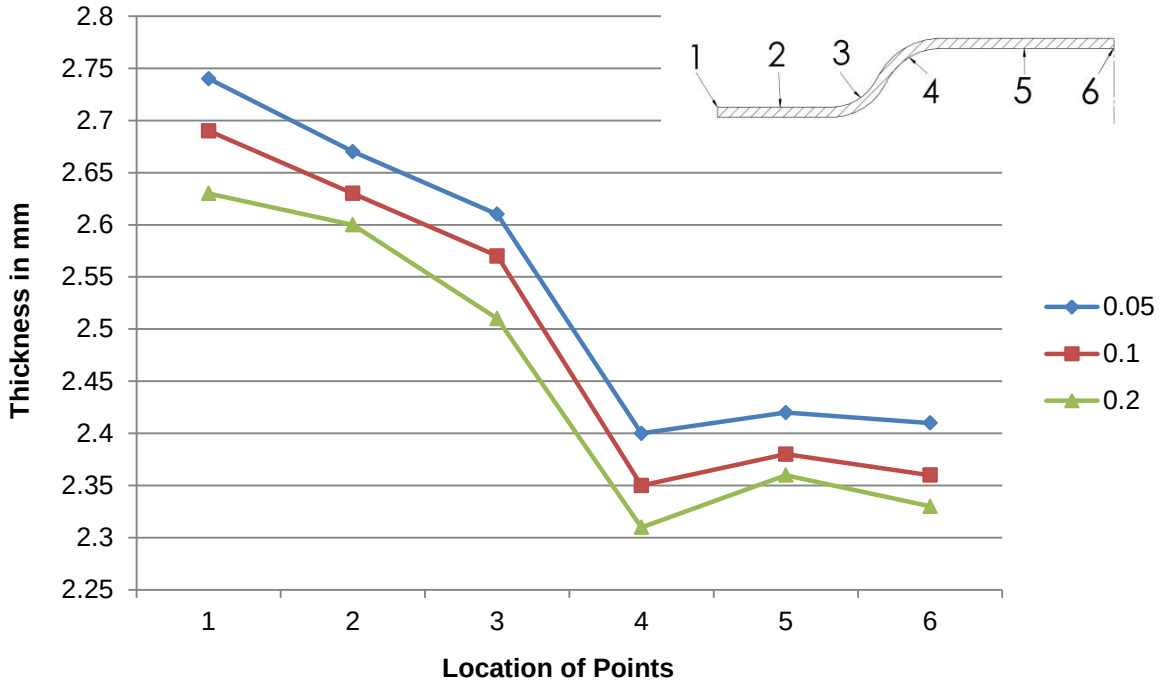

Figure 6.15: Thickness distribution of AA5754-H22 for 200 kN and 100 mm distance away from the cup center to the edge of die for different friction coefficients

The thickness values of all three graphs are parallel to each other. The graph of the lowest friction coefficient lies above the other two. These values are the highest. The thinnest values are observed in the highest friction coefficient, 0.2. The thickness value of normal lubricant is between them. It explains that the higher friction coefficient, in other words less or no lubricant, causes more thinning than deep drawing process with lubricant. When more lubricant is used, then friction coefficient becomes lower which causes the thickness values become higher. If a deep drawing process causes excessive thinning, using lubrication can prevent failure. As it can be seen from the thickness values for deep drawing process of emergency valve cup, no lubricant is needed. The lubricant can be applied when the drawn cup becomes deeper.

Next, the effect of the mesh size is investigated. **Figure 6.16** indicates the thickness distribution of AA5754-H22 for three different mesh sizes.

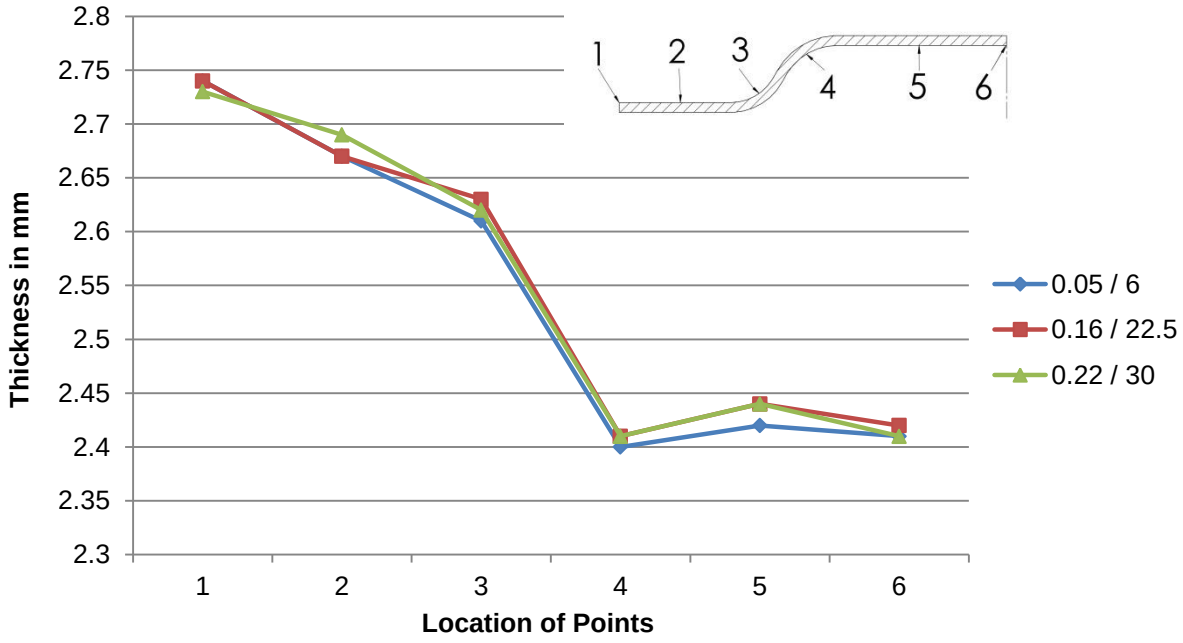

Figure 6.16: Thickness distribution of AA5754-H22 for 200 kN and 100 mm distance away from the cup center to the edge of die for different mesh sizes

All three curves coincide and have similar results. The mesh size has almost no effect on thickness values of the drawn cup. Finer mesh sizes means longer computational times but also smoother results in terms of thickness distribution images in the simulation software. AutoForm^{plus} R3 is an implicit solver software which requires less computational times than other programs. Because of this, the finest mesh size (0.05/6) can be chosen.

7 Cost Analysis

The cost analysis of this project has a significant role in the master thesis. In the first place, the reason to initiate this project was lowering the expense of the company. Instead of purchasing the hollow part of fuel filler flap panel from an external company and then adhere, the part is manufactured with deep drawing process at a hydraulic press in the factory.

The same deep drawn part is also located on the flap of the drivers' rest area. Each bus has two of the emergency valves to open the flaps manually. It is shown in **Figure 7.1.**

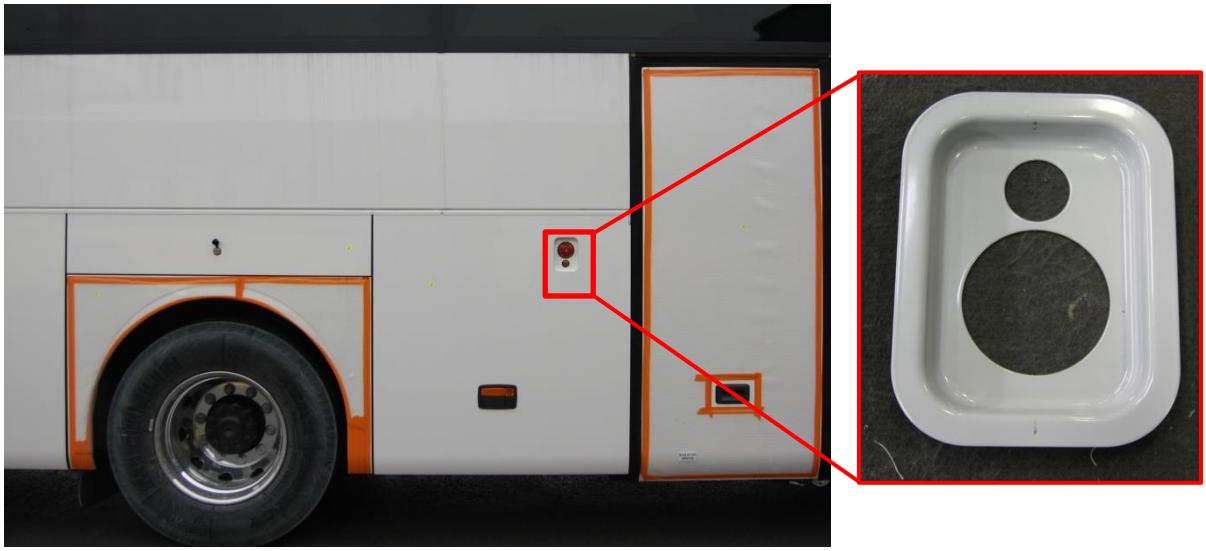

Figure 7.1: Emergency valve cavity on the flap of the drivers' rest area

First of all, the cost of the deep drawn part of fuel filler flap panel must be calculated. To produce a fuel filler flap, first the panel must be produced and then must be adhered to its framework. There are some holes on this panel which are cut in a CNC machining center and one of them has a deep drawn part which is adhered there. The deep drawn part is purchased from an external supplier. This part is needed to mount the emergency valve which opens the flap manually. Data provided by the ERP system SAP R/3used at Mercedes-Benz Türk A.Ş. show the production planning steps of the fuel filler flap panel. It includes the processes, their time and its cost if a material is used.. They are listed below in the **Table 7.1**. The process steps are the same for the same drawn part on the flap of the drivers' rest area.

Table 7.1: Cost of the hollow part of fuel filler flap panel with purchase and adhesive bonding

Explanation	Quantity	Unit cost	Cost
Hollow part	1 piece	1.5 €	1.5 €
Interply elastomer	4 piece	0.025 €/piece	0.01 €
Terokal 6015 adhesive	0.1 kg	4.75 €/kg	0.475 €
Teroson 700 hardener	0.02 kg	8 €/kg	0.16 €
Labour cost	5 min.	9 €/hour	0.75 €
		Total cost	**2.89 €**

The cost that is calculated is the extra cost which is caused by purchasing the hollow part to mount emergency valve. The production cost to make this hole with the whole fuel filler flap panel is shown in the Table 7.2 below. It includes only the labour cost as the same material is used as purchased hollow part and no adhesive bonding is necessary.

Table 7.2: Cost of the hollow part of fuel filler flap panel with deep drawing

Explanation	Quantity	Unit cost	Cost
Labour cost	1.2 min.	9 €/hour	**0.18 €**

The next table shows the cost difference of two production ways and how much it the company saves with choosing deep drawing of the emergency valve cavity over purchasing it.

Table 7.3: Total cost saving of with the deep drawn part with production instead of purchasing in a year

Saved cost for each part	Quantity of part at each bus	Quantity of bus in a year	Total cost saving
2.71 €	2	4200	**22,764 €**

This calculation is made on the sales prediction for 2015. At Hoşdere factory of Mercedes-Benz Türk A.Ş., 4700 busses are produced in a year and 500 of them is municipality type which do not have this deep drawn part. Cost difference of deep drawn part is calculated where the production methods are subtracted (2.89€ - 0.18 €) from each other. This amount is multiplied with the quantity of parts in bus and the

number of busses in a year. Total amount of saved cost is around 23,000 €. With ongoing production of busses over the years the amount saved will increase and become more significant.

The project is initiated by EvoBus and proposed to Mercedes-Benz Türk A.Ş to investigate two different aluminium materials AA5754-H22 and AA6061-T6. Apart from that it can lead to other projects for cost saving with reducing aluminium alloy sheet thickness.

8 Conclusion

In the scope of this thesis, two different aluminium alloys are compared in terms of deep drawability with experimental and numerical investigations.

First, the materials are characterized with tensile and Nakajima tests. Then deep drawing experiments with different process parameters are carried out to produce emergency valve cup. The experimental investigation is followed by a numerical analysis which investigates deep drawing process with AutoForm^{plus} R3 simulation software. The results of the material characterization tests are applied in the deep drawing simulation for a more realistic analysis and comparison with the experiments. The results of experimental and numerical investigations are not only interpreted separately but also compared to each other.

- The tensile test results show that AA5754-H22 has a higher anisotropy coefficient than AA6061-T6, which corresponds to good drawability. At high r values, the sheets exhibit significant resistance to thinning when being drawn into a cup.
- The forming limit diagram is generated according to the Nakajima test. In FLD the curve of AA5754-H22 is above than the curve of AA6061-T6, which means the extent of formability of AA5754-H22 is higher than the AA6061-T6.
- Deep drawing experiments show thickness distributions over different locations in drawn cup. The highest values of thickness are observed in the flange area and lowest values of thickness are observed in the bottom fillet area. It is observed that with increasing blankholder force, the overall thickness of the drawn cup reduces.
- Deep drawing experiment shows that smaller distances away from the cup center to the edge of the die causes the thickening which increases the chance of wrinkling. This flange thickening causes a gap between part and straight surface.
- Experimental and numerical results are in agreement with each other. Their results show that AA5754-H22 is more resistant to thinning than AA6061-T6 as it has higher thickness values at each different location of the drawn cup.

- According to FLD result of the simulation and the wrinkling criterion of the simulation, the wrinkling of both aluminium alloys is close to each other, whereas AA5754-H22 is more prone to wrinkling.
- According to further simulations, it can be stated that the mesh size has almost no effect on the results. On the other hand, use of lubrication leads to less thinning.
- From the results of the experiments and the simulations it can be concluded that the drawing of the cup can be achieved most efficiently and with required quality with 100 mm distance away from the cup center to the edge of die and 200 kN blankholder force. The first parameter, 100 mm distance to the edge of the drawn cup, provides a straight edge of the cup. The second one, 200 kN blankholder force, has no wrinkling to be observed and has highest thickness values.

Throughout this work, it is observed that these further investigations can be conducted:

- Different process parameters such as blankholder force can be chosen according to design of experiments (DOE) to have an optimum selection.
- The experiment and simulation can be repeated with other heat treatments of AA5754 or with other 5 series aluminium alloys and can be compared to AA5754-H22 in terms of drawability both experimentally and numerically.
- The experiments and simulations can be repeated with thinner than 2.5 mm thick (2.25 mm) sheets of AA5754-H22 in terms of drawability both experimentally and numerically to lower the cost of drawn part production.

Bibliography

Aleksandrović, S., Nedeljković, B., Stefanović, M., Milosavljević, D., Lazić, V. 2009. Tribological Properties of Steel and Al-Alloys Sheet Metals Intended for Deep Drawing. Tribology in industry, Volume 31, No. 3&4.

Aleksandrović, S., Stefanović , M., Adamović , D., Lazić, V. 2009. Variation of Normal Anisotropy Ratio "r" during Plastic Forming. Journal of Mechanical Engineering 55-6, 392–399.

Altan, T., & Tekkaya, A. E. 2012. Sheet Metal Forming Fundamentals. ASM International.

Boljanovic, V. 2004. Sheet Metal Forming Processes and Die Design, Industrial Press Inc. U.S.

Callister, William D., 2007. Material Science and Engineering–an Introduction, John Wiley & Sons Inc.

Cosovici, G., Comşa, D.S., Banabic, D. 2006. Evaluation of the Performances of the Different Yield Criteria by Using the Deep Drawing Test.

Davis, J. R., 2004. Tensile Testing, ASM International.

Demirci, H.İ., Esner, C., Yasar, M. 2008. Effect of the blank holder force on drawing of aluminium alloy square cup: Theoretical and experimental investigation. Journal of materials processing technology 206, 152–160.

DIN ISO 6892-1 Standart. 2009.Metallic materials -Tensile testing -Part 1: Method of test at room temperature

DIN ISO 12004-2 Standart. 2009.Metallic materials- Sheet and strip -Determination of forming-limit curves- Part 2: Determination of forming-limit curves in the laboratory

El Khaldi, F., 2002. New requirements and recent development in sheet metal stamping simulation

Fırat, M., 2007. Computer aided analysis and design of sheet metal forming processes: Part I – The finite element modeling concepts. Materials and Design 28 (4), 1298–1303.

Girjob C., Racz G., Bologa O., 2010. The Determination of Forming Limit Curve using a Modular Device, Academic Journal of Manufacturing.

Groover, Mikell P., 2012. Springer Handbook of Experimental Solid Mechanics, Wiley.

Herdawandi, H., Wilkinson, D.S., Niewczas, M., 2007. The Portevin–Le Chatelier (PLC) effect and shear band formation in an AA5754-H22 alloy. Acta Materialia 55, pp 4151–4160.

Nakajima. K., Kikuma T., Hasuka, K., 1971. Yawata Tech. Rep. No 284, pp 678-680

Kalpakjian, S., & Schmid, S., 2007. Manufacturing Processes for Engineering Materials Edition 5. Pearson Prentice Hall, New Jersey.

Kleiner, M., Geiger, M., Klaus, A., 2003. Manufacturing of Lightweight Components by Metal Forming. Manufacturing Technology. Volume 52, Issue 2, pp 521–542.

Lange, K., Pöhlandt, K., 1985. Handbook of metal forming. McGraw-Hill.

Lange, Kurt. 2006. Handbook of Metal Forming. Society of Manufacturing Engineers.

Magar, S. M., Khire, M. Y., 2010. Deep drawing of cup shaped steel component: finite element analysis and experimental validation. International Journal on Emerging Technologies 1,pp 68-72.

Marciniak, Z., Duncan, J.L., Hu, S. J., 2002. Mechanics of Sheet Metal Forming, 2nd Edition, Butterworth- Heinemann, Oxford.

Miller, W.S., Zhuang, L., Bottema, L., Wittebrood, A.J., De Smet, P., Haszler, A., Vieregge, A., 2000. Recent development in aluminium alloys for the automotive industry, Materials Science and Engineering A280, pp 37–49.

N. N., 2011,AutoFormplus R3- Oustanding Accuracy and Speed, http://www.autoform.com/en/news-events/news/autoform-plus-r3-outstanding-accuracy-and-speed. Retrieved on 02.07.2014

N. N.,2013, Aluminium in Cars, European Aluminium Association (EAA) http://www.alueurope.eu/wp-content/uploads/2013/10/EAA-Aluminium-in-Cars-Unlocking-the-light-weighting-potential_September2013_03.pdf .Retrieved on 10.06.2014

N. N., 2014, Classification of the Wrought Alloy Series http://aluminium.matter.org.uk/content/html/eng/default.asp?catid=214&pageid=2144417045. Retrieved on 01.06.2014

N. N., 2014, Aluminium Alloy - Commercial Alloy - 5754 – H22 Sheet http://www.aalco.co.uk/datasheets/Aluminium-Alloy-5754-H22-Sheet-and-Plate_153.ashx. Retrieved on 01.06.2014

N. N., 2014, " Aluminium Alloy - Commercial Alloy - 6061 - T6 Extrusions" http://www.aalco.co.uk/datasheets/Aluminium-Alloy-6061-T6-Extrusions_145.ashx. Retrieved on 01.06.2014

N.N., 2014, AutoForm Profile, http://www.autoform.com/en/company/profile Retrieved on 02.07.2014

Ozturk, F., Esener ,E., Toros ,S., Picu, R.C., 2010. Effects of aging parameters on formability of 6061-O alloy. Materials and Design 31,pp 4847–4852.

Raju, S., Ganesan, G., Karthikeyan R., 2010. Influence of variables in deep drawing of AA 6061 sheet. Trans. Nonferrous Met. Soc. China. 20, pp 1856- 1862.

Ramesh, G., Reddy, G.C.M., 2013. Analysis of Optimization of Blank Holding Force in Deep Drawing by Using LS DYNA. International Journal of Engineering Research and Applications. Vol. 3, Issue 4, pp 1975–1995.

Schüler Gmbh., 1998. Metal Forming Handbook, Springer-Verlag, Berlin.

Semiatin, S.L. 2005. Introduction to Bulk-Forming Processes, ASM Handbook, Volume 14A.

Soliman, A. A., 2006. Numerical Simulation of Metal Sheet Plastic Deformation Processes through Finite Element Method. PhD Thesis, University of Naples Fedeiico II. Department of Materials and Producion Engineering.

Tekkaya, A. E., Bunge, H., Pöhlandt, K., & Banabic, D., 2000. Formability of Metallic Materials: Plastic Anisotropy, Formability Testing, Forming Limits. Springer,

Tisza, M., Kovács, Z. P. 2012. New Methods for Predicting the Formability of Sheet Metals. Production Processes and Systems, Volume 5. No 1, pp 45-54.

Tisza, M., 2013. Material Developments in Sheet Metal Forming 6. Production Processes and Systems, pp 79-88.

Yalçin, S., 2010. Analysis and Modeling of Plastic Wrinkling in Deep Drawing.

Zein, H., El-Sherbiny, M., Abd-Rabou, M., El Shazly, M. 2013. Effect of Die Design Parameters on Thinning of Sheet Metal in the Deep Drawing Process. American Journal of Mechanical Engineering, Vol. 1, No. 2, pp 20-29.